UNIVERSITY OF BIRMINGHAM

Luminescence Lifetime-Based Sensing Solid Interfaces for the Determination of Perfluoroalkyl substances (PFAS)

by

KUN ZHANG

A thesis submitted to the University of Birmingham for the degree of DOCTOR OF PHILOSOPHY

School of Geography, Earth and Environmental Sciences

College of Life and Environmental Sciences

University of Birmingham

April 2024

Abstract

The presence of per- and polyfluoroalkyl substances (PFAS) in humans arises from their large-scale use in multiple industrial and consumer applications. Such uses have led to human exposure via a range of pathways of which is concerning given evidence of the adverse health impacts of PFAS. However, conventional LC-MS methods for measuring PFAS are economically and logistically unsuited to monitoring compliance with this limit, and less expensive, faster and user-friendly methods for the quantification of PFAS are urgently required. Luminescence lifetime is an attractive analytical method for detection due to its high sensitivity and stability, and there is great interest for the design of detection platforms for monitoring of PFAS concentrations in different environmental contents. Herein, three novel luminescence lifetime-based sensing platforms were developed for the accurate and rapid detection of PFAS (e.g. PFBA, PFOA, PFNA, PFDA, etc) in different environmental contexts.

Chapter III describes the fabrication and function of a novel and facile luminescence sensor for PFOA detection based on iridium modified gold surfaces. These surfaces were modified with lipophilic iridium complexes bearing alkyl chains, namely, **IrC_6** and **IrC_{12}**, and Zonyl-FSA surfactant. Upon addition of PFOA, the modified surfaces **IrC_6-FSA@Au** and **IrC_{12}-FSA@Au** show the largest change in the red luminescence signal with changes of the luminescence lifetime that allow monitoring of PFOA concentrations in aqueous solutions. The platform was tested for measurement of PFOA in aqueous samples spiked with known concentrations of PFOA, and demonstrated capacity to determine PFOA at concentrations >100 µg/L (240 nM).

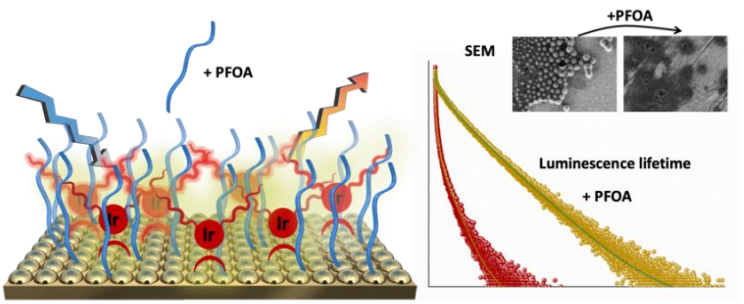

Chapter IV describes a functionalised gold surface based on a SAcbisDBM ligand and Europium(III) to rapidly and accurately measure the concentrations of C_4 to C_{10} PFCA in waste fabrics. The surface was modified with SAcbisDBM ligand, subsequently coordinated with Europium(III), namely **Eu-SAcbisDBM@Au** surface, displaying high affinity towards perfluoroalkyl carboxylic acids (PFCA) and is reusable. Under optimal conditions, the surfaces can detect >80 nM PFCA. The potential utility of the sensor is demonstrated by the good agreement between concentrations recorded by the sensor and LC-MS measurements of C_4-C_{10} PFCA in 34 leather, leatherette, and textile samples.

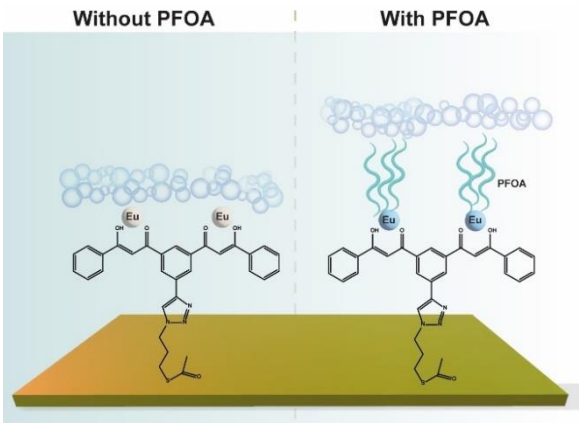

Chapter V investigates the use of near infrared-emitting lanthanides, such as Neodymium(III) and Ytterbium(III) coordinated with the SAcbisDBM ligand, in solution (**Nd/Yb-SAcbisDBM**) or on plasmonic gold (pAu) surface (**Nd-pAu** and **Yb-pAu**), to detect PFCA such as PFOA, PFNA, and PFDA in water. Upon the addition of PFCA (e.g. PFDA), both Nd-SAcbisDBM and Yb-SAcbisDBM show a significant increase in luminescence, displaying a detection range as low as 2 μM and 10 μM, respectively. The luminescence properties of Nd-pAu and Yb-pAu also present a positive correlation with the concentration of PFCA. The sensing systems exhibit enormous potential for the detection of PFAS, offering valuable insights for environmental monitoring.

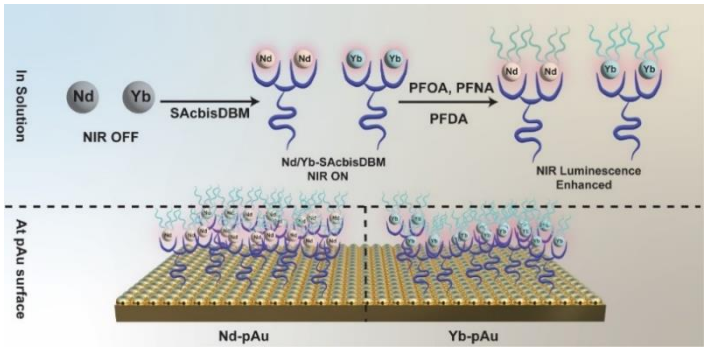

Acknowledgements

When I was writing this section, it was already two in the morning. Thoughts tend to flow more freely when the night is quiet.

Sometimes I think, if someone had told me when I was a child that I would become a doctor in the future, I would have thought that person was probably insane. I was born in a poor village in southern China. My father went to work in the mega city shortly after my birth, leaving only my mother and me in the countryside. I don't have many memories of rural life, just that summers were hot, mosquitoes were everywhere, while winters were cold, and food was always scarce. For a family like ours, my father was already proud that I could go to college. However, when I told him I wanted to pursue a master and even a doctoral degree, he fell silent. In my father's perspective, there was nothing happier than having his children by his side. Fortunately, with my mother's support, I had the opportunity to come this far. When I was young, I was naive, only wanting to step onto a bigger stage. But looking back on these 12 years away from home, my parents must have missed me a lot.

September 2019 marked the beginning of my doctoral journey. At that time, I was full of ambition, but the arrival of the pandemic poured cold water on me. Due to the pandemic, my wife and I were trapped in a tiny 17-square-meter room, enduring five difficult months. During that time, worries about rent, food, academic stagnation, and the panic brought by the pandemic kept tormenting me, causing me to suffer from severe gastritis. I had to apply for a 7-month leave of absence. It was my wife's constant companionship and encouragement that helped me get through this difficult time.

Later, just before my graduation, I regretted not having undertaken any academic visits. Therefore, I resolutely applied for a one-year exchange program at the Southern University of Science and Technology. Although this visit further delayed my graduation, the achievements I made here and the friendships I formed will benefit me for a lifetime.

Compared to my colleagues, friends, and peers, it does took me quite a long time to reach where I am today. Now, I feel it's time to bring it to an end and move on to the next stage of my life.

I am grateful to all the people I have met in my life, there are just too many, so I can only try to mention a few.

First and foremost, I express my sincere gratitude to my esteemed supervisors, Professor Stuart Harrad and Professor Zoe Pikramenou, I will never forget the invitation letter from Stuart in the summer of 2019; it was the first time I felt how refreshing Guangzhou could be. Over the past three years of working for Stuart and Zoe, I have gained invaluable insights that will benefit me for a lifetime.

Special appreciation is extended to the dedicated members of our research groups within the School of Geography, Earth, and Environmental Sciences, and the School of Chemistry at the University of Birmingham. I am grateful to Dr. Mohamed Abdallah, Dr. Daniel Drage, Dr. Ovokeroye Abafe, Dr. William Stubbings, Dr. Nicholas Davidson, Dr. Chuanzi Gao, Dr. Yulong Ma, Shijie Wang, Jinxi Jin, Dr. Oddny Ragnarsdottir, Dr. Muideen Gbadamosi, Dr. Simeon Onoja, Dr. Misbah Alghamdi, Dr. Affiong Asuquo, Dr. Abdalkarim Dawood, Dr. André Henrique Rosa, Dr. Maria Odyniec, Hassan Ageel, Muneera Al-Mansoori, Dr. Elena del Giorgio, Dr. Asier Rodriguez-Muguruza, Dr. Patrícia Gírio, Dr. Jamie Bradley, Dr. Luke Watson, Joseph Hughes, and Grace Ball. Their collaborative spirit and collective efforts significantly enriched my research experience. Among them, I am most grateful to Elena, a beautiful Italian girl. For a Chinese person who doesn't understand Western culture, integrating into the local culture can be challenging, but Elena has always shown me genuine kindness, for which I am deeply grateful. It is regrettable that there are too many individuals to reasonably list.

I would also like to express my gratitude to my friends, Dr. Congbo Song, Dr. Peng Zhang, Dr. Jingsha Xu, Dr. Yuqing Dai, Dr. Jiali Feng, Dr. Mao Du, who stood by me during the highs and lows of this academic endeavour. Your camaraderie and encouragement have made this journey more meaningful.

I would like to express my deepest gratitude to my parents and younger brother, they are Mr. Yuanxiang Zhang, Mrs. Ruiling Chen and Mr. Wei zhang. I have seen many people smarter and more talented than me give up pursuing a doctoral degree due to various family reasons. My parents and brother worked hard to contribute to this family, allowing me to pursue academic dream without worries. As I move forward, they give me unparalleled courage.

Lastly, I want to thank my wife. Her cooking is really bad, to the point where even the Little Bench

wants to bury it in the cat litter. By the way, Little Bench is our cat, now sleeping soundly by my feet. I want to continue complaining about my wife, but I can't seem to find any more faults with her. Oh, I remember one thing, I spent all my savings to buy her a diamond ring, but she thought it was too small. I've always remembered this little incident, but she still agreed to marry me in the end.

That is it, I'm starting to feel sleepy, good night world.

Contents

List of Acronyms

6:2 FTS: 6:2 Fluorotelomer sulfonate

ACQ: Aggregation caused quenching

AIE: Aggregation Induced Emission

Bpy: 2,2'-bipyridine

DBM: Dibenzoylmethane

DLS: Dynamic Light Scattering

EDX: Energy Dispersive X-Ray

EtOH: Ethanol

GC-MS: Gas chromatography coupled with mass spectrometry

LC-MS: Liquid chromatography coupled with mass spectrometry

LC-QTOF-MS: Liquid chromatography coupled with quadrupole time-of-flight mass spectrometry

Ln(III): Lanthanide(III)

LOD: Limit of Detection

MeCN Acetonitrile

MeOH: Methanol

MS Mass Spectrometry

NIR: Near Infrared

NMR: Nuclear Magnetic Resonance

PET: Photoinduced electron transfer

PFAS: Perfluoroalkyl substances

PFBA: Perfluorobutyric acid

PFBS: Perfluorobutanesulfonate

PFCA: Perfluoroalkyl carboxylic acid

PFDA: Perfluorodecanoic acid

PFHpA: Perfluoroheptanoic acid

PFHxA: Perfluorohexanoic acid

PFHxS: Perfluorohexane sulfonate

PFNA: Perfluorononanoic acid

PFOA perfluorooctanoic acid

PFOA: Perfluorooctanoic acid

PFOS: Perfluorooctane sulfonate

PFPeA: Perfluoropentanoic acid

PFSA: Perfluoroalkyl sulfonic acid

ppy 2-phenylpyridine

S/N=3: Signal/noise=3

SEM: Scanning Electron Microscopy

THF: Tetrahydrofuran

TOF-SIMS: Time-of-flight secondary ion mass spectrometry

UV- Vis: Ultraviolet-Visible Spectrum

XPS: X-Ray Photoelectron Spectroscopy

ε: Molar Absorptivity

λ_{max}: Wavelength with Maximum Intensity

τ: Luminescence lifetime

Chapter 1: Introduction

1.1 State-of-the-art with respect to environmental contamination with PFAS

1.1.1 Basic information on PFAS

Perfluoroalkyl substances (PFAS) are a group of synthetic chemicals that include thousands of fluorinated compounds (Figure 1.1).[1] Their molecular structures are made up of carbon-fluorine (C-F) chains with different lengths, terminal with hydrophilic sulfonate, carboxylates or aliphatic groups.[1] Due to the desirable industrial characteristics of PFAS such as oil and water repellency with good physical and chemical stability, these chemicals have been used extensively as surfactants and emulsifiers in a variety of industrial, commercial, and household products around the world since their onset of their manufacture in the 1940s.[2] Research has since reported the presence of PFAS in drinking water, food, indoor/outdoor air, dust and soil.[3, 4] This is because - while attractive in an industrial context - the strength of the C-F bond renders PFAS highly resistant to thermal, chemical and biological degradation,[5] with the result that they are capable of bioaccumulation and long-range environmental transport (exemplified by their presence in the Arctic),[6] thereby exacerbating their many negative health outcomes.

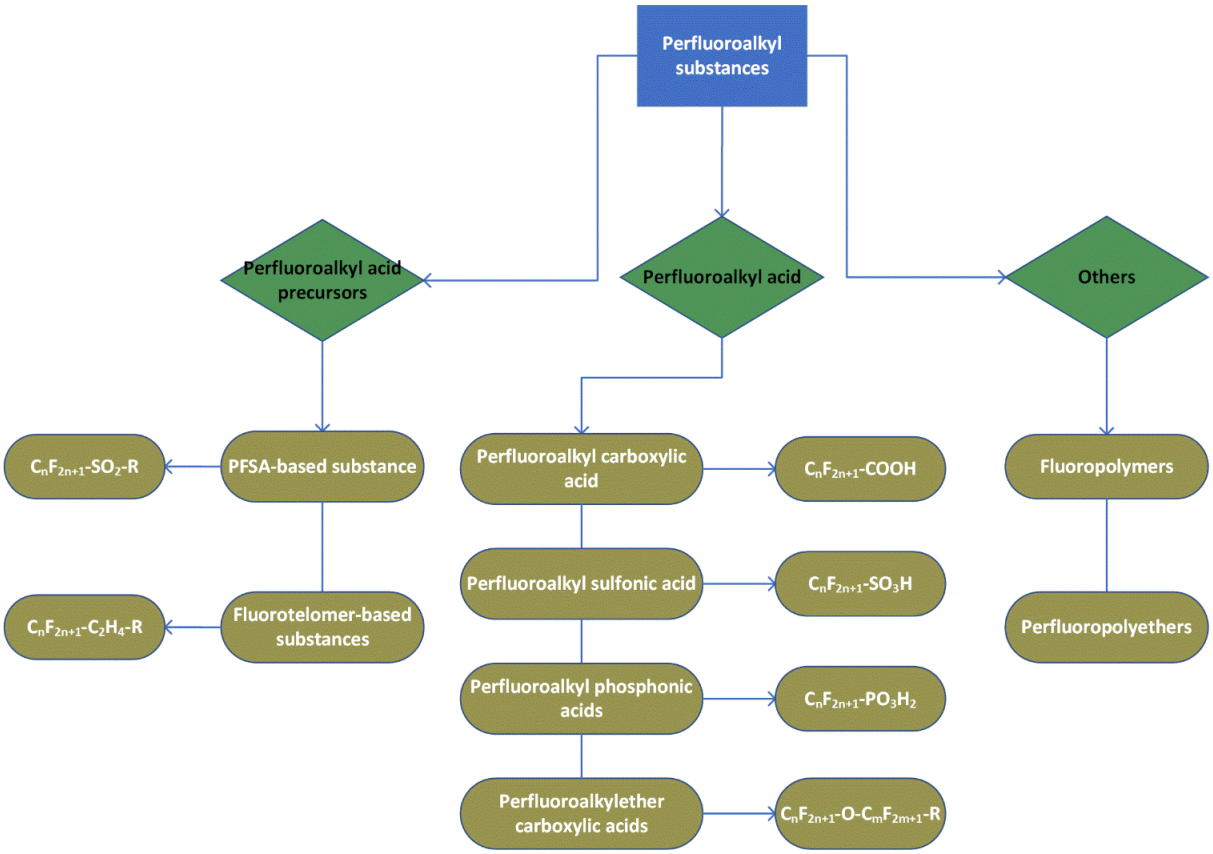

Figure 1.1. Classification of PFAS. This diagram categorizes PFAS into three main groups: Perfluoroalkyl acid precursors, Perfluoroalkyl acids, and Others. The Perfluoroalkyl acid precursors are further divided into PFSA-based substances and Fluorotelomer-based substances, with the general formulas C_nF_{2n+1}-SO_2-R and C_nF_{2n+1}-C_2H_4-R, where R also represents functional groups such as -OH, -COOH, etc. Perfluoroalkyl acids include Perfluoroalkyl carboxylic acids, Perfluoroalkyl sulfonic acids, Perfluoroalkyl phosphonic acids, and Perfluoroalkylether carboxylic acids. The 'Others' category includes Fluoropolymers and Perfluoropolyethers.

Given the vast number of chemicals that may be classed as PFAS, this review focuses on those PFAS defined as of high-concern by the Swedish Food Agency.[7] Their information are provided as Table 1.1.

Table 1.1. Nomenclature and physicochemical properties of 11 PFAS

Name	Acronym name	Molecular weight (g/mol)	Chemical structure	pKa*	Ref
Perfluorobutyric acid	PFBA	214.04	C_3F_7COOH	0.394	8
Perfluoropentanoic acid	PFPeA	264.05	C_4F_9COOH	0.569	8
Perfluorohexanoic acid	PFHxA	314.05	$C_5F_{11}COOH$	0.84	8
Perfluoroheptanoic acid	PFHpA	364.06	$C_6F_{13}COOH$	2.4	9
Perfluorooctanoic acid	PFOA	414.07	$C_7F_{15}COOH$	3.8±0.1	10
Perfluorononanoic acid	PFNA	464.08	$C_8F_{17}COOH$	2.575	8
Perfluorodecanoic acid	PFDA	514.09	$C_9F_{19}COOH$	2.606	8
Perfluorobutanesulfonate	PFBS	300.10	$C_4HF_9O_3S$	-3.31	11
Perfluorohexanesulfonate	PFHxS	400.11	$C_6HF_{13}O_3S$	-3.45	12
Perfluorooctanesulfonate	PFOS	500.13	$C_8HF_{17}O_3S$	<3.27	13
6:2 Fluorotelomer sulfonate	6:2 FTS	428.17	$C_8H_5F_{13}O_3S$	-	-

*: reported pKa value differs between studies. -: uncertain

1.1.2 Sources of PFAS

Sources of PFAS are varied. They are mainly released from industrial facilities, use of aqueous film forming foam (AFFF) in fire-fighting training and emergency response, farmland and residential areas, and wastewater treatment plant discharge (Figure 1.2).[14] Manufacturing plants involved in the production of fluorinated compounds and products using PFAS as raw materials are notable sources.[15] As depicted in Figure 1.2, these facilities discharge PFAS to nearby watercourses and the atmosphere directly via sewage outlet and atmospheric discharges. Research indicated that rivers proximate to industrial zones exhibit elevated PFAS concentrations compared to urban and agricultural regions.[16] Moreover, airborne emissions of PFAS will undergo atmospheric transport, followed by wet and dry deposition to the surface.[17] Part of the rain containing PFAS that has fallen will directly flow to nearby rivers; with some leaching to deeper soil layers and groundwater.[18]

Another significant source of PFAS comes from the consumption and use of products containing these compounds. PFAS from such releases migrate to the environment contexts by use, transport, abrasion, degradation and so forth.[19-21] For instance, the runoff water and wastewater near the firefighter training area (frequently use AFFF) were detected a large amount of PFAS.[22] AFFF will migrate to the groundwater by sewage system or to underground water via leaching. Also, PFAS are emitted from waterproof clothing, leather, etc by abrasion of PFAS-treated fibres/particles.[20] To date, PFAS have been reported in non-stick cookware, textiles, leather, food packaging, paint, cleaning agents, cosmetic products and firefighting foams (Figure 1.2).[20, 23-26]

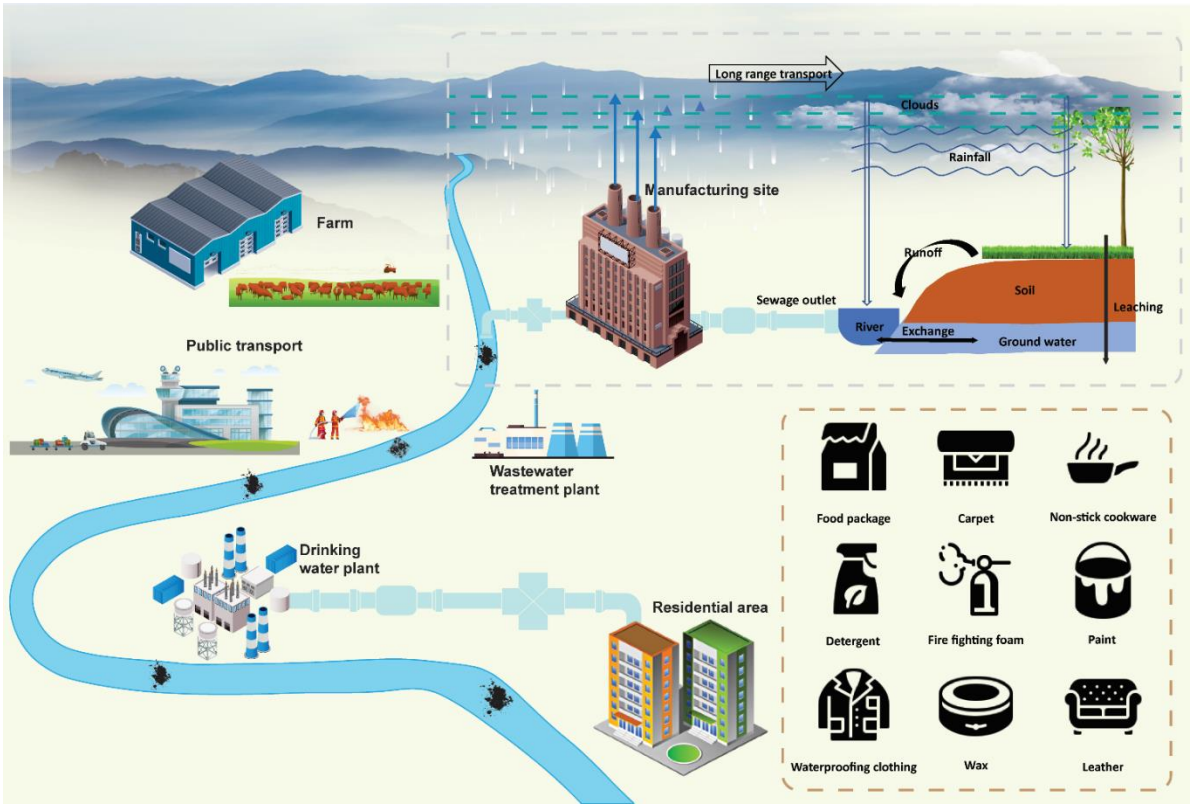

Figure 1.2. Various sources of PFAS in the environment.

1.1.3 Human exposure pathways

PFAS enter the human body through diet, ingestion of contaminated water, inhaled dust and air as well as direct dermal uptake (Figure 1.3). Of these pathways, ***dietary intake***[27] is estimated to be the main pathway of human exposure to PFAS leading to their ubiquitous presence in human serum.[28] Sources of dietary exposure to PFAS include migration from food packaging[29] and non-stick cooking[30] utensils. Based on assessment of the evidence for their adverse health effects in humans, the European Food Safety Authority (EFSA) announced a tolerable weekly intake (TWI) opinion for four main PFAS on September 17, 2020; specifically, the weekly dietary intake of the sum of PFHxS, PFOS, PFOA and PFNA should not exceed 4.4 ng/kg.[31]

Ingestion of contaminated water[32] is a significant pathway of human exposure to PFAS. Notably, some PFAS compounds terminate with carboxylic and sulfonic groups, which greatly enhance their solubility in water compared to other halogenated organic chemicals.[10]

Meanwhile, ***inhalation of indoor air and dust***[33] - especially in occupational environments like fluoropolymer manufacturing factories can also constitute a significant pathway for some individuals. Eva et. al. found that participants with high cumulative workplace exposure had 34% higher serum PFOS levels compared to participants without occupational exposure.[34]

Dermal uptake presents an additional potential avenue for PFAS exposure.[35] It may occur via skin contact with PFAS sources, including but not limited to clothing and upholstery, cosmetics, and house dust. However, it's important to acknowledge that our understanding of PFAS absorption through the skin remains incomplete. As a result, current assessments primarily consider dermal exposure via hands as a reference point, given the available data and knowledge base.[36]

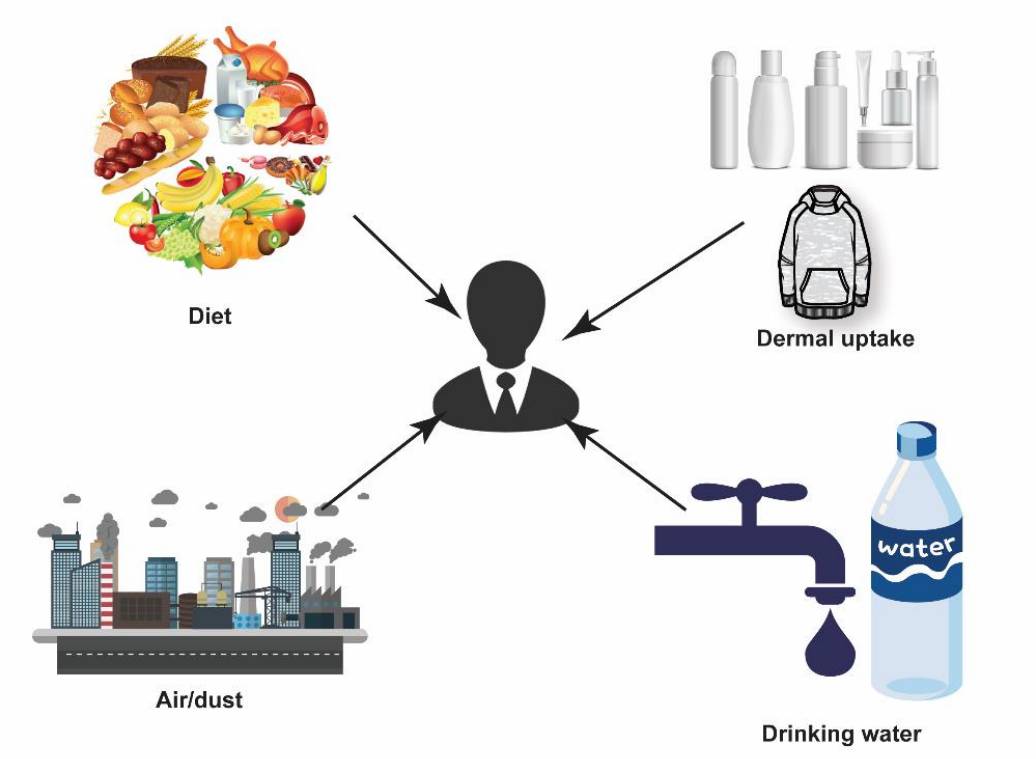

Figure 1.3. Pathways of human exposure to PFAS.

1.1.4 Human health effects of PFAS

PFAS are ubiquitously detected in the serum of workers and residents living near fluorinated manufacturing plants, as well as in the general population.[33, 37] In a survey undertaken in 2003-2004 PFAS were detected in > 98% of the serum samples of the general U.S. population ≥ 12 years of age.[38] Such evidence of near-universal exposure has driven consideration of the potential health implications. The European Food Safety Authority (EFSA) highlighted several possible adverse human health effects of PFAS, such as lower birth weight, increased serum cholesterol levels, and reduced antibody response to vaccination. Concretely, PFOS, PFHxS, PFOA, and PFNA are regarded as 'likely' carcinogens by the European Chemicals Agency (ECHA), and are associated with functional thyroid disease, testicular cancer, and kidney cancer etc.[39, 40] Of these substances, PFOA has recently been classified as a human carcinogen by the International Agency for Research on Cancer (IARC).[41] Epidemiological evidence links PFOS and PFOA exposure with pregnancy-induced hypertension/pre-eclampsia, increased risk of decreased fertility, and low birth weight.[42] A survey of results shows a positive correlation between PFOS, PFHpA, PFOA, and PFNA in plasma and alanine aminotransferase (ALT) - increased of ALT activity is the clinical marker for impaired liver function.[43] Other evidence links PFOS, PFOA, and PFHxS with decreased antibody response to vaccines,[44] and PFOS, PFOA, and PFNA are linked with increased serum lipids, particularly total cholesterol and low-density lipoprotein (LDL) cholesterol.[45]

1.1.5 PFAS limits and relevant regulations

Given the persistence, bioaccumulation potential and toxicity of PFAS, some PFAS (apart from PFOS, use of which was banned in 2004),[46] were registered for use in the European Union (EU) under the Registration, Evaluation, Authorization and Restriction of Chemicals (REACH) legislation (Table 1.2).[47, 48] The ECHA classified these 11 PFAS as persistent (P) because of their strong C-F bonds.[2] This in turn leads to their long human serum elimination half-lives; for instance, that of PFOA is 3.5-3.8 years, of PFOS is 4.8-5.4 years, of PFHxS is 7.3-8.5 years,[49] of PFBS is 25.8 days[50] and for PFBA 44-152 hours.[51] PFHxS, PFOS, PFHxA, PFOA, PFNA, and PFDA were classified as bioaccumulative (B)

and toxic (T),[2] resulting in each being listed on ECHA's List of Substances of Very High Concern (SVHC),[52] or in the case of PFOS, banned.[46] Among these high concern chemicals, PFOA, PFNA, and PFDA are considered 'possibly carcinogenic' by the EU.[2] It is worth noting that PFBS was classified as not B and T,[2] but is still listed as SVHC[52] because PFBS has become the primary substitute for PFOS.[53] In contrast, of the remaining PFAS, 6:2 FTS, PFBA, and PFPeA were classified as neither B nor T,[2] with the classification of PFHxA considered as yet uncertain. It illustrates that PFAS with shorter carbon chains likely display lower bioaccumulation and toxicity.

In an effort to minimise the negative effects of PFAS on environmental and human health, PFOA and related PFOA compounds, as well as PFOS and PFHxS are listed for elimination under the Stockholm Convention on Persistent Organic Pollutants (POPs).[54] Additionally, C_9-C_{21} PFCA are under active consideration for listing under the Stockholm Convention. Moreover, the EFSA has set a challenging tolerable weekly intake value of 4.4 ng/kg body weight for the sum of PFOA, PFOS, PFNA, and PFHxS;[31, 55] and as part of a recast of its Drinking Water Directive, the EU has set a limit of 100 ng/L for the sum of C_4-C_{13} perfluorosulfonic acids (PFSA) and PFCA in drinking water.[56] Further, in March 2023, the US Environmental Protection Agency (EPA) announced proposed maximum contaminant levels (MCLs) for 6 PFAS in drinking water with that for PFOS and PFOA set at 4 ng/L, respectively, and PFHxS, PFNA and GenX chemicals set at 10 ng/L, respectively.[57] Also pertinent, the European Council set a maximum limit value for both PFOA, and PFHxS and their salts as well as PFOA-related and PFHxS-related compounds in waste at 1 mg/kg and 40 mg/kg, respectively.[58]

Table 1.2. Environmental regulatory status of selected PFAS. The regulations are set by ECHA.

Name	SVHC	REACH	PBT			Remarks
			P	B	T	
Perfluorobutane sulfonic acid (PFBS), its salts and related substances: 12 PFBS derivatives and 1 ester						
Perfluorobutanesulfonamide (FBSA)	√	√	√	×	×	
N-Ethyl perfluorobutanesulfonamidoethanol (EtBSE）	√	√	√	×	×	
N-(4-Hydroxybutyl) N-methyl perfluorobutanesulfonamide	√	√	√	×	×	
Perfluorohexane-1-sulphonic acid (PFHxS) and its salts						
Ammonium perfluorohexane-1-sulphonate	√	√	√	√	√	
Potassium perfluorohexane-1-sulphonate	√	√	√	√	√	
Perfluorohexane-1-sulphonic acid	√	√	√	√	√	
Tridecafluorohexanesulphonic acid, compound with 2,2'-iminodiethanol (1:1)	√	√	√	√	√	
Perfluorooctane sulfonic acid (PFOS) and its derivatives, Metal salt, halide, amide, and other derivatives including polymers: approximately 21 chemicals in this group	×	×	√	√	√	PFOS chemicals is restricted under Commission Regulation No 850/2004 on Persistent Organic Pollutants [59] Possibly Carcinogenic, Toxic to Reproduction
6:2 fluorotelomer sulfonate (6:2-FTS)						
6:2 fluorotelomer sulfonamide alkyl betaine (6:2 FTSAB)	×	√	√	×	×	6:2 FTS is less toxic and less persistent in the environment and does not bioaccumulate
6:2 fluorotelomer sulfonamide propyltrimethylammonium iodide (6:2 FTSAQ)	×	√	√	×	×	
Perfluorobutyric acid (PFBA) and its salts						
Perfluorobutyric acid (PFBA)	×	●	√	×	×	
Butanoic acid, heptafluoro-, anhydride (PFBA anhydride)	×	●	√	×	×	
Perfluoropentanoic acid (PFPeA) and its salts						
Perfluoropentanoic acid (PFPeA)	×	●	√	×	×	
Pentanoic acid, nonafluoro-, ammonium salt (ammonium PFPeA)	×	●	√	×	×	
Perfluorohexanoic acid (PFHxA) and its salts						

undecafluorohexanoic acid (PFHxA), its salts and related substances	√	√	√	√	√	
Hexanoic acid, undecafluoro-, ammonium salt (ammonium PFHxA)	√	√	√	√	√	
Perfluoroheptanoic acid (PFHpA) and its salts						
Perfluoroheptanoic acid (PFHpA)	×	●	√	-	-	
Heptanoic acid, tridecafluoro-, ammonium salt (ammonium PFHpA)	×	●	√	-	-	
Pentadecafluorooctanoic acid (PFOA) and its salts						
Pentadecafluorooctanoic acid (PFOA)	√	√	√	√	√	Possibly Carcinogenic, Toxic to Reproduction
Ammonium pentadecafluorooctanoate (APFO)	√	√	√	√	√	Possibly Carcinogenic, Toxic to Reproduction
Perfluorononan-1-oic-acid (PFNA) and its salts						
Ammonium salts of perfluorononan-1-oic-acid	√	√	√	√	√	Possibly Carcinogenic, Toxic to Reproduction
Perfluorononan-1-oic-acid	√	√	√	√	√	Possibly Carcinogenic, Toxic to Reproduction
Sodium salts of perfluorononan-1-oic-acid	√	√	√	√	√	Possibly Carcinogenic, Toxic to Reproduction

Nonadecafluorodecanoic acid (PFDA) and its salts						
Decanoic acid, nonadecafluoro-, sodium salt	√		√	√	√	
Ammonium nonadecafluorodecanoate	√		√	√	√	Possibly Carcinogenic, Toxic to Reproduction
Nonadecafluorodecanoic acid	√		√	√	√	Possibly Carcinogenic, Toxic to Reproduction

SVHC: substance of very high concern; REACH: Registration, Evaluation, Authorization and restriction of chemicals; P: persistence; B: bioaccumulative; T: toxicity.

The current need for a simple and rapid sensing technique for detecting PFAS concentrations is driven by the increasing recognition of the adverse environmental and health impacts of PFAS. These substances are persistent in the environment, bioaccumulative, and have been linked to various health issues. As regulatory agencies worldwide implement stricter guidelines and lower permissible limits for PFAS in water and other media, there is an urgent demand for efficient, user-friendly, and cost-effective methods to monitor these contaminants accurately and promptly.

1.2 Overview of the technologies for the detection of PFCAs

1.2.1 General technologies

Measuring concentrations of PFAS to e.g. facilitate monitoring compliance with regulatory standards, requires accurate, reproducible measurement methods that ideally are inexpensive and rapid. Currently, liquid chromatography - mass spectrometry (LC-MS) and gas chromatography - mass spectrometry (GC-MS) are the methods of choice for the determination of PFAS, due to their high sensitivity, reproducibility and selectivity toward the target molecules.[60] These methods offer detection limits between 0.1 ng/L to 3 ng/L with a RSD range 2% to 16%,[61, 62] depending on the specific PFAS compound, sample size and level of blank contamination (Table 1.3). While accurate and reproducible, such methods are time-consuming, require expert operators, are expensive, and cannot be carried out in the environment in real-time. Instead, samples must be transported to a laboratory for analysis with accompanying time delays.

Table 1.3. Summary of the limits of detection and quantification (LOD/LOQ) of HPLC-MS/MS and GC-MS/MS methods for the detection of PFAS

Technique	Analytical Performance				Matrix	Ref.
	Targets	LOD (ng L^{-1})	LOQ (ng L^{-1})	RSD (%)		
LC-MS/MS	PFBA	0.59	0.75	4	Wastewater Surface water Drinking water	71
	PFPeA	0.71	0.89	5		
	PFHxA	0.87	1.1	6		
	PFHpA	0.84	1.1	6		
	PFOA	0.28	0.35	2		
	PFNA	0.61	0.77	4		
	PFDA	0.71	0.89	4		
	PFBS	0.49	0.62	3		
	PFHxS	0.69	0.88	5		
	PFOS	0.78	1.0	5		
	6:2 FTS	0.56	0.7	4		
GC-MS/MS	PFHxA	0.40	0.86	16	Aqueous matrices	61, 62
	PFHpA	0.17	0.37	12		
	PFOA	0.11	0.24	8		
	PFNA	0.08	0.17	13		
	PFDA	1.2	2.5	16		

1.2.2 Electrochemical sensors

In comparison to the methods required for bench-top instrument, electrochemical sensor measurements of PFAS can be performed in situ using portable potentiostat.[63] It is less costly than LC-MS yet can provide high sensitivity (down to pg/L or even lower) for the detection of PFAS. Based on current research (Table 1.4), this thesis categorizes them into two distinct types. ***Indirect assay*** (IDA) currently is the main avenue being explored for development of such a sensor, especially given that most PFAS are electrochemically inert. Typically, this approach involves modifying a recognition layer on the electrode [e.g., glassy carbon electrode (GCE) or gold micro/macro electrode (AuE)], followed by the addition of redox mediator (e.g., ferrocene carboxylic acid), and finally, the introduction of PFAS. The electron transfer between the recognition layer and redox mediator will be affected in the presence of the PFAS, leading to the alteration in current,[64-67] resistance[68, 69] and other electrochemical signal. ***Direct assay*** (DA) utilises the redox reaction of PFAS on the electrode to quantify PFAS directly. The terminal groups of PFAS, such as carboxylic and sulfonate groups, can also undergo electron transfer. To date, there are some materials that electrochemically sensitive to PFAS were reported, including Cr-MIL-101 MOF,[69] Co/Fe bi-metallic MOFs,[70] hafnium-doped tungsten oxide (Hf.WO3)[71] and poly(vinyl chloride) membrane plasticized with 2-nitrophenyl octyl ether.[72] While processing strong sensitivity, the electrochemical sensor is susceptible to interference from other compounds present in the sample matrix, despite its high sensitivity. These interferences can lead to false positive or false negative results, reducing the accuracy and reliability of the sensor.

Table 1.4 Summary of current studies about the development of electrochemical sensor for the detection of PFAS

Electrode	Analytes	Matrix	Analytical performance		Remark	Ref
			Detection range	LOD (S/N=3)		
o-PD@GCE	PFOS	-	0-0.05 nM	0.05 nM	IDA. ferrocene carboxylic acid as the redox mediator	64
o-PD@Au electrode	PFOS	Drinking water	-	0.04 nM	IDA. ferrocene carboxylic acid as the redox mediator	65
o-PD@Au microelectrode	GenX (HFPO-DA)	River water	1-5000 pM	250 pM	IDA. ferrocene methanol as the redox mediator	66
o-PD-AuNSs@GCE	PFOS	Drinking water	-	0.015 nM	IDA. ferrocenecarboxylic acid as the redox mediator	67
O-PD@GC macroelectrode	PFOS	River water	0-0.5 nM	3.4 pM	IDA. O2 as the indicator. Alter the resistance of the electrode	68
Cr-MIL-101 MOF interdigitated microelectrode	PFOS	-	-	0.5 ppt	DA. PFOS absorbed with MOF will reduce the conductivity of MOF, thus changing the resistance of the microfluid platform	69
Hf.WO3@CPE	PFOA	Drinking water Soil & fruit	70 nM-0.3 mM	18.3 nM	hafnium-doped tungsten oxide (Hf.WO3) toward PFOA	71
oNPOE/PVC@Au	PFOS	-	0-0.5 ppb	25 ppt	DA. PFOS has good lipophilicity and prone to transfer to oNPOE/PVC membrane from water.	72
Co/Fe bi-metallic MOFs@electrospun film	PFOA	-	10 nM-90 uM	1.073 nM	DA. Co/Fe bi-metallic MOFs has high affinity toward PFOA	70

IDA: Indicator displacement assay

DA: Direct assay

1.2.3 Luminescence sensors

Luminescence is a very sensitive detection method which can reach sensitivities down to single molecule level.[73] It offers distinct advantages of rapid screening, simple operation, low cost, environmentally-friendly reusability, fast readouts and high sensitivity.[73] Such technologies have been extensively investigated for a range of applications, for example, detection of biomacromolecules (e.g., protein and glucose), physical signals (e.g., pH, temperature and humidity), inorganic ions (e.g., metal ions and gaseous molecules), etc.[74-76]

Research in utilizing luminescent technology for detecting PFAS has already established some foundation. For instance, luminescent sensors designed to detect PFOS/PFOA and other prevalent PFAS have been developed using quantum dot,[77-80] fluorescence dye,[81-87] functionalised gold/SiO_2 nanoparticles,[88-90] metal-organic frameworks[91-93] and optical fibres[94-96] (Table 1.5). These studies have demonstrated many reliable methods. Nevertheless, a key limitation in analytical detection arises from the mode of detection solely relying on luminescence intensity, which requires additional reference controls and testing to exclude interferences with scattering, excitation light or lumophore bleaching.[80, 85, 87,97]

Table 1.5. Summary of current studies about the development of luminescence sensor for the detection of PFAS.

Probe Material	Analytes	Analytical performance		Mechanism	Ref.
		Detected range	LOD (S/N=3)		
Quantum dots_01	PFOA	207.0 μg/L-16.6 mg/L	124.2 μg/L	Aggregation caused quenching	77
Quantum dots_02	PFOS	150.0 ng/L-80.0 μg/L	150 ng/L	Aggregation induced enhancement	78
Quantum dots_03	PFOA	4.1-29.0 mg/L	0.74 mg/L	Photoinduced electron transfer	79
Quantum dots_04	PFOA	103.54 μg/L-6.2 mg/L	10.4 mg/L	Photoinduced electron transfer	80
Fluorescence dye_01	PFOS PFOA	0-17.5 mg/L and 0-7.0 mg/L	10.7 μg/L and 10.9 μg/L	Photoinduced electron transfer	81
Fluorescence dye_02	PFOS	0-1.0 mg/L	75.0 μg/L	Photoinduced electron transfer	82
Fluorescence dye_03	PFOS PFOA	20.0 μg/L-5.0 mg/L	6.4 mg/L and 4.7 mg/L	Photoinduced electron transfer	83
Fluorescence dye_04	PFOA, PFOS and PFHxS	-	-	-	84
Fluorescence dye_05	PFAS	-	10 μg/L	-	85
Fluorescence dye_06	PFOS	20.0 μg/L -4.0 mg/L	2.1 μg/L	Photoinduced electron transfer	86

Functionalised SiO_2 nanoparticles_01	PFOS	5.57-48.54 μg/L	5.57 μg/L	Photoinduced electron transfer	87
Functionalised gold nanoparticles_01	10 PFAS	0.01 mg/L to 10 mg/L	10 μg/L	Aggregation caused quenching	88
Functionalised gold nanoparticles_02	PFOA	>103.5 mg/L	-	Aggregation caused quenching	89
Metal-organic frameworks_01	PFOS	90.0 pg/L-9.0 ng/L	75.0 pg/L	Photoinduced electron transfer	91
Metal-organic frameworks_02	PFOA	<200 uM (82.8 mg/L)	19 μg/L	Photoinduced electron transfer	92
Metal-organic frameworks_03	PFHxA	PFHxA: -	-	Photoinduced electron transfer	93
	PFHpA	PFHpA: 0.1-2 mg/L	0.044 mg/L		
	PFOA	PFOA: 0.1-10 mg/L	0.046 mg/L		
	PFNA	PFNA: 0.1-2 mg/L	0.047 mg/L		
	PFDA	PFDA: 0.1-1 mg/L	0.045 mg/L		
	PFOS	PFOS: 0.1-1 mg/L	0.037 mg/L		
Metal-organic frameworks_04	PFOA PFOS PFNA	-	40 nM	Photoinduced electron transfer	90

	PFHpA				
	PFHxA				
	PFHxS				
	PFDA				
Optical fibre_01	PFOA	4.8 mg/L-60 mg/L	5 mg/L	Refractive index alteration	94
Optical fibre_02	PFOS and PFOA	0-100 ng/mL	0.21 ng/mL	Refractive index alteration	95
Optical fibre_03	PFOA	0-200 ng/mL	0.5 ng/mL	Refractive index alteration	96

1.3 Strategies of PFAS-luminescence sensor development

1.3.1 Photo-induced electron transfer in the design of sensor systems

Photo-induced electron transfer (PET) is predominantly used in design of luminescence turn-on/off system for the detection of PFAS. As depicted in Figure 1.4a, the luminescence 'turn-on/off' probe is mainly composed of chromophore, spacer and receptor.[98] The spacer is the bridge to connect the chromophore and the receptor, while the receptor normally loads with many recognition sites that able to capture the target molecules. With respect to the luminescence turn-off sensor (Figure 1.4b), for instance, the excited electrons of the anthracene are promoted to the lowest unoccupied molecular orbital (LUMO) when it absorbed the outer photons[99]. In alkaline environments, the electron from the lone pair of -NR transfers to the HOMO, blocking the electron return from the LUMO and preventing luminescence. Upon protonation (mid pH), the energy of the -NR receptor drops and no longer transfer electrons to HOMO, resulting in the luminescence revived.

In terms of luminescence turn-on sensing system (Figure 1.4a right), which is similar to the 'turn-off' sensing system but the target recognition group also plays the role of quencher.[100] In the conventional operation mode shown in Figure 1.4c, the diphenylphosphine moiety (receptor) donates electrons to carbon dots (chromophore), saturating their HOMO. This prevents the carbon dots from accepting electrons from their LUMO, leading to luminescence quenching.[101] In the presence of H_2O_2 (strong oxidant), the diphenylphosphine moiety likely donate electrons to H_2O_2 and form R-P=O. As a results, the electrons at the carbon dots' LUMO can return to the HOMO, and generate luminescence.

With respect to the detection of PFAS based on PET, the hydrophilic side (e.g. $-COO^-$ and $-SO_3^-$) of the PFAS can donor its electron to the chromophore or the receptor, causing the alteration in luminescence signal.

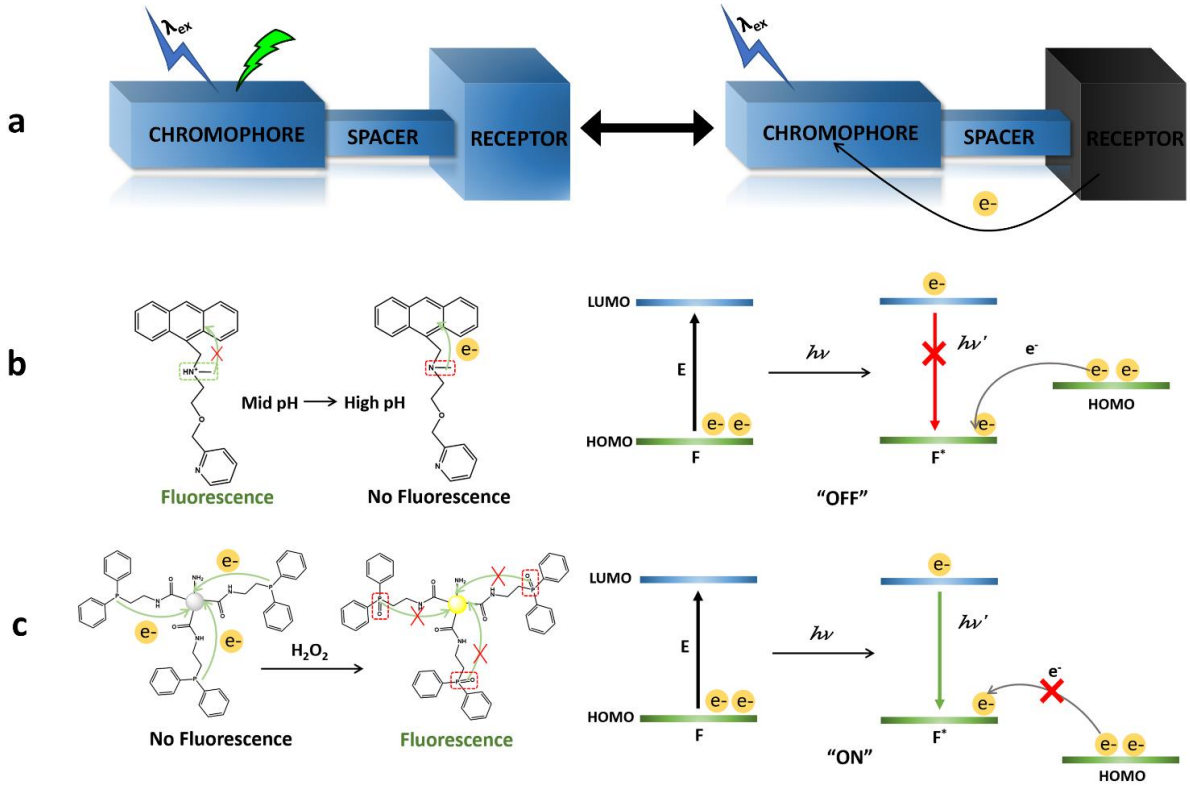

Figure 1.4. (a) Schematic diagram of luminescence 'turn-off/on' sensing system based on PET mechanism. (b) Schematic diagram of an example of turn-off sensing - anthracene-based chromophore for the detection of pH. (c) Schematic diagram of an example of turn-on sensing - the carbon dot modified with diphenylphosphine moiety for the detection of H_2O_2.

1.3.2 Aggregation-caused quenching in the design of sensor systems

Aggregation-caused quenching (ACQ) refers to a phenomenon observed in luminescent probes, typically those containing disc-shaped aromatic groups such as pyrene. When their concentrations reach a certain level, these probes tend to aggregate, leading to a decrease in luminescence intensity.[102] As shown in Figure 1.5a, excited or ground state pyrene molecules stack together via strong π-π interactions, forming 'sandwich-shaped' excimers and exciplexes. This aggregation of excited pyrene molecules results in the loss of energy through non-radiative pathways, thereby reducing luminescence intensity. However, in practical applications, the ACQ effect often hinders the utilization of luminescent probes. Specifically, when the probe concentration is high, luminescence is significantly diminished, and while

at low concentrations, luminescence intensity can be weakened.[103] Despite some attempts have been carried out to mitigate this phenomenon, progress has been limited. For example, increasing the diameter of quantum dots can help inhibit luminescence quenching caused by probe aggregation and Förster resonance energy transfer (FRET).[104] However, the preparation of quantum dots is complex and may cause adverse environmental consequences.[105] Another approach to addressing the ACQ effect is through solid-state luminescence, which successfully avoids aggregation. However, solid-state luminescent materials may exhibit more severe scattering than their liquid-state counterparts, posing additional challenges.[106]

1.3.3 Aggregation-induced emission in the design of sensor systems

In contrast to the ACQ effect, the aggregation-induced emission (AIE) effect presents a reverse phenomenon where luminescent materials exhibit enhanced light emission when aggregated. Tang et al. initially observed this phenomenon in the light-emitting material 1,1,2,3,4,5-Hexaphenyl-1H-silole, which appears dark when dispersed but shows robust emission when aggregated.[107, 108] As illustrated in Figure 1.5b, this specific phenomenon can be attributed to the restriction of intramolecular rotation (RIR).[109] Compounds susceptible to RIR typically feature multiple aromatic substituents connected to a core molecule via a conjugated system through a rotatable bond.[110] In a dispersed state, the self-rotation of aromatic substituents consumes the excited-state energy through non-radiative pathways, leading to decreased or eliminated luminescence. However, in aggregation, molecular self-rotation encounters significant obstacles due to limited space. With the non-radiative pathway blocked, excited photons can only return to the ground state via radiative decay, resulting in considerably enhanced luminescence.[111] Many PFAS have exceptional hydrophobicity and lipophobicity, which has the potential to manipulate the distance between molecules. This alteration is required by the ACQ effect and AIE effect.

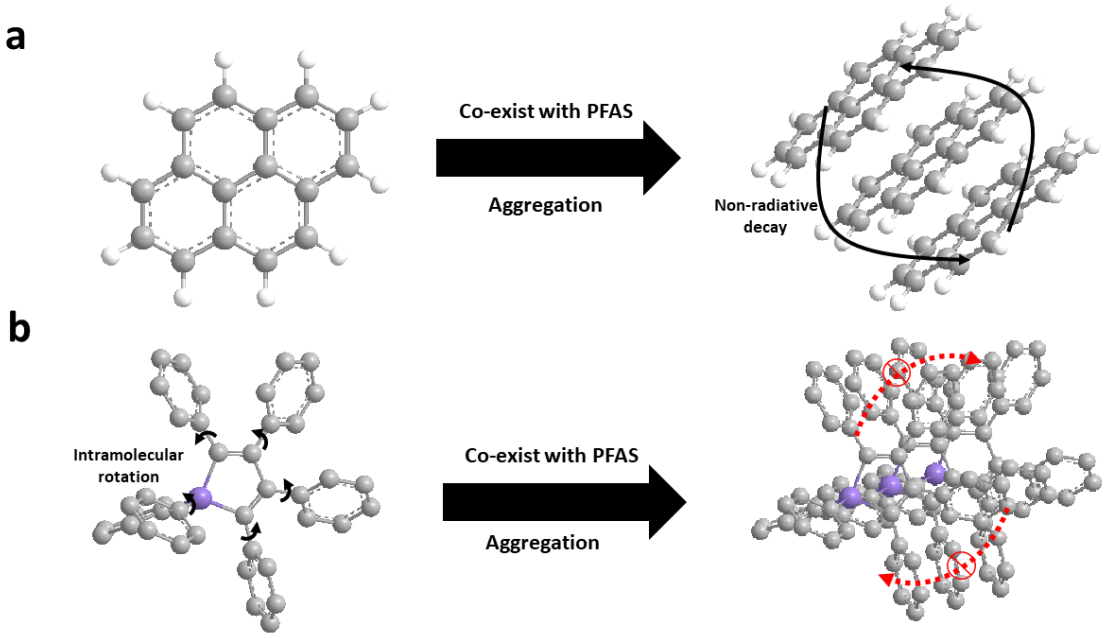

Figure 1.5. (a) Schematic diagram of pyrene ACQ effect. (b) Schematic diagram of 1,1,2,3,4,5-Hexaphenyl-1H-silole AIE effect.

1.3.4 Others approaches in the design of sensor system

There are also many other approaches has been proposed to develop a luminescence sensor for the detection of PFAS. Each method possesses its unique characteristics, and therefore, we provide only brief descriptions here. Generally, many sensors operate indirectly, meaning they cannot directly detect PFAS but instead detect substances that are significantly influenced by PFAS. For example, the refractive index of light links to the thickness of modified optical fibres, and PFAS can alter the thickness of certain modified materials, such as polyvinylidene fluoride (PVDF).[94] Alongside this, PFAS can affect biomolecules - studies have shown that PFAS can modify the permeability of cell membranes, intracellular pH levels, and cause DNA damage.[112-114] These responses offer a feasible means to link PFAS to specific molecules for detection. For instance, PFAS can easily bind to peroxisomal proliferator-activated receptor-alpha-retinoid X receptors (PPARα-RXRs) complexes in a certain proportion, while the PPARα-RXRs complexes is detectable by quantum dots.[115]

1.4 Possible interactions occur to PFAS

1.4.1 Electrostatic interaction

Electrostatic interaction is a fundamental physical phenomenon involving the attraction and repulsion between charged objects.[129] This force arises from the interaction between electric charges, where positive charges attract negative charges, and the same charges repel each other. According to Coulomb's law,[130] the magnitude of this interaction force is inversely proportional to the square of the distance between the charges and directly proportional to the product of their charges. As the distance between two charged objects decreases, the interaction force between them increases; conversely, the force decreases as the distance increases. Electrostatic interactions (ranging from 1.2 to 48 kJ/mol)[131] are commonly observed in the adsorption process of PFAS. For instance, the polymeric weak anion exchange SPE cartridge is frequently used in the extraction of PFAS from water sample.[123] In aqueous environments, PFAS predominantly exist in the form of anionic ion, attributed to their low acid dissociation constant (pKa) as depicted in Table 1.1. Consequently, these anionic PFAS species tend to associate with sensing components possessing a positive charge.

1.4.2 Hydrogen bonding interaction

The recognition of the perfluorinated compounds also relies on non-covalent bonding.

Several types of hydrogen bonding related to PFAS have been reported so far.[116] As shown in Figure 1.6a, the hydrogen bonding interaction occurs between the terminal groups of PFAS, such as sulfonyl group (-SO_3H) and carboxyl group (-COOH), and the chemicals processing hydrogen bond donor (X-Y) or acceptor (Y). These interactions exhibit bonding energies ranging from 0.2 to 40 kcal/mol.[117] For instance, O=C-OH···O=C-OH provides 7.4 kcal/mol of energy, falling within the range of moderate hydrogen bonds (4-15 kcal/mol).[116, 118] It is noted that sulfonyl and carboxyl not only act as the hydrogen bond donor (-OH, X-Y), whereas form the hydrogen bond with the nucleus exhibiting large electronegativity and short radius, but also serve as the hydrogen bond acceptor (=O, Y), providing the

hydrogen bonding site.

Another non-covalent bond pattern that is easily overlooked but is actually prevalent in PFAS, is the interaction between organic fluorine (C-F) as the hydrogen bond acceptor and the other hydrogen bond donor (H-X).[119] The ability of halogen atoms to act as hydrogen bond acceptors was discovered and calculated as early as the 1920s.[120, 121] In most cases, the distance of the C-H···F-R hydrogen bond at around 2.5 Å with an angle of near 130°, although the distance can be as low as 2.02 Å when the angle approaches 180° under ideal conditions.[119] The approaches to forming H···F hydrogen bond are diverse and exhibit different performances (Figure 1.6b). For instance, in scenario (I), the bond energy, distance and angle of C-H···F-C are 0.43 kcal/mol, 2.53 Å and 180°, respectively. In scenario (II), that of H_3C-F···H-F are 5.65 kcal/mol, 1.761 Å and 169.7°, respectively. In scenario (III), that of H_2C=CHF···H-F are 3.89 kcal/mol, 1.845 Å and 173.1°, respectively. In scenario (IV), that of HC≡CF···H-F are 0.82 kcal/mol, 2.107 Å and 173.7°, respectively, and in scenario (V), that of H_3CF···OH_2 are1.4 kcal/mol and 2.51 Å, respectively.[122-124] The bond energy and length directly decide the interaction between the bonding substances. Studies have reported that the number of fluorine substituents influences the performance of the hydrogen bond, with an increase in the number of fluorine substituents resulting in larger or lower hydrogen bond energies.[125] For example, Alkorta et al. found that the H_3CH···OH_2 interaction energy increases by approximately 1 kcal/mol with each additional fluorine atom (from H_3CH to F_3CH), and their distance shorten around 0.1 Å for each additional fluorine atom, from 2.78 Å (H_3CH···OH_2) to 2.28 Å (F_3CH···OH_2).[126]

1.4.3 Fluorine-fluorine interaction

Fluorine-fluorine interactions have provided numerous innovative insights for PFAS recognition and capture, leading to the development of a series of noteworthy techniques for PFAS detection. The existence of C-F···F-C interactions was confirmed by Robert et al. in 2011 (Figure 1.6c) based on Atoms-in-Molecules study, and their precise energies of 1-4 kcal/mol were calculated through computational chemistry investigations.[127] The magnitude of interaction between PFAS ranges from 0.26 to 29.64 kcal/mol, depending on the length of the C-F chains and the type of interaction.[127] It is

undeniable that this level of energy is strong enough to arise the self-assembling between fluorinated compounds. Additionally, Karnoukhova et al. found that the energy of C-F···F-C interactions predominately depend on the distance between the fluorine atoms and irrespective of the directionality of C-F···F.[128] Interestingly, it is noted that this theory is different from that of hydrogen bonding mentioned above. According to their calculation, the most optimal distance between fluorene atoms is 2.819 Å (equal to 1.5 kcal/mol), while the secondary distance is 2.900 Å (equal to 0.5 and 0.5 kcal/mol).

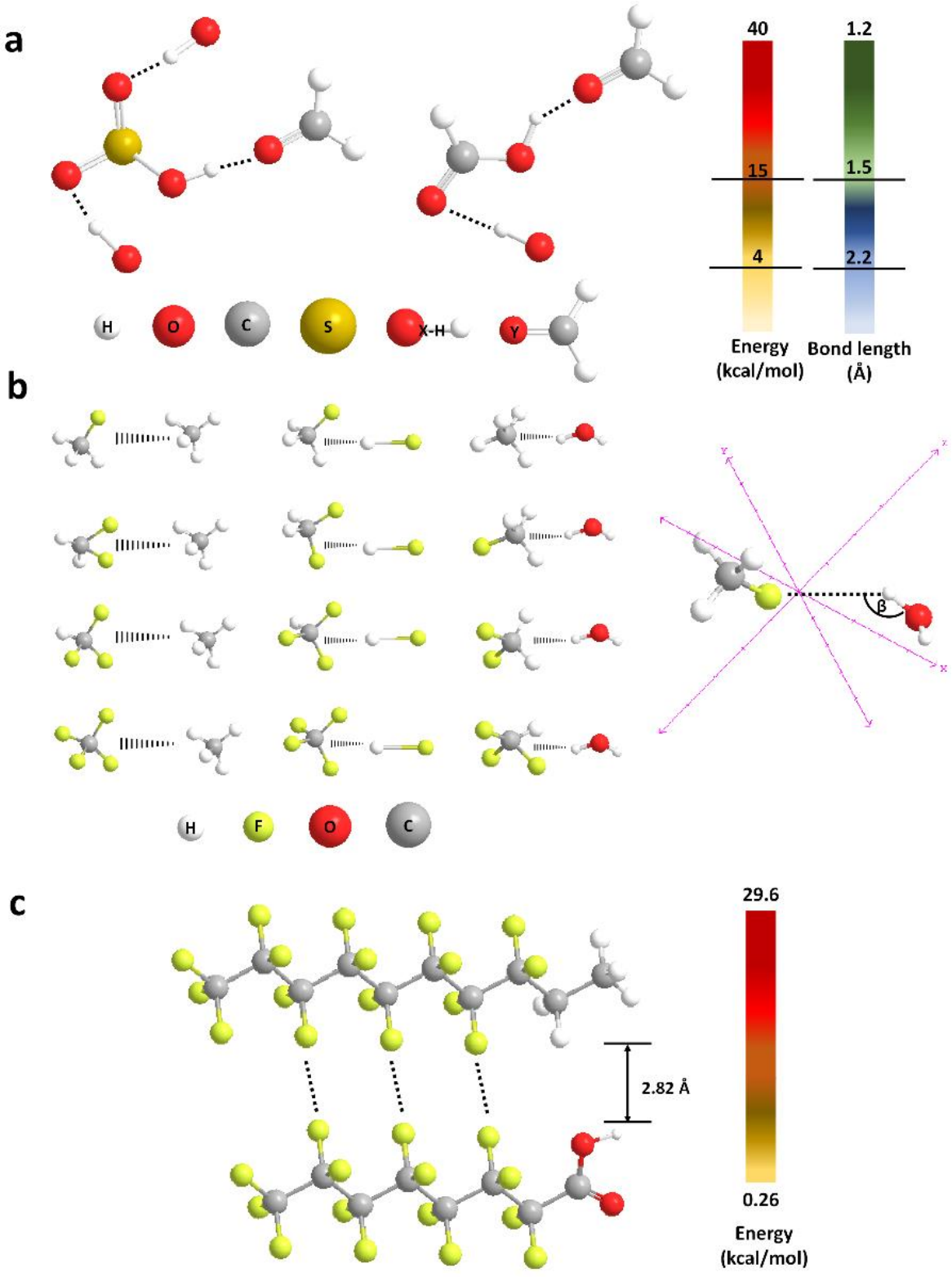

Figure 1.6. Schematic diagram of (a) -SO_3H and -COOH hydrogen bonding patterns, X-H regard as hydrogen bond donor and Y as acceptor. (b) hydrogen bonding patterns between carbon-fluorine bond and C-H, H-F, OH_2. (c) fluorine-fluorine interaction.

1.5 Luminescence lifetime as a signal for sensing

Any changes in spectroscopic characteristics, such as luminescence intensity, shift in excitation/emission wavelength and luminescence lifetime, linked with the PFAS concentration are theoretically usable as signal for PFAS detection.[98] Current studies (Table 1.5) primarily focus on luminescence intensity as it is sensitive, can be easily collected and read-out due to the updated photosensitive components as well as capable of offering visual detection process.[132] Nevertheless, light-emitting intensity usually associated with poor photostability because of the luminophores leaching or bleaching, as well as scattering or absorbance of the excitation light.[97] Moreover, the accuracy will be easily influenced by probe concentration and interferents.

Luminescence lifetime offers several advantages for sensing applications, including long-term stability, environmental sensitivity, less susceptible to photobleaching, reduced interference and versatility,[133, 134] which is demanded in real-world application. The use of luminescence lifetime for sensing has been proposed years ago.[98] Currently, the implementation of luminescence lifetime concentrates on the monitoring of pH, oxide, and temperature,[135-137] cell image[138] as well as background interference elimination (time-delay),[139] yet has not been applied to the determination of emerging contaminants like PFAS. Luminescence lifetime as sensing signal is feasible for PFAS detection, due to the lifetime of the luminophore is susceptible to its surrounding environment (e.g. polarity and viscosity).[140] Most PFAS act as fluorinated surfactants with hydrophobicity and lipophobicity, effectively altering the nature of the solution. For instance, our group previously found that the fluorinated surfactants can affect the lifetime of the transition metal complexes - the lifetime of Ir(III) complex change from 130 ns to 64 ns, 245 ns and 462 ns, respectively, with the addition of Zonyl 7950, Zonyl FSA and Zonyl FS-300.[141] Additionally, it also found that the lifetime of Ru(III)-functionalised gold nanoparticle increase in the presence of Zonyl 7950, due to the fluorinated surfactants can prevent the aggregation of gold nanoparticles.[142]

Utilising luminescence lifetime as the sensing signal provides an alternatively and attractive mode of PFAS detection, which is worth attempting.

1.6 Functionalised sensing platform formation

1.6.1 Function of solid interfaces

Immobilisation of sensing components at solid interface is a way to optimize their physical and chemical properties such as number, orientation and even the accessibility, allowing for the development of a wide range of advanced devices and functional materials.[143] Currently, techniques such as self-assembly,[144] microcontact printing,[145] spin coating,[146] Langmuir-Blodgett film formation[147] and laser ablation[148] can be employed to form thin films on surfaces. In this thesis, self-assembly is mainly employed. This method involves immersing a prepared gold, copper, or glass substrate into a solution of an alkanethiol for a specific period, followed by washing and drying under nitrogen. As a results, the coated molecules are well-arranged on gold surface in comparison with when they are in solution, which greatly reduce molecular aggregation and avoid quenching.[149] Our group previous study has shown that the surface modified with transition-metal complex exhibit enhanced luminescence lifetime in comparison with when it is in solutions (Figure 1.7).[150] Additionally, immobilising the luminophore on a solid-state surface makes it easier to store, transport, and use, potentially making it suitable for in-situ monitoring of contaminants.

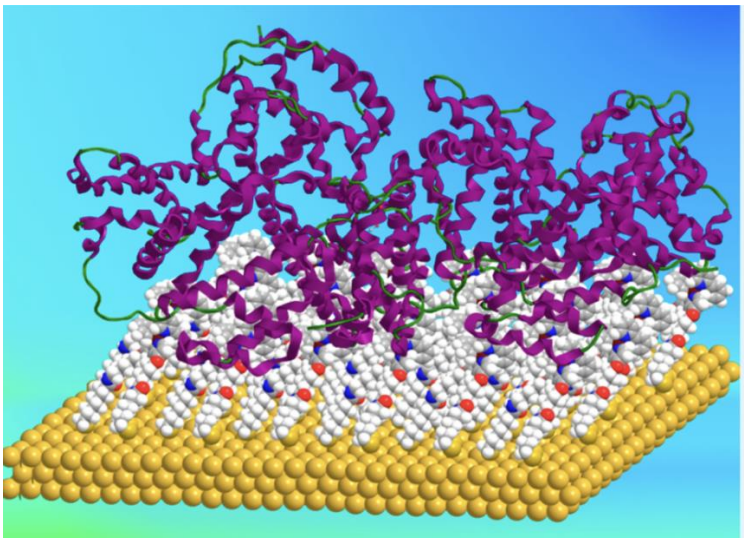

Figure 1.7. Luminescence gold surface modified with transition metal probes for sensing and imaging. Adapted from reference 150.

1.6.2 Choice of suitable luminophore

A luminescence lifetime-based sensing platform requires probes with long-lived lifetimes to reduce the difficulty in numerical read-out and to eliminate environmental background caused by autofluorescence and short-lived interferents.[98] Traditional fluorescent dyes often have small Stokes shifts, short luminescence lifetimes and low photostability, which are unsuitable in this context.

Transition metal complexes, such as iridium(III) complexes, exhibit well-studied photophysical properties. Iridium-based luminescent probes have long-lived luminescence, typically in hundreds of nanoseconds range, with signals in the visible range of the spectrum, with demonstrated sensitivity to the analytes and has reasonable quantum yield.[151, 152] Due to these attractive properties, they have been particularly employed in sensing application such as cell studies,[151] detection of saccharide[152] and protein.[150]

Trivalent lanthanide (Ln^{3+}) such as europium(III), neodymium(III) and ytterbium(III), displays sharp line band emission profiles due to f-f transitions that are caused by the highly shielded character of the f orbitals.[153] Moreover, owing to their metal-centred luminescence, the Stokes shift of Ln(III) is usually large (> 100 nm).[153] As a result, the excitation wavelength can be cleanly separated from the emission wavelength, providing a well signal-to-noise ratio for all measurements. Coordinating to the appropriated ligand, such as SAcbisDBM ligand, the luminescence lifetime of surface-active luminescent lanthanide(III) can extend well into millisecond (ms) timescale. This property makes them ideal probes for the detection of PFAS.

1.7 Thesis outline

Given environmental and human health concerns about PFAS, there is an increasing need for a proper technique that can measure these contaminants accurately, rapidly, and inexpensively on a wide scale. While current chromatographic-mass spectrometric methods are accurate, they are also time-consuming and expensive, and thus are unsuited to meeting the vast future demand for PFAS monitoring in matrices such as drinking water, waste effluents, and waste consumer products. This thesis aims to develop and evaluate three luminescence sensors for the accurate and rapid detection of one or more PFAS in different environmental matrices.

Chapter two summarises the methodology employed in developing these sensors.

Chapter three describes the preparation of an Ir(III)-functionalised surface based on lipophilic iridium complexes bearing alkyl chains (namely, IrC_6 and IrC_{12}) and Zonly-FSA surfactant. The morphology, elemental composition, Raman spectra, contact angle and optical properties of the Ir(III)-functionalised surfaces are characterised. Furthermore, the analytical performance of the Ir(III)-functionalised surface toward PFOA was examined, and the sensing mechanism is discussed. Finally, the Ir(III)-functionalised surface is used to detect PFOA in drinking water samples.

Chapter four outlines the development of a solid-state sensing platform based on Europium(III), SAcbisDBM ligand and plain gold surface. The characterization of the surface's morphology, elemental composition and variation upon the addition of C_4-C_{10} PFCA, amount of coordinated Eu(III) on the surface, and Raman spectrum are discussed. The pH optimisation of the sensor is also addressed. Additionally, the sensing mechanism is discussed, along with the sensitivity, anti-interference ability and reusability of the sensor. Finally, the Eu(III)-functionalised surface is applied to detect the C_4-C_{10} PFCA in waste leather, leatherette and textile samples.

Chapter five reports the development of a near-infrared (NIR) luminescence sensor based on Neodymium(III) and Yttrium(III), SAcbisDBM ligand and plasmonic gold surface (pAu). The morphology, Raman spectrum and optical properties of the surfaces are discussed. Subsequently, possible factors that may alter the emission intensity and lifetime of the functionalised surface are

explored. Finally, the analytical performance of Nd(III)/Yb(III)-SAcbisDBM in solution or immobilised on plasmonic surface toward PFOA, PFNA and PFDA are tested, respectively.

Finally, in chapter six, a comprehensive conclusion is presented, summarizing the key findings and contributions made throughout the research. Additionally, we humbly propose possible avenues for future development of such sensors. These proposals may include further optimization of sensor design and performance, exploration of new sensing materials or ligands, enhancement of sensitivity and selectivity, and validation of sensor performance in real-world scenarios.

Chapter 2: General Methods

2.1 Materials

Gold slides (30 nm on silicon with 5 nm Ti priming layer) were purchased from Georg Albert PVD, Germany. Plasmonic gold slides were purchased from Nirmidas Biotech, USA. Zonyl-FSA fluorosurfactant was purchased from Sigma-Aldrich, USA. Native standards of: PFBA (98.0%), PFPeA (97.0%), PFHxA (≥98.0%), PFHpA (97%), PFOA (95%), PFNA (97%) and PFDA (98.0%) used for evaluating performance of the prepared sensors were purchased from Sigma-Aldrich, USA. The PFBA, PFPeA, PFHxA, PFHpA, PFOA, PFNA and PFDA native reference standard (1.2 mL, 50 µg/mL in methanol), the ^{13}C-PFBA, $^{13}C_3$-PFPeA, ^{13}C-PFHxA, $^{13}C_4$-PFHpA, $^{13}C_8$-PFOA, ^{13}C-PFNA and $^{13}C_6$-PFDA internal (surrogate) standard (1.2 mL, 50 µg/mL in methanol), and the $^{13}C_4$-PFOS and $^{13}C_4$-PFOA recovery determination (syringe) standard (1.2 mL, 50 µg/mL in methanol) used for LC-MS analyses were purchased from Wellington Laboratories, Canada. Europium(III) chloride hexahydrate ($EuCl_3$•$6H_2O$, 99.9%), Neodymium(III) chloride hexahydrate ($NdCl_3$•$6H_2O$, 99.9%) and Ytterbium(III) chloride hexahydrate ($YbCl_3$•$6H_2O$, 99.9%) were purchased from Sigma-Aldrich, USA. The rest of the chemical agents and solvents used in this study were obtained from Sigma-Aldrich, Fluka, Fisher Scientific or Acros Chemicals and used without further purification.

2.2 Techniques

2.2.1 Liquid chromatography coupled with quadrupole time-of-flight mass spectrometry

Liquid chromatography-mass spectrometry (LC-MS) is a powerful analytical technique that combines the physical separation capabilities of liquid chromatography with the mass analysis capabilities of mass spectrometry. LC-MS is widely used in many fields such as environmental analysis, pharmaceuticals, and biochemistry due to its high sensitivity, specificity, and the ability to analyse complex mixtures. Herein, LC-MS was chosen because it is a gold standard method to detect and quantify PFAS,[60] which

is critical for validating the feasibility and accuracy of the sensor we designed.

In this study, the liquid chromatography coupled with quadrupole time-of-flight mass spectrometry (LC-Q-TOF-MS) determination of various PFAS in samples was conducted using a Sciex Exion HPLC coupled to a Sciex 5600+ triple TOF MS, equipped with a Restek Raptor C18 column (1.8 μm particle size, 50 mm length, 2.1 mm internal diameter). The liquid chromatography elution program and MS/MS transitions employed are detailed in the corresponding chapter.

2.2.2 Solid-Phase Extraction

Solid-phase extraction (SPE) is a sample preparation process used to extract and concentrate analytes from liquid samples, improving the detection sensitivity and selectivity of the analytical method.[154] SPE is widely used in environmental analysis, pharmaceuticals, and food safety due to its effectiveness in isolating target compounds from complex matrices.

In this study, the extraction of PFBA, PFPeA, PFHxA, PFHpA, PFOA, PFNA, and PFDA from samples was performed using Phenomenex Strata TM-X-AW 33 μm polymeric weak anion 200 mg/6 mL SPE cartridges. The SPE process involves passing the sample through a cartridge containing a solid adsorbent material, which selectively retains the analytes of interest while allowing other components to be washed away. The retained analytes are then eluted using a suitable solvent for further analysis. Specific SPE procedures are detailed in the corresponding chapter.

The use of SPE in this study is crucial for several reasons. Firstly, it concentrates the PFAS from large volumes of environmental samples, enhancing the sensitivity of the subsequent LC-MS analysis. Secondly, SPE helps to remove potential interferences from the sample matrix, which could otherwise affect the accuracy and reliability of the analytical results. By employing SPE, we ensure that the PFAS are effectively isolated and concentrated, leading to more precise and accurate quantification. This step is essential to validate the performance of the sensor we designed, as it allows for a clear comparison between the sensor's readings and the known concentrations of PFAS obtained through a reliable extraction and analysis method.

2.2.3 Steady-state and Time-resolved Spectroscopy

Steady state and time resolved luminescence studies were conducted on an Edinburgh Instruments FLS 920 and FLS980 spectrophotometer fitted with a 450 W Xenon arc lamp as excitation source and a Hamamatsu R928 photomultiplier tube as detection system. The emission monochromator was equipped with gratings at 395 nm, 435 nm, and 575 nm. The data was collected with F980 software and corrected for photomultiplier tube and instrument responses. Liquid-state probes were accommodated in 1 cm path length quartz cuvettes.

Luminescence Lifetime (τ) spectra were obtained with an EPL-375 laser or 100 W flashlamp (90 - 260 V, 50/60 Hz) as excitation source. Lifetimes were fitted with Edinburgh Instruments FAST software. Luminescence lifetimes were fitted to two components or three components (if necessary), with an estimated error of 10% and chi-squared (χ^2) within 1 ± 0.2.

Time-Correlated Single Photon Counting (TCSPC) is a highly sensitive technique used to measure the fluorescence lifetimes of samples. It involves detecting single photons emitted by the sample after excitation by a short light pulse and measuring the time interval between the excitation and emission events. This method provides a histogram of photon arrival times, which is then used to determine the decay kinetics of the sample.

The basic principle of TCSPC can be described by the following steps: (1) A short pulse of light (typically from a laser) excites the sample. (2) The sample emits photons as it returns to the ground state. (3) A single photon is detected by a photomultiplier tube (PMT) or a single-photon avalanche diode (SPAD). (4) The time between the excitation pulse and the detection of the photon is recorded. (5) This process is repeated many times to build up a histogram of photon arrival times.

The fluorescence decay curve I(t)) obtained from TCSPC can be described by an exponential function:

$$I(t) = I_0 \exp\left(-\frac{t}{\tau}\right)$$

where: I(t) is the intensity at time t, I_0 is the initial intensity and τ is the fluorescence lifetime.

The fluorescence lifetime τ is determined by fitting the decay curve with the exponential model. In cases where multiple decay processes are present, a multi-exponential model may be used:

$$I(t) = \sum_i I_{0i} \exp(-\frac{t}{\tau})$$

where τ are the lifetimes of different decay components and I_{0i} are their respective initial intensities.

By using TCSPC, we can accurately measure the fluorescence lifetimes of our luminescent materials, which is critical for optimizing the performance of the sensors and ensuring their reliability in detecting PFAS.

2.2.4 UV/Vis absorption spectroscopy

The UV/Vis spectrophotometer plays a crucial role in our research by allowing us to determine the absorbance of the samples at specific wavelengths. This information helps in identifying and characterizing the electronic transitions of the compounds, providing insights into their structural and electronic properties.

In this study, UV/Vis spectra were conducted using a Cary 60 UV-Vis spectrophotometer. The spectra were recorded at a scan rate of 600 nm min^{-1} with a 1 cm path length quartz cuvette at room temperature. Baseline correction was performed by utilizing a matching solvent as a reference to the analysed sample.

2.2.5 Dynamic Light Scattering and Zeta Potentials

Dynamic light scattering (DLS) is a technique used to determine the size distribution of small particles in suspension or polymers in solution. By analysing the scattering of light caused by the Brownian motion of particles, DLS provides information about the hydrodynamic diameter and size distribution of the particles. Zeta potential measurements, on the other hand, are used to assess the surface charge of particles, which is crucial for understanding their stability and interactions in suspension.

DLS and zeta potential measurements were conducted using a Malvern Zetasizer nano ZSP. Samples were assessed with a 1 cm DTS0012 disposable cuvette for size analysis and a folded capillary cell for zeta potential measurements. The instrument was left to equilibrate at 25 °C for 180 seconds before recording measurements.

For DLS samples, three measurements were taken, each comprising 15 runs, and the average was then

presented. Zeta potential samples underwent 10 runs with values ranging between 10 and 100, and the average was presented accordingly. Data were recorded and processed using the Malvern Zetasizer software. The polydispersity index is calculated from the equation below, where the standard deviation (σ) of the particle diameter is divided by the mean particle diameter.

$$PDI = \left(\frac{\sigma}{2a}\right)^2$$

2.2.6 Scanning Electron Microscopy - Energy-dispersive X-ray spectroscopy

The morphology of the functionalised surfaces were analysed by two systems of Scanning Electron Microscopy (SEM): i) at University of Birmingham a CFEI Quanta 3D FEG FIB-SEM fitted with an Oxford Inca 300 Energy Dispersive X-ray Spectrometer (EDS) and ii) at BAM a Zeiss Supra 40 SEM with a Schottky field emitter having attached a Thermo Fisher Scientific EDS (Waltham, MA, USA). The gold sputtering was carried out by Emscope SC 500 Au-Pd Sputter Coater.

The sample preparation for SEM is as follows: firstly, the functionalised surface prepared is affixed onto a 3 cm × 3 cm round copper sample holder using specialised conductive adhesive. Subsequently, silver conductive adhesive is applied around the edges of the surface, and finally, gold sputtering can be employed to further enhance the sample's conductivity.

2.2.7 Time-of-Flight Secondary Ion Mass Spectrometry

Time-of-Flight Secondary Ion Mass Spectrometry (TOF-SIMS) is a powerful surface analysis technique used to determine the composition and distribution of elements and molecules on the surface of materials. TOF-SIMS operates by bombarding the sample surface with a focused primary ion beam, which causes the ejection (or sputtering) of secondary ions from the surface. These secondary ions are then analysed based on their mass-to-charge ratio (m/z) using a time-of-flight mass analyzer. The resulting mass spectrum provides detailed information about the surface chemistry, including the presence of specific elements, isotopes, and molecular fragments. TOF-SIMS is widely used in various fields, including material science, semiconductor industry, pharmaceuticals and environmental science.

In this study, TOF-SIMS was employed to observe changes in the surface composition of fluorinated compounds on the sensor materials. By using TOF-SIMS, we can precisely measure the amount and distribution of fluorinated species on the sensor surface, which is crucial for understanding the sensor's performance and its interaction with PFAS.

The semi-quantitative determination of surface chemical composition was carried out using a TOF-SIMS IV instrument (IONTOF, Münster, Germany). The prepared surface can be detected without further treatment.

2.2.8 X-ray photoelectron spectroscopy

X-ray Photoelectron Spectroscopy (XPS) is a widely used surface analysis technique that provides quantitative and chemical state information about the elements present on the surface of a material. XPS operates by irradiating a material with X-rays, which causes the emission of photoelectrons from the surface. The kinetic energy of these photoelectrons is measured, and their binding energies are calculated, allowing for the identification and quantification of elements present on the surface. XPS is used in various fields for elemental composition analysis, chemical state analysis, thin film characterization and surface contamination detection.

In this study, XPS was employed to observe the changes in the surface composition of various elements, particularly sulfur (S), fluorine (F), iridium (Ir), and europium (Eu). The XPS studies were conducted using a Thermo NEXSA XPS, fitted with a monochromated Al Kα X-ray source, a spherical sector analyzer, and 3 multichannel resistive plate 128 channel delay line detectors. The binding energy of the photoelectrons is calculated using the equation: $E_b = h\nu - E_k$, where Eb is the binding energy, hν is the photon energy, and E_k is the kinetic energy. The prepared surface can be detected without further treatment.

2.2.9 Raman spectrometer

Raman spectroscopy is a vibrational spectroscopic technique used to provide information about molecular vibrations, which can be used to identify molecules and study chemical bonding and molecular interactions. The technique involves irradiating a sample with a monochromatic laser light, which interacts with the molecular vibrations, phonons, or other excitations in the system. The scattered light is then analysed to provide a Raman spectrum, which contains information about the vibrational modes of the molecules.

In this study, Raman spectra were collected using Renishaw inVia™ confocal Raman microscopes. The spectra were recorded with a 532 nm diode laser employing 1800 and 1/mm gratings or a 785 nm diode laser with a 600 1/mm grating. The laser power was set at 0.1% and 1%, and the exposure time was set to 1 time/s.

2.2.10 NMR and Mass Spectrometry

Nuclear Magnetic Resonance (NMR) and Mass Spectrometry (MS) are powerful analytical techniques used for the structural elucidation and characterization of chemical compounds. NMR provides detailed information about the molecular structure and dynamics, while MS offers precise molecular weight determination and insights into the composition of the sample. By employing NMR and mass spectrometry, we aim to obtain comprehensive information about the molecular structure and composition.

^{1}H and ^{13}C NMR spectra were recorded on a Brüker AVIII300 and AVIII400 respectively. NMR spectra were processed using MestReNova. Electrospray mass spectroscopy was carried out on a Waters Micromass LCT- TOF mass spectrometer in an electrospray positive mode, using a nitrogen laser.

Chapter 3: Luminescence Lifetime-Based Sensing Platform Based on Cyclometalated Iridium (III) Complexes for the Detection of PFOA in Aqueous Samples

This chapter contains material taken verbatim from the following publication:

1. **Kun Zhang**, Andrew J. Carrod, Elena Del Giorgio, Joseph Hughes, Knut Rurack, Francesca Bennet, Vasile-Dan Hodoroaba, Stuart Harrad, and Zoe Pikramenou, Analytical Chemistry 2024, 96, (4), 1565-1575.

3.1 Introduction

3.1.1 General remarks on the significance of PFOA detection

Perfluorooctanoic acid (PFOA) possess desirable industrial characteristics such as oil and water repellency with good physical and chemical stability. They have been widely used in a range of applications: carpets, clothing, paper, and packaging to confer dirt, grease, oil resistance as well as in fire-fighting foams.[155] However, in an environmental context, the strength of the C-F bond renders PFOA highly resistant to thermal, chemical and biological degradation,[156] with the result that they are capable of bioaccumulation and long-range environmental transport, exemplified by their presence in the Arctic.[6, 157, 158] As a result, and combined with concerns about toxicity (including impaired response of children to vaccines),[159] perfluorooctanoic acid (PFOA) and related PFOA compounds are listed for elimination under the Stockholm Convention on Persistent Organic Pollutants (POPs).[54] Moreover, the EU has listed PFOA and related PFOA compounds as substances of very high concern, [52] whilst the European Food Safety Authority (EFSA) has set a challenging tolerable weekly intake value of 4.4 ng/kg body weight for the sum of PFOA, PFOS, perfluorononanoic acid and PFHxS;[55] furthermore, as part of a recast of its Drinking Water Directive, the EU has set a limit of 100 ng/L for the sum of C_4-C_{13}

perfluorosulfonic acids and PFCAs (including PFOA) in drinking water.[56] In March 2023, the United States Environmental Protection Agency (USEPA) announced proposed maximum contaminant levels (MCLs) for 6 PFAS in drinking water, with that for PFOA set at 4 ng/L.[160]

3.1.2 Challenges in developing a PFOA luminescence sensor

It is challenging to design sensor systems for PFOA based on its chemical properties.[161] Most sensor systems have relied on the interaction between organofluorines,[162, 163] which provide a recognition element for detection. Baker *et al.* estimated that the fluorine-fluorine (C-F • • • F-C) stabilization energy of up to 30 kcal/mol is adequate for perfluorinated molecules to be captured by another perfluorinated receptor.[127] Luminescence is a very sensitive detection method which can reach sensitivities down to single molecule level. Luminescent sensors for the detection of PFOA have been developed using quantum dots,[115] fluorescent organic dyes,[81, 87] gold nanoparticles[88] and metal organic frameworks.[92, 93] While the photostability of the lumophore and its fluorescence quantum yield are important considerations in the designs, a key limitation in analytical detection arises from the mode of detection solely relying on luminescence intensity,[80, 164] which requires additional referencing controls and testing to exclude interferences with scattering, excitation light or lumophore bleaching.

3.1.3 Design of Ir(III)-functionalised surface

Sensing systems based on luminescence lifetime provide an attractive mode of detection with high sensitivity and versatility.[165] Photostable luminophores with long luminescence lifetimes are ideal for using in bench-top instruments for luminescence lifetime detection and have received wide popularity in medical diagnostics as luminescence lifetime detection is available in many microplate readers.[166] Iridium-based luminescent probes have long-lived luminescence, in the range of hundreds of nanoseconds, in the visible, originating from triplet charge transfer states. The iridium luminescence is responsive to the local microenvironment around the metal complex with changes that affect the rigidity of the complex, polarity, aggregation and access of oxygen.[152, 167-170] We have previously anchored

cyclometalated iridium complexes on gold solid supports using a thiol active ligand (bpySS) which prevented quenching from gold surface and studied the influence of the luminescent signal of the iridium films in presence of proteins.[141, 150, 151] Herein, we report the development of a novel solid-state luminescence lifetime sensing platform for PFOA detection based on cyclometalated iridium complexes bearing lipophilic chains of six and twelve carbons respectively, IrC_6 and IrC_{12} (Figure 3.1).

3.1.4 Influence of PFOA on Ir(III)-functionalised surface

The hydrocarbon chains provide lipophilic tentacles on the iridium complex, ideal for inducing aggregates or organized self-assembled structures of the cationic iridium complexes. Agents such as PFOA which bear hydrophilic groups and lipophobic chains may interfere with the local iridium environment. We have examined the influence of PFOA on gold surfaces modified with two iridium complexes, **IrC_6@Au** and **IrC_{12}@Au**, by a series of surface characterization and analytical techniques. The luminescence lifetime of the iridium photoactive center is monitored in different conditions in order to optimize detection sensitivity and provide a monitoring tool for PFOA detection.

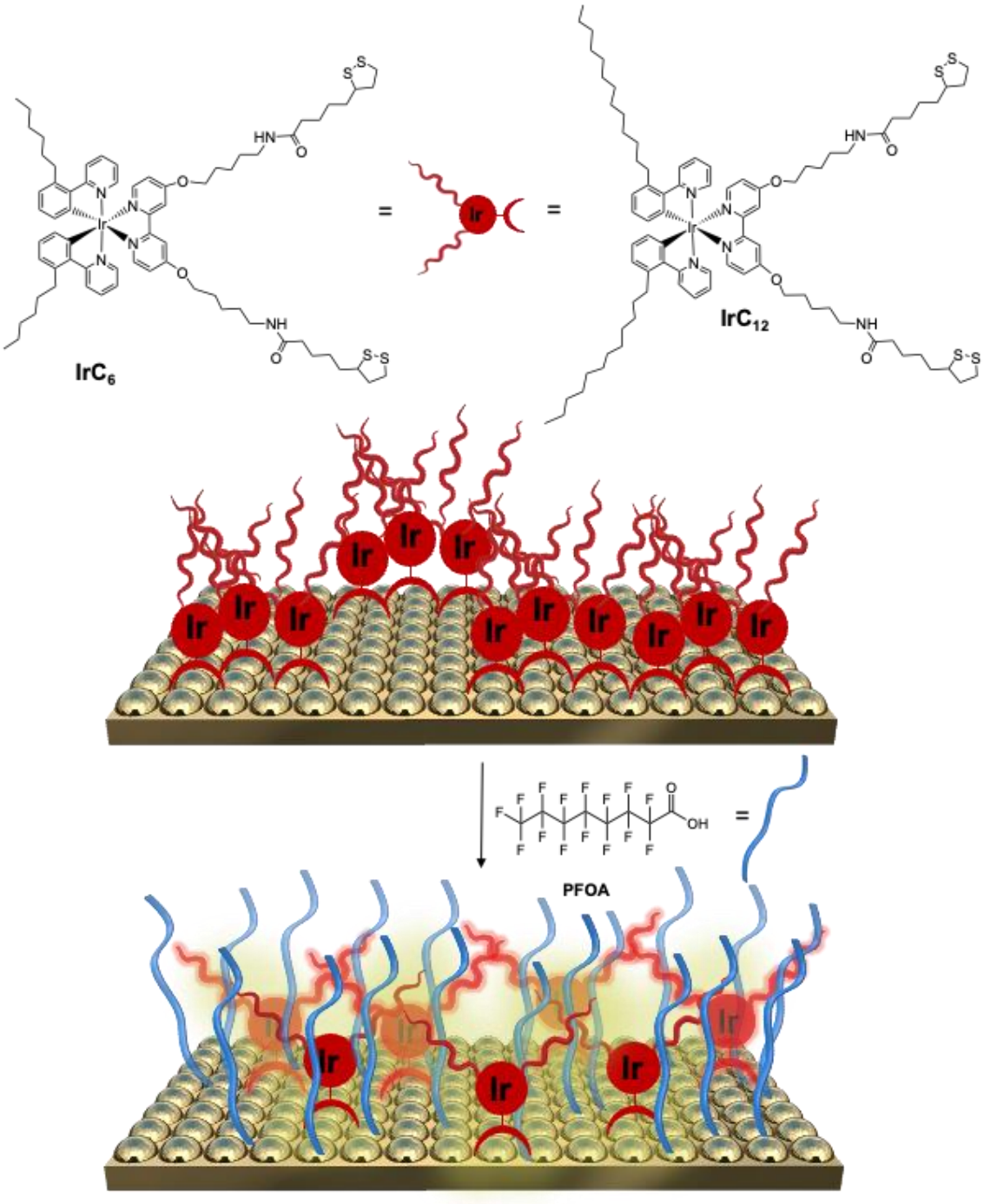

Figure 3.1. Schematic diagram of the functionalised gold surfaces, **IrC_6@Au** and **IrC_{12}@Au** upon addition of PFOA.

3.2 Experimental

3.2.1 Synthesis of IrC_6 and IrC_{12}

The complexes IrC_6 and IrC_{12} (chemical structure see below) are prepared as previously reported.[167]

IrC_6

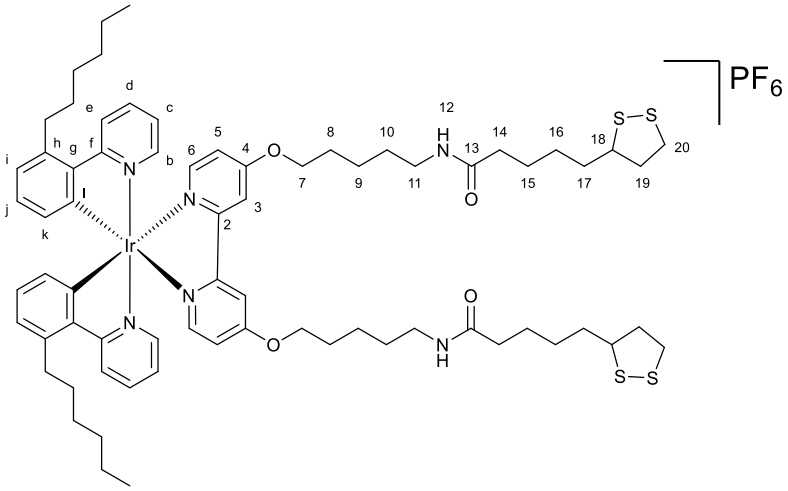

IrC_{12}

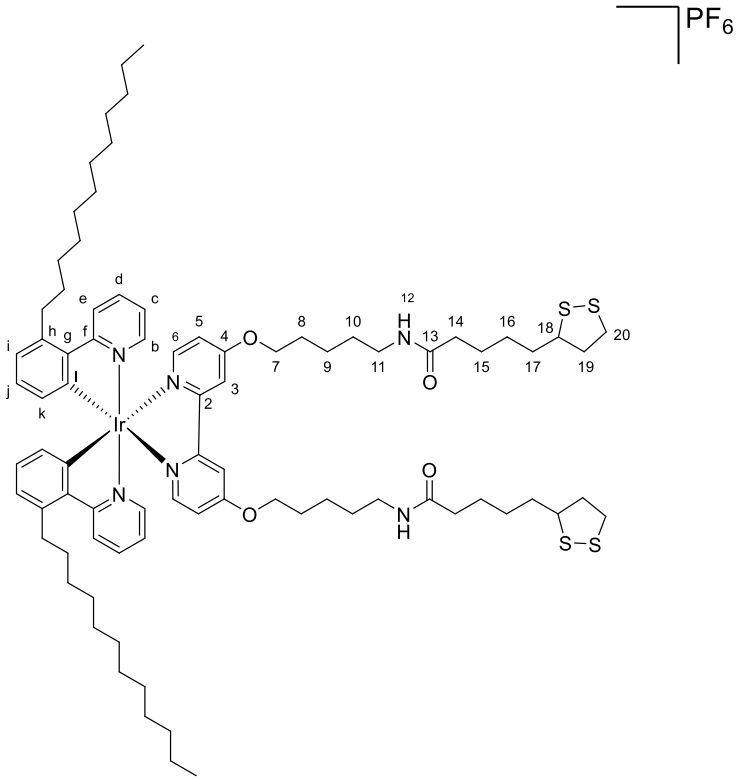

3.2.2 preparation of Ir(III)-functionalised surface

IrC_6@Au and **IrC_{12}@Au**. Gold slides were rinsed thoroughly with acetonitrile and milli-Q water sequentially for three times before immersion in 80 ℃ piranha solution (concentrated sulfuric acid and hydrogen peroxide in proportion of 3:1 (v/v)) for 15 min to eliminate all organic residues on the surface. The cleaned surfaces were subsequently washed with milli-Q water and dried with a stream of nitrogen and stored in ethanol until use. The **IrC_6@Au** and **IrC_{12}@Au** surfaces were prepared by immersing the gold slides in 0.74 μM IrC_6 acetonitrile solution or 0.62 μM IrC_{12} acetonitrile solution for 18 h. The **IrC_6-FSA@Au** and **IrC_{12}-FSA@Au** surfaces, were prepared by immersion in a 0.74 μM IrC_6 acetonitrile solution with 2% Zonyl-FSA or a 0.62 μM IrC_{12} acetonitrile solution with 2% Zonyl-FSA for 18 h, in a final solvent composition of 92% MeCN, 4% water and 4% isopropyl alcohol. All modified surfaces were washed with small amounts of acetonitrile after immersion and dried with a stream of nitrogen. The prepared surfaces were finally stored in a dark environment under nitrogen atmosphere until use.

3.2.3 Detection of PFOA

For the detection of PFOA, the IrC_6@Au and IrC_{12}@Au surfaces were immersed in phosphate-buffered solutions (pH of 7.4) with different concentrations of PFOA for 30 min incubation, and subsequently rinsed with slight amount of acetonitrile and dried with a stream of nitrogen.

3.2.4 Drinking water sample collection

Twenty-nine samples were prepared for evaluation of the sensor. These comprised: bottled water (8 still mineral waters, 6 sparkling waters, and 5 flavored water samples) purchased from supermarkets, along with tap water sampled from 10 different household kitchens in Birmingham, UK. The water samples were collected between October and November 2020. For quality control, blank samples were prepared

in the guise of distilled deionized (Milli-Q) purified laboratory reagent water collected in a PET sample bottle. Bottled water samples (different brands/water sources/types) were purchased from four different shops in Birmingham in October 2020. All samples were transferred promptly to the laboratory and stored at 4 ℃ before analysis.

The water samples were firstly analysed by LC-TOF-MS to measure the concentration of PFOA before detection by the iridium functionalied surfaces. To evaluate the performance of the prepared sensor, the same water samples were then spiked with known concentrations of PFOA within the range detectable by the sensor (herein, 10 mg/L and 100 µg/L).

3.2.5 Drinking water sample treatment

PFOA extraction was carried out using Phenomenex Strata ^{TM}-X-AW 33 µm polymeric weak anion, 200 mg/ 6 mL solid phase extraction (SPE) cartridges. To concentrate PFOA, this study adopted an approach that has previously been reported by our group.[3] Briefly, 50 µL of 1 ng/µL internal standard (M8-PFOA) dissolved in methanol was first added in the 500 mL filtered water, subsequently pass them through a 0.45 µm membrane for removing impurities. The solid-phase extraction (SPE) cartridges were conditioned with 2×6 mL of 0.1% NH_4OH/methanol and 6 mL Milli-Q water in advance before extracting the spiked water samples at around 1-2 drops per second. Once the entire sample has passed through the cartridge, rinsed the cartridge with 2×6 mL of Milli-Q water, and dried using vacuum pump for 30 min. After that, the PFOA was eluted with 6 mL of 0.1% NH_4OH/methanol. Finally, the extracts were evaporated to approximately 300 µL with nitrogen stream at 40 ℃ before passing them through the 0.2 µm syringe filter and transferred to autosampler vials, then further concentration to dryness. The autosampler vials were reconstituted with 200 µL methanol for further analysis by LC-TOF-MS. All the samples should store in 4 ℃ until used.

3.2.6 LC-MS methods for the determination of PFOA in water

LC-MS determination of concentrations of PFOA in water samples was conducted using a Sciex Exion

HPLC coupled to a Sciex 5600+ triple TOF MS equipped with a Restek Raptor C18 column (1.8 μm particle size, 50 mm length, 2.1 mm internal diameter). Firstly, 10 μL of extract was injected into the LC fitted with a Raptor C18 column (1.8 μm particle size, 50 mm length, 2.1 mm internal diameter, Restek). Details of the LC conditions employed are provided as Table S3.1.

The TOF-MS is equipped with a Turbo V source operated in negative mode using electrospray ionization (ESI) at a voltage of −4500 V. The curtain gas and nebulizer gas (source gas 1) were both 25 psi, while the drying gas (source gas 2) was 35 psi. The CAD gas was set to medium, and the temperature was 450 °C. Mass spectrometric data was acquired using automatic information-dependent acquisition (IDA) with two experiment types: (i) survey scan, which provided TOF-MS data, and (ii) dependent product ion scan using a collision energy of -40 V and a collision spread of 30 V. PFOA was quantified in Multiquant 2.0 using MS/MS transitions and retention time for identification (Table S3.2).

3.3 Results and discussion

3.3.1 Characterisation of Ir(III)-functionalised surfaces

The luminescent iridium probes, IrC_6 and IrC_{12}, have been designed with surface active dithiol groups for covalent attachment to gold surfaces. The surfaces have been fully characterised by analytical techniques to examine morphology and elemental constitution. Firstly, SEM was used to characterise the morphology of the modified surfaces, IrC_6@Au and IrC_{12}@Au (Figure 3.2a). Interestingly, both IrC_6 and IrC_{12} show the formation of well-dispersed micelle-type structures on the Au surface. Their mean sizes were found to be 250 ± 40 nm in IrC_6@Au and 230 ± 30 nm in IrC_{12}@Au (Figure 3.3a,b). Upon investigation of the analogous iridium complexes without the liphophilic six and twelve carbon chains ($Ir(ppy)_2bpy$ and IrbpySS), carrying either dithiol chains as anchor or not, no micelles were observed on the surfaces (Figure S3.1). EDS elemental mapping analysis of the IrC_6@Au and IrC_{12}@Au (Figure 3.2c) shows the clear presence of Ir and organic content on the micelle-type structures. Independent DLS analysis of acetonitrile solutions of IrC_6 and IrC_{12} confirmed the presence of micelles in solution, with sizes of 210±6 nm and 190±3 nm for IrC_6 and IrC_{12}, respectively which are in the same range but

slightly smaller than the ones observed on gold surfaces (Table 3.1). The smaller size of the IrC_{12} micelles can be attributed to more efficient packing of the aliphatic chains hence smaller sizes micelles are observed. We have independently examined surfaces coated with the iridium complexes under the same conditions but at low concentrations (0.15 mM) which is below the estimated critical micelle concentration of the iridium complexes assessed in water and no micelles were observed on the surfaces. Upon addition of PFOA the morphology of the IrC_6@Au and IrC_{12}@Au surfaces was examined. A significant disruption of the micelle-type structures can be observed (Figure 3.2a). It is postulated that the hydrophobic and oleophobic fluorosurfactant PFOA interacts with the hydrophobic micelle interior leading to micelle disassembly. The coating of the surfaces with iridium was also examined in the presence of a fluorinated surfactant Zonyl-FSA, which was previously used with iridium surface active complexes on gold surfaces,[28-29] as its fluorinated chain was envisaged to affect the PFOA interaction. The IrC_6-FSA@Au and IrC_{12}-FSA@Au surfaces show iridium aggregation with elongated shape structures around micelle-type features (Figure 3.2b), and upon EDS analysis, it was found that the elemental composition of fluorine was 32 at. % (Figure 3.3c). Addition of PFOA led to the disruption of the structures (Figure 3.2b) and EDS analysis reveals a lower fluorine content (20% at.) possibly due to loss of the Zonyl-FSA (Figure 3.3c).

Table 3.1. DLS size analysis of acetonitrile solutions of IrC_6 and IrC_{12} PDI: polydispersity index.

	PDI	**Z-ave (d.nm)**	**Mean size by intensity (nm)**	**Mean size by number (nm)**
IrC_6	0.12	210±6	150±39	200±60
IrC_{12}	0.33	190±3	140±30	160±33

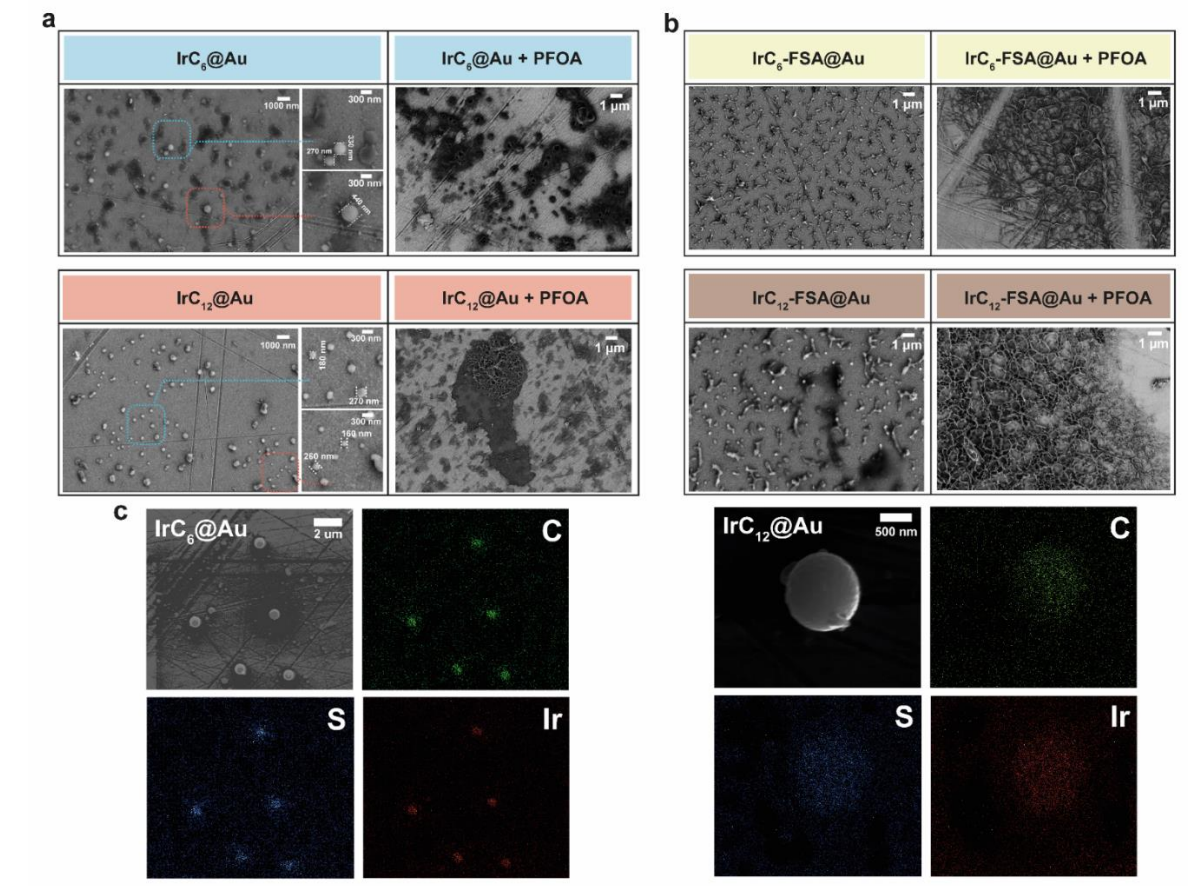

Figure 3.2. (a) SEM images of **IrC$_6$@Au** and **IrC12@Au** without and with PFOA and (b) **IrC$_6$-FSA@Au** and **IrC$_{12}$-FSA@Au** without and with PFOA. Solution of PFOA: 1 g/L for **IrC$_6$@Au** and **IrC$_{12}$@Au** and 10 mg/L for **IrC$_6$-FSA@Au** and **IrC$_{12}$-FSA@Au**. (c) EDS elemental mapping analysis (Carbon, Sulfur and Iridium) for **IrC$_6$@Au** and **IrC$_{12}$@Au**.

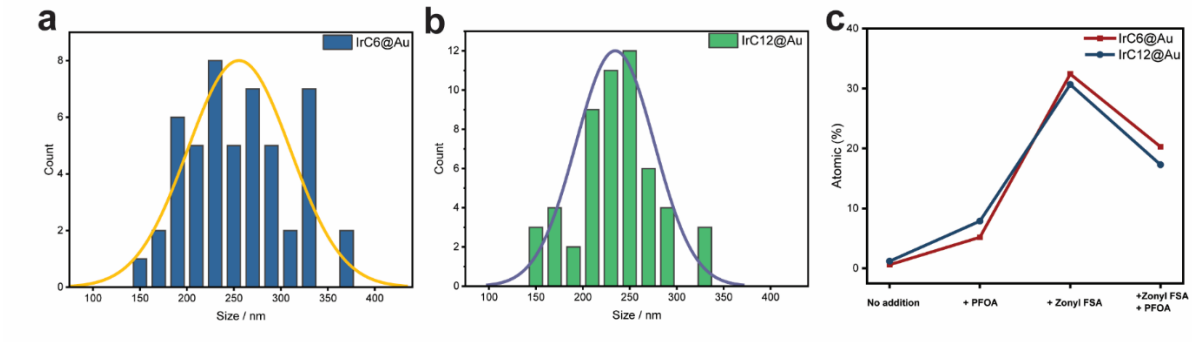

Figure 3.3. Size distributions of (a) IrC$_6$@Au and (b) and IrC$_{12}$@Au from SEM images (Figure 2) with N>50. (c) Variation of fluorine composition in different substrates.

Contact angle measurements of gold surfaces coated with IrC_6 and IrC_{12} were carried out to probe the effect of chain length on the relative hydrophobicity of the surfaces. The trend of the measurements (Figure 3.4) from 60° of the plain gold surface to 73° IrC_6@Au and 80° IrC_{12}@Au shows that modification of the surface with the iridium complexes led to increase of surface hydrophobicity.

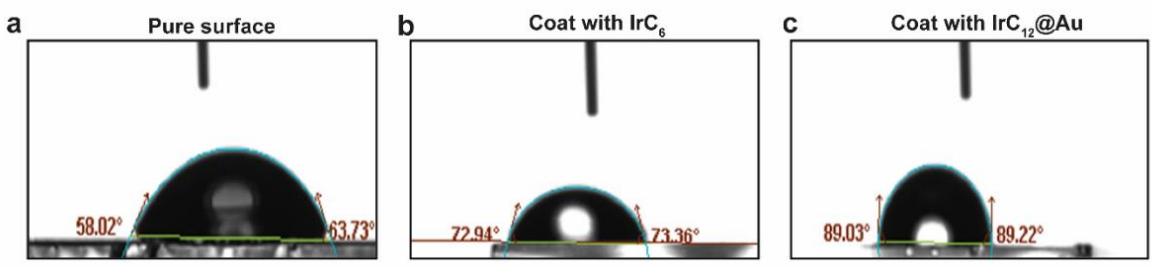

Figure 3.4. Representative images of the contact angle observed between the gold surface and water droplet a) uncoated gold surface, b) IrC_6@Au and c) IrC_{12}@Au.

X-ray photoelectron spectroscopy (XPS) was used to further characterize the modified surfaces. The characteristic Ir 4f and S 2p peaks confirm attachment of the complexes to the surfaces. The characteristic peaks are similar for IrC_6@Au and IrC_{12}@Au, hence only selected peaks for IrC_{12}@Au are shown in Figure 3.5 and the peaks for IrC_6@Au are shown in Figure 3.6. The peaks for Ir (Figure 3.5a) appeared at 61.8 eV ($4f_{7/2}$) and at 64.8 eV Ir ($4f_{5/2}$) in all modified surfaces The binding energy and the symmetric peak shape confirms the ionic character of the Ir.[30] The S 2p region for IrC_6@Au and IrC_{12}@Au (Figure 3.5b) revealed peaks at 162.5 eV, and 163.7 eV, (characteristic of $2p_{3/2}$ peaks) assigned to thiolate (48%) and disulfide (28%).[31] The two additional peaks at 165.2 eV (16%), and 166.8 eV (8%) are attributed to oxidized sulfur as previously reported. The presence of disulfide may be attributed to some of the surface-active groups not attached to the surface with some Ir(III) complexes binding only with one thiolate capped leg. The remaining oxidized species are usually regarded as sulfonate as previously observed.[32] Furthermore, upon addition of PFOA, the peaks of CF_2 (291.8 eV) and CF_3 (294.2 eV) appear clearly in the region of the carbon peaks (Figure 3.5c) and the F peaks are shown with addition of PFOA (Figure 3.5d).

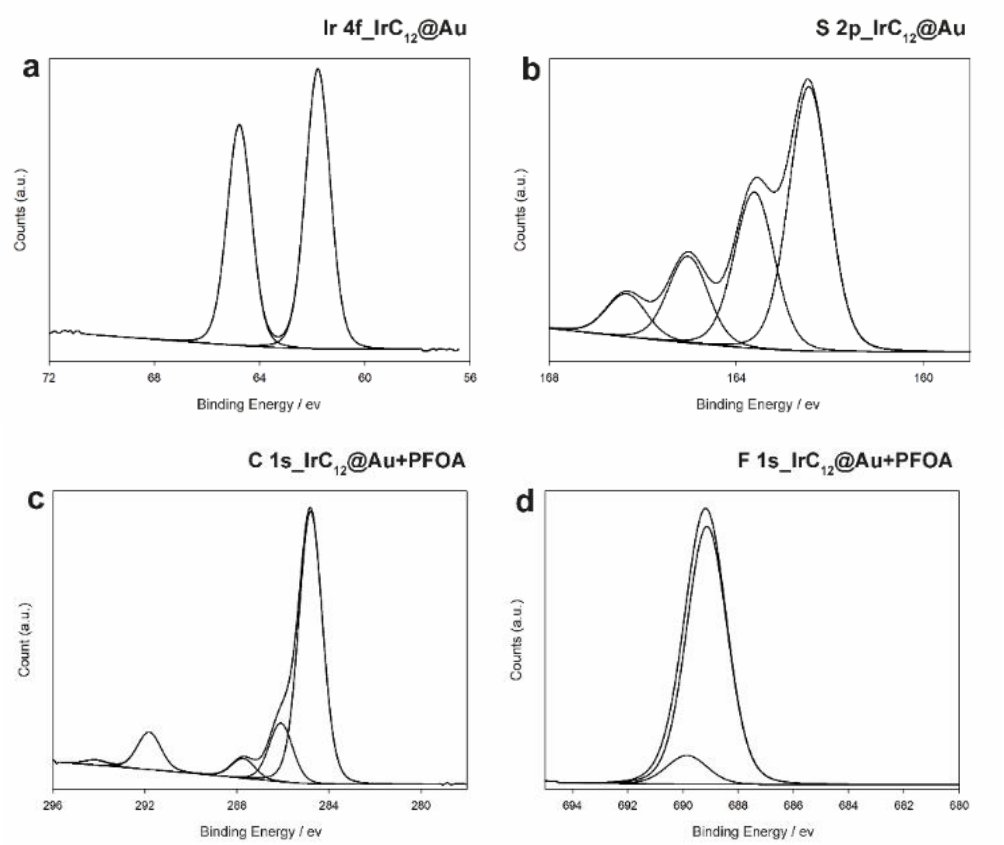

Figure 3.5. XPS spectra of (a) Ir 4f spectrum of IrC_{12}@Au, (b) S 2p spectrum of IrC_{12}@Au, (c) C 1s spectrum of IrC_{12}@Au with PFOA (PFOA concentration: 100 mg/L) and (d) F 1s spectrum of IrC_{12}@Au with PFOA (PFOA concentration: 100 mg/L).

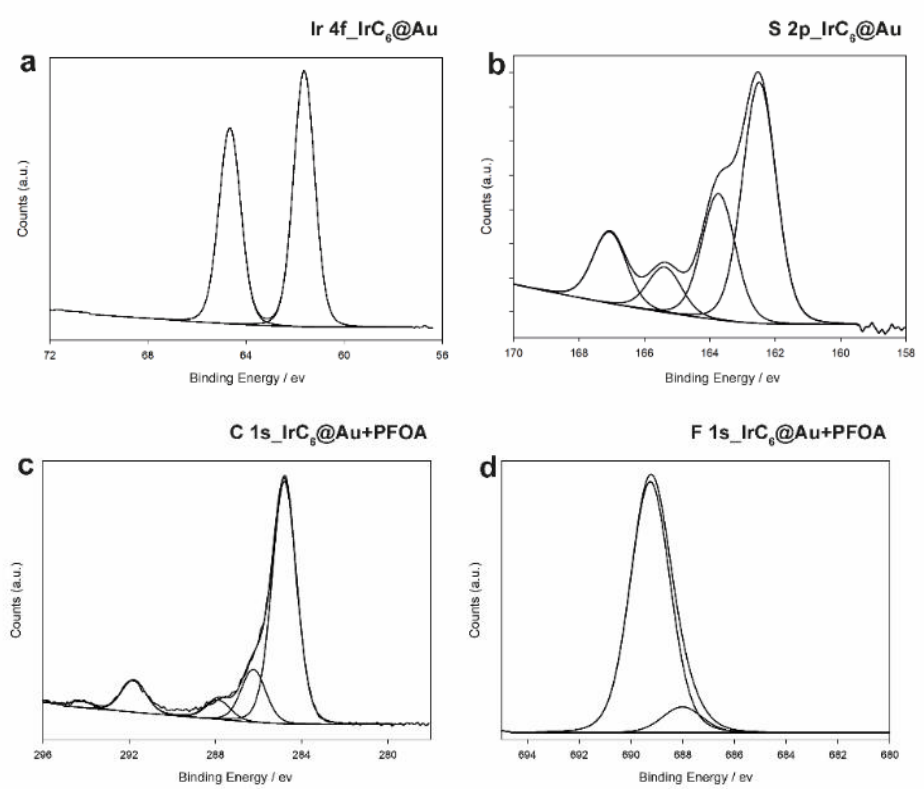

Figure 3.6. XPS spectrum of (a) Ir 4f spectrum of IrC_6@Au, (b) S 2p spectrum of IrC_6@Au, (c) C 1s spectrum of IrC_6@Au with PFOA (PFOA concentration: 100 mg/L) and (d) F 1s spectrum of IrC_6@Au with PFOA (PFOA concentration: 100 mg/L).

3.3.2 Probing immobilization of PFOA and Zonyl-FSA on coated surfaces

The immobilization of PFOA or Zonyl-FSA on coated surfaces was measured by TOF-SIMS which is a highly surface-sensitive method capable of analysing the top 1-3 nm of a substrate.[33] The primary ion beam used for TOF-SIMS analysis causes molecular fragmentation of the analyte, and the presence of certain species can be identified by their characteristic ions. Because the yield of secondary ions is dependent on several parameters including the surrounding matrix, TOF-SIMS studies may draw conclusions from the presence or absence of peaks as well as large variations (orders of magnitude) in peak intensities, however a fully quantitative study is possible only under set conditions.[34-35] The correct interpretation of peak intensities in this study relies on suitable scaling of the y-axis. Here, all peaks were scaled to the area of the $C_3H_7NO^+$ peak from the amide group in the IrC_{12} complex, which is common to all samples, and was present in a suitably high intensity to give reliable scaling. Other peaks

such as those related to Ir did not provide a high enough signal intensity to be suitable as a reference peak. It is also demonstrated from the EDS atomic composition results that the same amount of iridium complex is deposited on the different surfaces.

The CF^+ secondary ion is readily formed from fluorocarbons and is common to both Zonyl-FSA and PFOA, and is therefore useful for a comparison of the relative adsorption of PFOA or Zonyl-FSA on the substrate (Figure 3.7). A comparison of the IrC_{12}@Au substrate before and after PFOA treatment indicates some immobilization of PFOA on the substrate (Figure 3.7a). The weak CF^+ signal for the unexposed substrate IrC_{12}@Au may be caused by residual CF species in the TOF-SIMS instrument, or alternatively from cross-contamination between samples. A comparison of the substrates IrC_{12}@Au+PFOA and IrC_{12}-FSA@Au (Figure 3.7b) show an order of magnitude change in the CF^+ peak, indicating that Zonyl-FSA has extensive adsorption on the substrate. Interestingly, the IrC_{12}-FSA@Au substrate shows a significant drop in the CF^+ peak, suggesting that PFOA interferes with the immobilization of Zonyl-FSA (Figure 3.7c). Comparisons of peak areas are shown in Figure S3.2 for both CF^+ and Li^+ peaks. The Li^+ peak is an independent indicator of Zonyl-FSA. The significantly higher peak area for the IrC_{12}-FSA@Au compared to IrC_{12}-FSA@Au + PFOA supports the conclusions drawn from the CF^+ peak, that PFOA has affected the Zonyl-FSA immobilization. These results are supported by EDS analysis and further examined by luminescence lifetime measurements below.

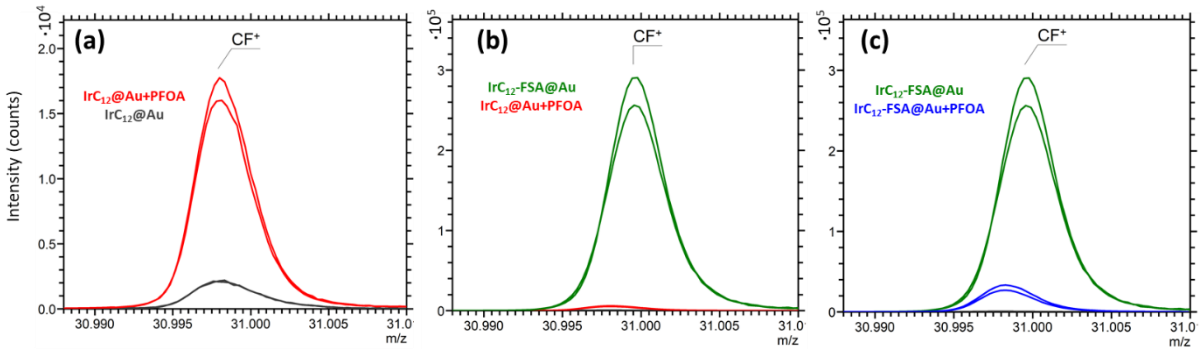

Figure 3.7. TOF-SIMS spectra showing the characteristic CF^+ peak for presence of PFOA and Zonyl-FSA in comparisons of substrates: (a) IrC_{12}@Au (black) and IrC_{12}@Au+PFOA (red), (b) IrC_{12}-FSA@Au (green) and IrC_{12}@Au+PFOA (red) (c) IrC_{12}-FSA@Au (green) and IrC_{12}-FSA@Au+PFOA (blue). Spectra were normalised to the $C_3H_7NO^+$ peak at *m/z* = 73.05 present from the amide group in the IrC_{12} complex. Samples were analysed in duplicate, with repeats shown as separate lines.

3.3.3 Optical behaviour of the iridium luminescence

The luminescence properties of the iridium micelles on surfaces were characterised by steady-state and time-resolved spectroscopy and compared with the complexes in solution before and after addition of PFOA and in the presence of the FSA-surfactant. The iridium-modified surfaces, IrC_6@Au and IrC_{12}@Au exhibit characteristic luminescence originated from the triplet charge transfer state with maxima at 570 and 574 nm upon excitation at 375 nm (Table 3.2 and Figure 3.8). The luminescence signal is significantly blue shifted compared to the acetonitrile solutions of the complexes at 608 and 611 nm, Table 3.3). Interestingly the corresponding luminescence lifetime of the iridium signal on the surface (Table 3.1) is significantly longer (the major component 150 ns and 165 ns for IrC_6@Au and IrC_{12}@Au, respectively) and compared to the corresponding solutions of the complexes (55 and 62 ns for IrC_6 and IrC_{12}, Table 3.3) which is unusual based on the expected quenching of metal complex luminescence most commonly observed by gold surfaces.[171, 172] It is worth noting the multicomponent luminescent lifetime is commonly observed for iridium complexes based on the mixed character of the triplet excited state and we focus the comparisons on the longer, major component. We attribute the longer lifetimes of IrC_6/IrC_{12} on the gold surface to the better arrangement of the complexes on the

surface. Exposure of the IrC_6@Au and IrC_{12}@Au surfaces to PFOA leads to significant further blue shift of the signal at 560 nm, accompanied by an increase of the luminescence lifetime of 31 ns for IrC_6@Au and 26 ns for IrC_{12}@Au (Figure 3.8). The addition of PFOA in the solutions of IrC_6 and IrC_{12} did not show any changes of the maximum of the emission intensity and small changes in luminescence lifetime (Table 3.3). The effect of PFOA on the Ir-modified surfaces may be attributed to the disassembly of the micellar structures as also observed by SEM which can be driven by association of the PFOA with the iridium complex leading to a number of factors that influence the luminescence lifetime such as protection from luminescence quenching by $^3O_2$, change of the polarity of the environment around the metal centre due to the disruption of the micellar structure. We examined the iridium surfaces co-coated with the Zonyl-FSA surfactant which was previously shown to lead to lengthening of luminescence lifetime of metal complexes.[141] It was envisaged the presence of the surfactant on the surface (as confirmed by the surface analysis) will enhance the interaction of PFOA with the surface due to the presence of its fluorinated chain. The co-coated surfaces with the fluorinated surfactant, IrC_6-FSA@Au and IrC_{12}-FSA@Au exhibit long luminescence lifetimes (446 and 502 ns respectively), as anticipated, while the micellar structures are maintained with elongated assemblies evidenced by SEM (Figure 3.2). Upon addition of PFOA the luminescence lifetimes are decreased by 139 ns for IrC_6-FSA@Au and by 194 ns for IrC_{12}-FSA@Au, which are much larger changes than the ones observed with the IrC_{16}@Au and IrC_{12}@Au surfaces. These changes are attributed to replacement of the Zonyl-FSA by PFOA in the iridium microenvironment accompanied by changes of the surface assemblies. The replacement of Zonyl-FSA is also supported by the aforementioned results by EDS and TOF-SIMS analyses which confirm the change of fluorine content on the surfaces.

Table 3.2. Emission maxima and luminescence lifetimes of iridium modified gold surfaces upon addition of PFOA. PFOA solutions added: 1 g/L for IrC_6@Au, IrC_{12}@Au and 10 mg/L for IrC_6-FSA@Au, IrC_{12}-FSA@Au. The amplitude of each component of the lifetime is shown in brackets. Estimated errors: λ_{em} ± 1 nm and luminescence lifetimes error with standard deviation (n = 3).

Name	**λ_{em} (nm)**	**τ (ns)**	
		1st component	**2nd component**
IrC_6@Au	570	13±1 (21%)	150±4 (79%)
IrC_6@Au + PFOA	561	49±3 (24%)	191±2 (76%)
IrC_6-FSA@Au	562	119±6 (19%)	446±5 (81%)
IrC_6-FSA@Au + PFOA	571	76±1 (25%)	307±7 (75%)
IrC_{12}@Au	574	32±3 (26%)	165±2 (74%)
IrC_{12}@Au + PFOA	560	54±2 (23%)	194±3 (77%)
IrC_{12}-FSA@Au	569	167±5 (20%)	502±4 (80%)
IrC_{12}-FSA@Au + PFOA	578	93±7 (25%)	308±3 (75%)

Table 3.3. Photophysical properties of solutions of the Ir (III) complexes in acetonitrile showing the effect of mixing with Zonyl FSA and addition of PFOA. PFOA solution added: 41.4 mg/L. The amplitude of each component of the lifetime is shown in brackets. Estimated errors: λ_{em} ± 1 nm and luminescence lifetimes error with standard deviation (n = 3).

Name	**λ_{em} (nm)**	**τ (ns)**	
		1st component	**2nd component**
IrC_6	608	30±0 (21%)	55±0 (79%)
IrC_6 + PFOA	608	47±0 (77%)	81±1 (23%)
IrC_6 + FSA	612	33±1 (26%)	69±1 (74%)
IrC_6 + FSA + PFOA	610	38±1 (45%)	63±1 (55%)
IrC_{12}	611	35±1 (39%)	62±2 (61%)
IrC_{12} + PFOA	608	49±0 (85%)	83±2 (15%)
IrC_{12} + FSA	615	33±0 (24%)	74±1 (76%)
IrC_{12} + FSA + PFOA	611	39±2 (36%)	61±1 (64%)

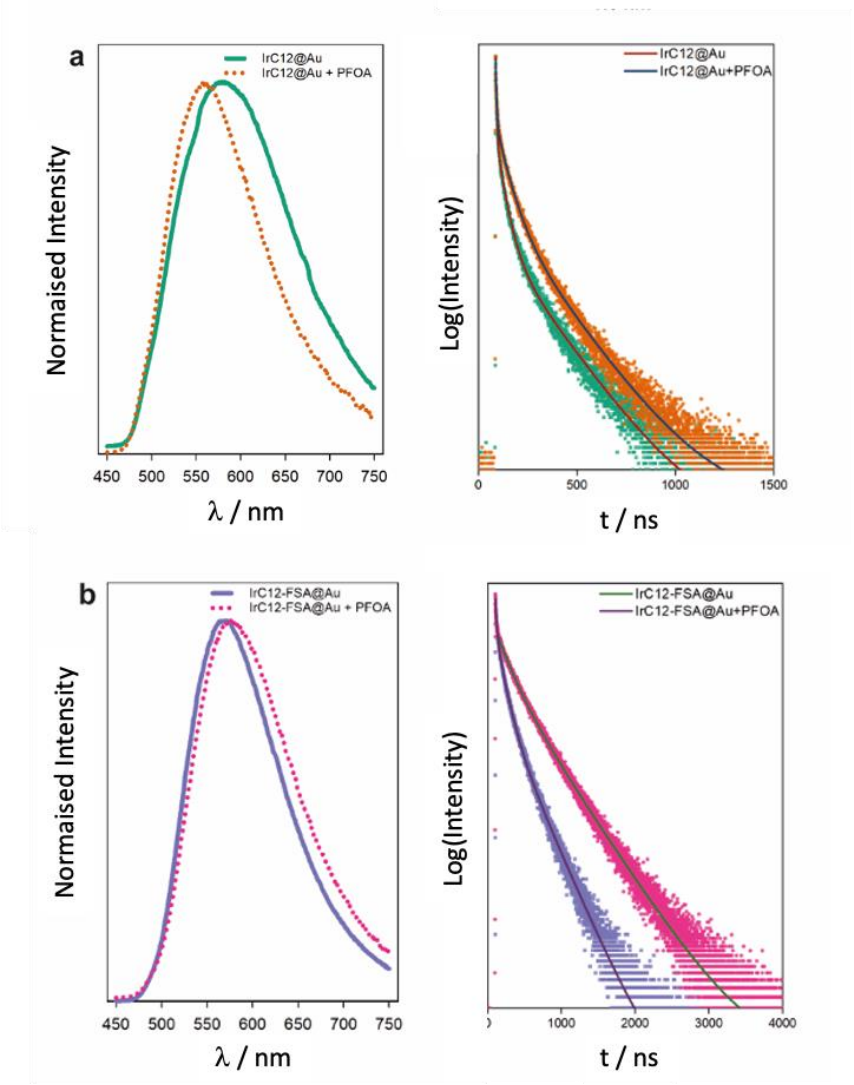

Figure 3.8. Selected luminescence spectra and normalised lifetime decays (fit-solid line) upon addition of PFOA to (a) IrC_{12}@Au ([PFOA] = 1g/L) and (b) IrC_{12}-FSA@Au ([PFOA] = 10 mg/L).

3.3.4 Analytical performance for PFOA detection

To examine the sensitivity and range of the platform, the luminescence lifetime was monitored across a range of PFOA concentrations for the surfaces with IrC_6-FSA@Au, IrC_{12}-FSA@Au and without the Zonyl-FSA surfactant - IrC_6@Au or IrC_{12}@Au. All surfaces show an exponential dependence of the luminescence lifetime upon addition of PFOA (Figure 3.9 and Figure S3.3). If the PFOA interaction was based on a bimolecular event between the PFOA and the Ir(III) complex a linear Stern-Volver dependence would have been expected between the luminescence lifetime and the concentration of

PFOA. However, the exponential dependence with the concentration of PFOA is consistent with luminophores sensing within micelles.[173, 174] It is expected that the PFOA will interact with the luminophores within the micelle according to previously studied models.[175, 176] The shifts of the emission maxima observed also agree with a ground state quenching as well as dynamic quenching of the PFOA within the micelles, indicating the ground state association of PFOA within the micelles on the surface. Nevertheless, this dependence correlates well the luminescence lifetime and allows the estimation of concentration. The Limit of Detection (LOD) was estimated to be of 8.2 mg/L (20 µM, S/N=3) IrC_6@Au + PFOA and 67 mg/L (162 µM, S/N=3) for IrC_{12}@Au surface when the co-coated surfaces showed a higher LOD as expected from the initial screening of luminescence properties with LOD for IrC_{12}-FSA@Au + PFOA of 39 µg/L (94 nM, S/N=3) and detection range from 100 µg/L (0.24 µM) to 1 g/L (2.42 mM) whilst IrC_{12}-FSA@Au + PFOA surface has a LOD of 6.2 µg/L (15 nM, S/N=3) and detection range from 10 µg/L (24.2 nM) to 1g/L (2.42 mM) (Table 3.4).

The surfaces show reproducible performance with standard deviations as indicated in luminescence lifetimes tables. The surface reproducibility was examined with 50 independent measurements of luminescence lifetime of iridium coated surfaces.

We have examined the possible interference of metal cations and other acids, reported for a large number of luminescence sensors and resulting in inaccuracies of the measurements.[36] We examined common salts and other aliphatic acids including Na^+, Ca^{2+}, Mg^{2+} Zn^{2+}, Cu^{2+}, Ni^{2+}, Mn^{2+} and Co^{2+} valeric acid, hexanoic acid, heptanoic acid, octanoic acid, decanoic acid and dodecanoic acid for possible interference on the luminescence of IrC_{12}-FSA@Au. The luminescence lifetime of IrC_{12}-FSA@Au before and after the addition of the metal ions was monitored. (Figure 3.10) The variation (-2% to 2%) of the luminescence lifetime in the presence of the interferents is very small and in the range of error. In conclusion, both the selected metal ions and the aliphatic acids did not display any interferences with the platform's luminescence signal.

Overall, the performance of the iridium surfaces shows strong potential for further development of the luminescence lifetime as detection technique. Analysis of polluted waste water effluents has revealed concentrations of PFOA of 160 µg/L.[177] It is challenging to compare the different detection approaches

for development of novel sensors as many factors need to be taken into consideration apart from sensitivity of detection: interferences, time to response, detection versatility, stability. Optical techniques offer great advantage of rapid detection compared to electrochemical sensors although the latter have reported high sensitivities.[65, 68] Most of the reported platforms require incubation time between 20-30 min which compare well with the iridium surface platform (incubation time of 30 min) although some methods require preconcentration steps or longer incubation periods.[69, 178] The iridium platform also provides great stability of the chromophore compared to organic counterparts and has strong potential in development of a portable device.[179]

Table 3.4 Luminescence lifetime of IrC_6-FSA@Au and IrC_{12}-FSA@Au upon addition of PFOA χ^2 within 1.0 ± 0.2**, n=3**

C_{PFOA} (mg/L)	IrC_6-FSA@Au τ /ns		C_{PFOA} (mg/L)	IrC_{12}-FSA@Au τ /ns	
1000	56±3 (15%)	187±12 (85%)	1000	65±8 (19%)	196±14 (81)
100	68±7 (22%)	237±13 (78%)	100	83±12 (20%)	249±21 (80%)
10	76±1 (25%)	307±7 (75%)	10	93±7 (25%)	308±3 (75%)
1	86±3 (24%)	348±4 (76%)	1	106±10 (20%)	366±12 (80%)
0.1	102±5 (19%)	409±16 (81%)	0.1	129±2 (18%)	434±11 (82%)
0	119±6 (19%)	446±5 (81%)	0.01	164±3 (22%)	469±3 (78%)
			0	167±5 (20%)	502±4 (80%)

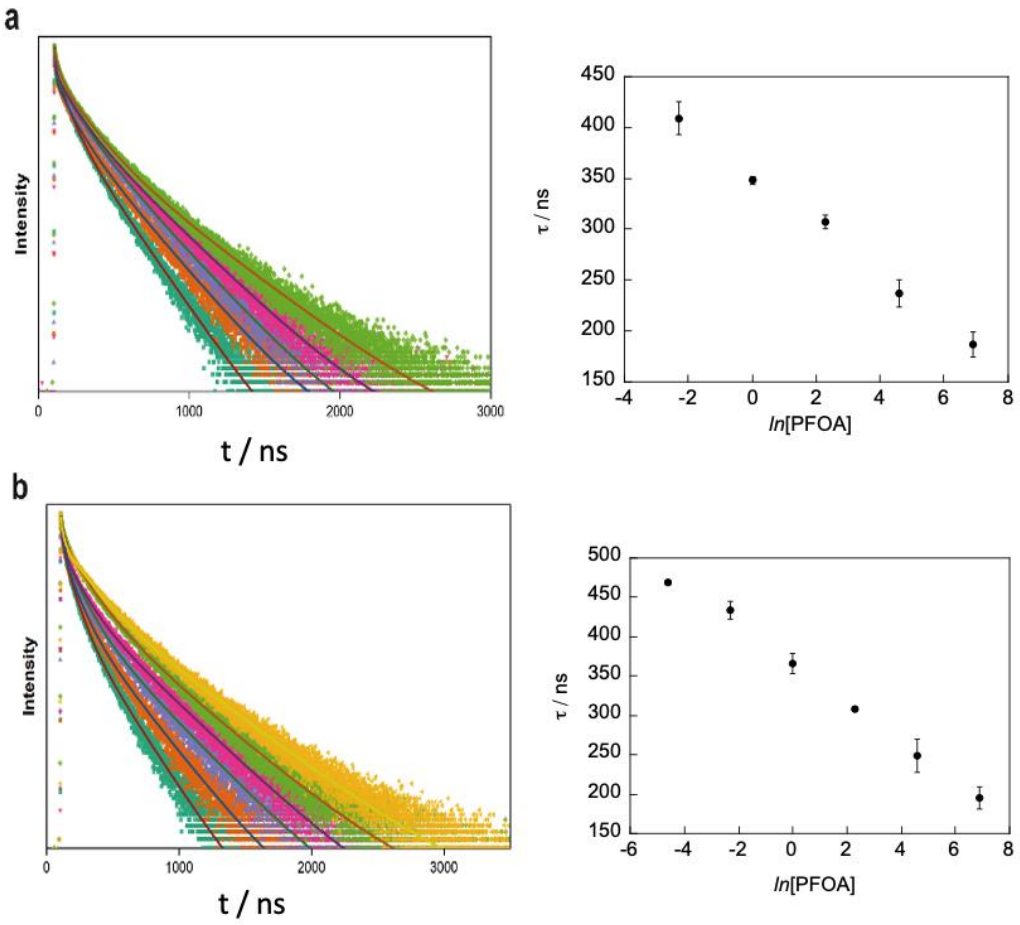

Figure 3.9. Luminescence lifetime decays (normalised, fit - solid line) of (a) IrC_6-FSA@Au and (b) IrC_{12}-FSA@Au upon addition of PFOA in different concentrations at pH of 7.38 (range for IrC_6-FSA@Au 100 µg/L to 1 g/L, and for IrC_{12}-FSA@Au 10 µg/L to 1 g/L, [PFOA] in mg/L.

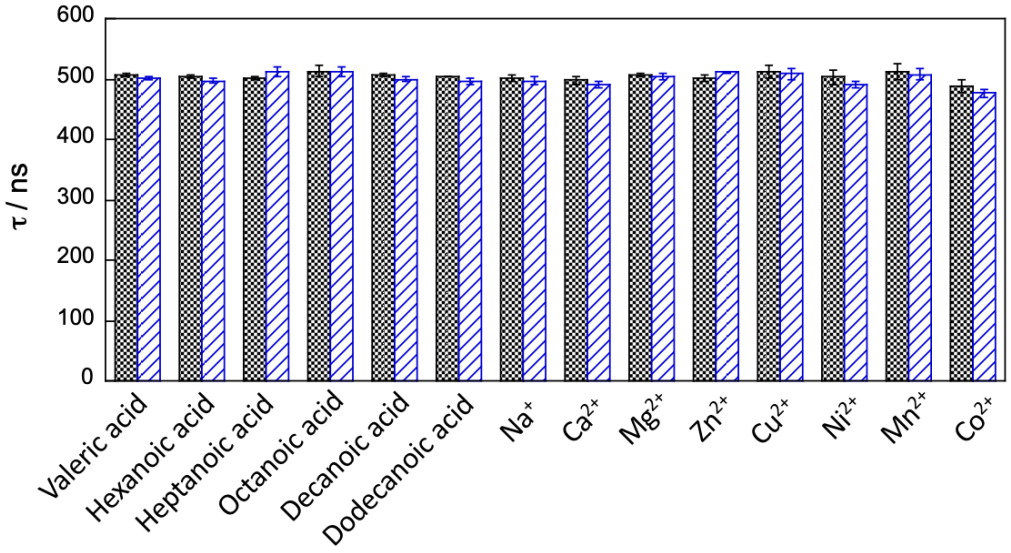

Figure 3.10. Influence of possible interferents Na^{+}, Ca^{2+}, Mg^{2+} Zn^{2+}, Cu^{2+}, Ni^{2+}, Mn^{2+}, Co^{2+} and valeric acid, hexanoic acid, heptanoic acid, octanoic acid, decanoic acid and dodecanoic acid (1 mg/L) to the luminescence lifetime of iridium, upon addition of interferent to IrC_{12}-FSA@Au surface; before (dark) and after (light).

3.3.5 Drinking water analysis

To evaluate the feasibility of the sensing platform, IrC_{12}-FSA@Au was applied to the analysis of 29 samples of drinking water from the UK West Midlands. These samples were firstly analysed for their PFOA content using LC-TOF-MS before being analysed by our sensor. As shown in Table 3.5, concentrations of PFOA in unspiked bottled water ranged between 0.67 and 3.9 ng/L PFOA while those in tap water contained 0.82-1.4 ng/L PFOA. These concentrations were well within the EU drinking water directive limit (100 ng/L for the sum of C_4-C_{13} PFCAs and PFSAs) but were in some instances close to exceeding the MCL for PFOA announced recently by the USEPA of 4 ng/L.[11] Compared with previously reported data (Table S3.3), PFOA concentrations in our UK samples are very similar to those reported in: Ireland, Norway, Germany, Belgium, and the Netherlands, but are exceeded by those reported for: Italy (northern Milan), Spain (Catalonia), the USA (24 contiguous states) and China (79 cities). Given that the concentrations of PFOA in UK drinking water samples are below the detection

limit of our sensor, samples were instead spiked with PFOA reference standard at two concentrations. Tap water spiked at: 10 mg/L; and at 100 µg/L, and these were measured using the sensor. In the 10 mg/L spiked samples, PFOA was detected between 7-14 mg/L while in the 100 µg/L spiked samples, PFOA was detected in the range 88 to 151 µg/L. These data suggest that in aqueous samples like industrial effluent and wastewater that contain e.g. up to 160 µg/L[177] or groundwater near military base that contain up to 220 µg/L,[180] this luminescence sensor is applicable and reliable. We believe further optimisation of our approach, will yield lower detection limits and thus widen its applicability.

Table 3.5. Concentrations of PFOA detected in drinking water unspiked[a] and spiked[b] at 100 µg/L and 10 mg/L

Water type	PFOA Concentration		
	Unspiked Tap Water (ng/L)	Tap Water (spiked at 10 mg/L) (mg/L)	Tap Water (spiked at 100 µg/L) (µg/L)
Mineral water 1	0.68	12	120
Mineral water 2	0.71	12	89
Mineral water 3	0.69	13	109
Mineral water 4	0.72	11	112
Mineral water 5	0.71	9	97
Mineral water 6	0.72	12	134
Mineral water 7	0.83	12	137
Mineral water 8	0.73	14	120
Sparkling water 1	0.72	11	88
Sparkling water 2	0.76	11	110
Sparkling water 3	0.74	14	88
Sparkling water 4	0.72	9	94
Sparkling water 5	0.71	11	101
Sparkling water 6	0.67	7	88
Flavored water 1	0.67	13	126

Flavored water 2	3.9	11	116
Flavored water 3	1.7	8	96
Flavored water 4	1.0	10	142
Flavored water 5	2.2	14	105
Tap water 1	0.87	11	102
Tap water 2	0.98	8	127
Tap water 3	0.90	9	151
Tap water 4	1.0	9	114
Tap water 5	0.94	13	111
Tap water 6	0.96	8	124
Tap water 7	0.97	9	114
Tap water 8	0.90	9	127
Tap water 9	1.4	12	136
Tap water 10	0.82	13	93

a. determined using LC-TOF-MS. b. determined using IrC12-FSA@Au sensor

3.4 Discussion of high LOD, possible interferences and potential improvements

The LOD of the sensor for PFOA is 6.2 μg/L. While this LOD is sufficient for certain applications, it is higher than the stringent water quality standards set by the EU and USEPA. For example, the USEPA has set a maximum contaminant level (MCL) for PFOA in drinking water at 4 ng/L, which is significantly lower than our current detection limit.

It is also important to consider potential interferences from other PFAS or chemicals with similar structures. PFAS such as PFNA and PFBA may have similar interactions with the iridium complexes, potentially affecting the accuracy of PFOA detection. Additionally, other environmental contaminants, including organic compounds and metal ions, could interfere with the sensor's performance.

To improve sensitivity and reduce interference, several strategies could be considered:

Using Alternative Substrate Materials: Employing other substrate materials such as platinum (Pt) or plasmonic gold surfaces could enhance the sensor's performance. These materials may provide better surface plasmon resonance effects, leading to increased signal sensitivity.

Exploring Other Metal Complexes: Investigating other metal complexes such as europium (Eu) or ruthenium (Ru) as substitutes for iridium (Ir) could also be beneficial. These metals have different photophysical properties that might result in longer luminescence lifetimes and higher sensitivity to PFOA.

Optimizing Surface Functionalization: Further optimization of the surface functionalization process, including the use of different surfactants or surface modifiers, could improve the interaction between PFOA and the sensor, leading to lower detection limits.

Advanced Data Analysis Techniques: Utilizing advanced data analysis techniques, such as machine learning algorithms, to distinguish between signals from PFOA and other interfering substances, could enhance the accuracy and reliability of the sensor.

By addressing these aspects, we can significantly enhance the sensor's performance, making it more suitable for real-world applications and ensuring compliance with stringent water quality standards.

3.5 Conclusion

We have demonstrated that gold surfaces modified with IrC_6 and IrC_{12} metal probes provide a sensitive optical platform for the detection of PFOA based on the iridium luminescence lifetime signal. The iridium complexes have lipophilic chains which affect the assembly on gold with evidence of micellar type structures. Addition of PFOA affects the luminescence lifetime of the iridium probes which are known for sensitivity of the luminescence signal on local environment. Characterisation analysis of the surfaces shows that addition of PFOA disrupts the micellar-type assemblies on the surfaces. The change of the luminescence lifetime in the presence of PFOA is not observed in solution and is attributed to the interaction of PFOA with the iridium assemblies on the surface. The largest change of the lifetime which is best suited for analytical detection is observed for the gold surfaces co-coated with the fluorinated surfactant and IrC_6 or IrC_{12}. The surfactant not only enhances the PFOA interaction but by increasing

the luminescence lifetime provides a large, analytically well-exploitable change of the lifetime signal upon displacement with PFOA. The sensory surfaces effectively quantify PFOA concentrations in drinking water down to 100 µg/L (240 nM) and display strong anti-interference. In summary, the surface-based luminescence assays reported here provide a novel approach to monitoring PFOA and related PFAS based on iridium probe luminescence lifetime signal with rapid screening, large window of detection which can be further exploited for development of multi-analyte devices.

Chapter 4: A Europium-Functionalised Surface for the Detection of C_4-C_{10} PFAS in Waste Leather, Leatherette and Textile samples

4.1 Introduction

4.1.1 The importance of detection C_4-C_{10} PFCA

Perfluoroalkyl carboxylic acids (PFCAs, formula: $C_nF_{(2n+1)}CO_2H$) are compounds with different fluorocarbon chain lengths terminating with a carboxylic acid group, and belonging to the class of perfluoroalkyl substances (PFAS). Due to the strong carbon-fluorine (C-F) bonds,[123] PFCA possess a number of industrially useful physicochemical properties, including thermal stability, high surface activity, hydrophobicity and lipophobicity,[2] resulting in their extensive application in articles such as: non-stick cookware, textiles, leather, food packaging, cleaning agents, and firefighting foams.[20, 23, 25] Such widespread applications have led to demonstrable human exposure to PFAS *via* pathways such as: inhalation, ingestion of diet and dust, and dermal contact with PFAS-containing media[35, 181-183]. An investigation showed that >98% of serum samples collected from the general U.S. population (≥ 12 years of age) contained PFAS, including PFCA like perfluorooctanoic acid (PFOA), perfluorononanoic acid (PFNA), etc.[38] Such exposure is concerning, given human serum elimination half-lives of PFCA are of the order of several years,[184, 185] coupled with evidence of adverse human health outcomes linked with PFAS exposure, including kidney, testicular and thyroid cancer as well as impacts on levels of blood cholesterol.[186-190] These concerns about wide-range application, capacity for long range atmospheric transport, toxicity, environmental persistence and potential for bioaccumulation have led to listing PFOA, PFOS, PFHxS and their salts and related compounds under the Stockholm Convention, and the long-chain PFCA are also currently being reviewed.[191]

4.1.2 Challenges in monitoring PFCAs

As part of efforts to eliminate PFOA, the EU has set a limit on its maximum permissible concentration in waste of 1 mg/kg.[192] While welcome, monitoring compliance with such limits presents a formidable challenge, given the vast volume (e.g. 2,135 million tonnes in 2020)[193] of waste generated across the EU. The scale of this challenge is further compounded by the fact that the conventional LC-MS based techniques used to measure PFOA and other PFCA are destructive, time-consuming, and expensive. Against this backdrop, this paper reports a novel technique for the determination of C_4-C_{10} PFCA (see Table S4.1 for their chemical structures), namely: perfluorobutanoic acid (PFBA), perfluoropentanoic acid (PFPeA), perfluorohexanoic acid (PFHxA), perfluoroheptanoic acid (PFHpA), PFOA, PFNA, and perfluorodecanoic acid (PFDA). These chemicals are commonly present in leather, leatherette and textiles.[20, 194]

4.1.3 Surface sensing platforms

Surface sensing platforms are a new concept proposed by environmental analytical chemistry to adapt to different and tricky environments.[195] The portability, storability, transportability, and customizability of these platforms facilitate *in situ* measurement of contaminants. Compared with traditional liquid probes, surface sensing platforms can be customized for a variety of target contaminants or different matrix such as the atmosphere or the aquatic environment by tailoring of the specific recognition group.[196, 197] For instance, electrostatic interaction, H-bonding interaction, van der Waals interaction[198] and covalent interaction have provided abundant pathways for anchoring multifunctional materials targeting different molecules. Alongside this, a surface is able to give a more reasonable arrangement for the luminescence probes, thereby protecting them from aggregation.[150] Within our experience, the rough modification of the surface normally leads to a uneven distribution of the luminophore on the surface, resulting in a massive influence on those optical signals (e.g. emission intensity, refractive index and scattering) associated with the concentration of probes.

4.1.4 Eu-functionalised surface for PFCA detection

A luminescence lifetime readout is normally linked to the surrounding environment of the luminophores but independent of their concentration, making it the ideal transduction signal for surface sensing platforms. Yet, it has rarely been applied in the field of environmental analytical chemistry.[199] Lanthanide(III) ions exhibit long luminescence lifetimes, covering microsecond to millisecond time ranges. These are significantly quenched by high energy O-H oscillators, such as those of H_2O molecules.[200, 201] Given by the chemical properties of PFAS, this study hypothesises the addition of PFAS will reduce such deactivation pathway. As depicted in Figure 4.1, the carboxylic group at one end of PFAS (e.g. PFOA, pKa=3.8±0.1)[10] can coordinate to Eu(III), displacing coordinating H_2O molecules and reduce quenching, while the fluorocarbon chain at the other side processed robust hydrophobicity, which can effectively create a pocket to protect the Eu^{3+} from quenching by H_2O. The functionalised surface was achieved by anchoring the SAcbisDBM ligand on the gold substrate, following by coordination of Eu(III) ions to ligand.[202] The choice of SAcbisDBM lies in the excellent affinity of β-diketonates for lanthanides(III), as well as their suitability as sensitisers of Eu(III) luminescence, ensuring sufficient luminescent signal for the sensing readout. Furthermore, the design of the ligand includes a spacer unit to limit quenching from the metal surface and a terminal thioacetate group to anchor the ligand *via* Au-S bonds.

To our knowledge, this type of sensing system has never been reported before.

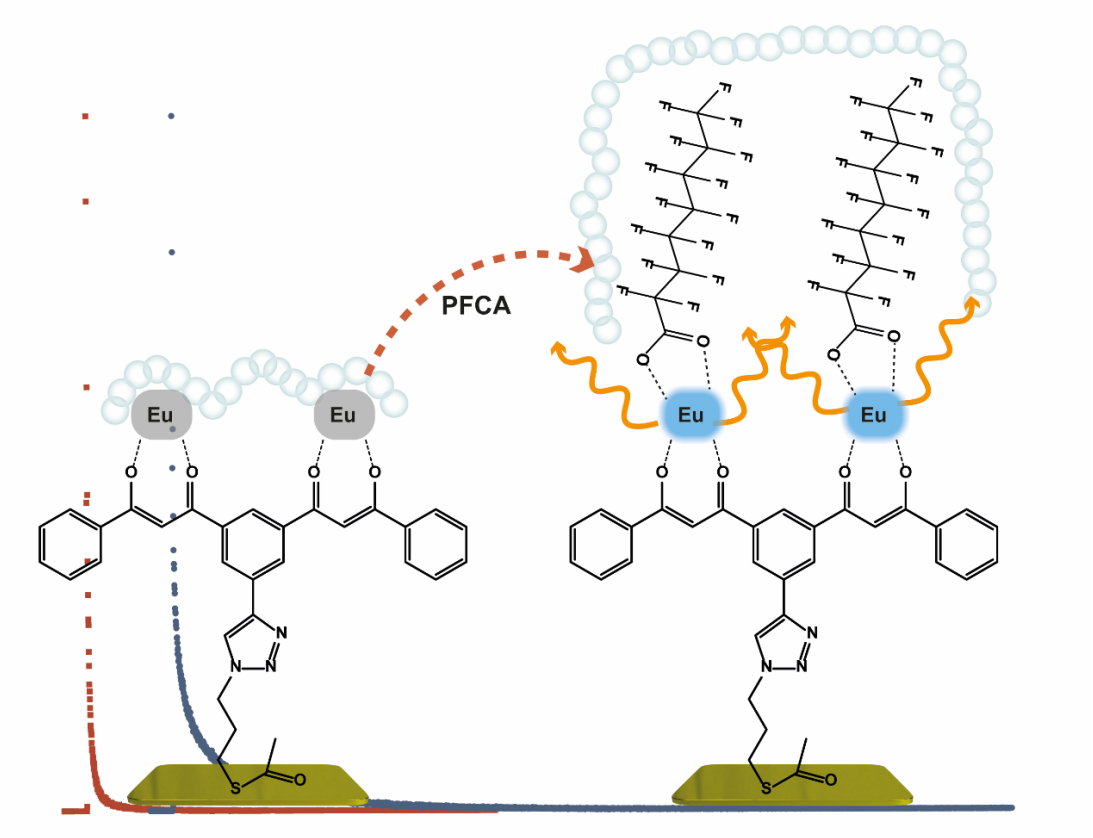

Figure 4.1. Schematic diagram of Eu-SAcbisDBM@Au surface, and the variation of the surface upon the addition of C_4-C_{10} Σ_7PFCA.

4.2 Experimental

4.2.1 Synthesis of SAcbisDBM ligand

The synthesis of the SAcbisDBM ligand followed our group's previous work.[203] The experimental process was shown in Figure 4.2. In brief, the design of the SAcbisDBM ligand involved a four-step synthesis process, relying on the copper-catalysed azide alkyne cycloaddition (CuAAC, known as click reaction). This synthesis requires the reaction between the alkyne bisDBM derivative 5 and the azide moiety of compound 6 to integrate the surface-active unit. This synthetic strategy demonstrates remarkable versatility, enabling the incorporation of various functional units in a single-step reaction without the need for further modification of derivative 4.

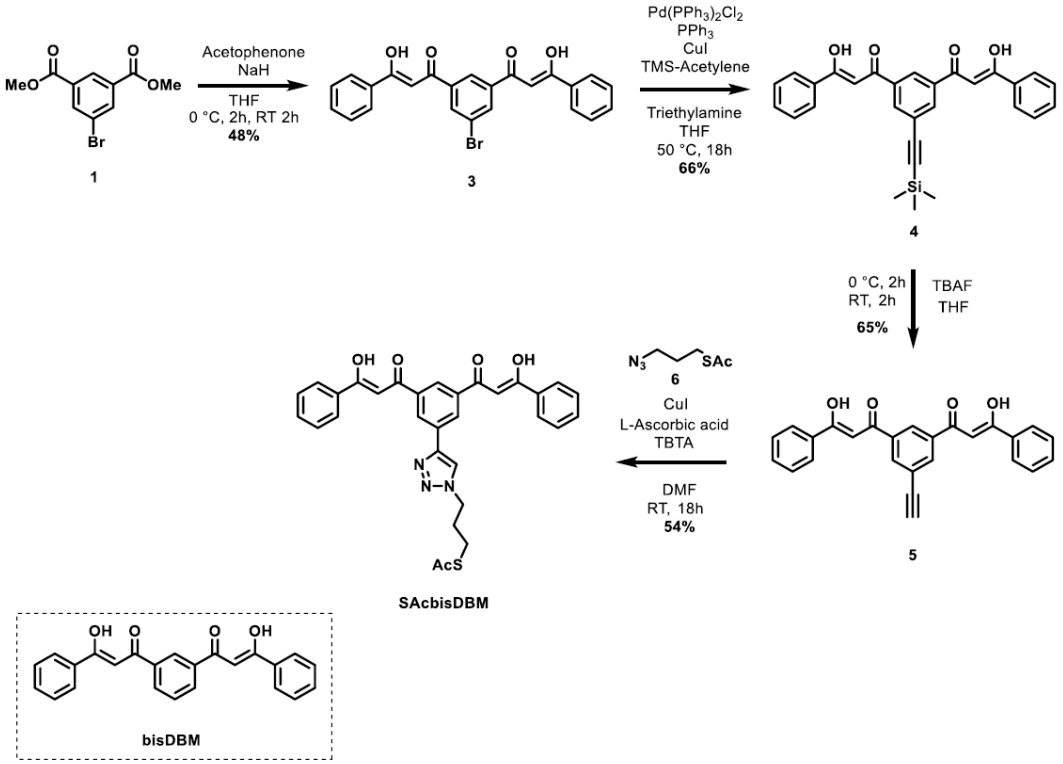

Figure 4.2. Synthesis route to SAcbisDBM ligand.

4.2.2 Preparation of Eu(III)-functionalised surface

Gold slides were rinsed thoroughly with acetonitrile and milli-Q water sequentially for three times before immersion in 80 °C piranha solution (95% sulfuric acid and 30% hydrogen peroxide in proportion of 3:1 (v/v)) for 15 min to eliminate all organic residues on the surface. The cleaned surfaces were dried under nitrogen flow and stored in ethanol until use.

The **SAcbisDBM@Au** surface was prepared by immersing the treated gold surfaces in a SAcbisDBM solution (1 mM in THF) for 18 hours. The modified surface was washed with small amounts of tetrahydrofuran and dried with a stream of nitrogen. The **Eu-SAcbisDBM@Au** surface was prepared by immersing SAcbisDBM@Au in a $EuCl_3$ solution (10 mM in H_2O) for 18 hours. The modified surface was washed with milli-Q water and dried with a stream of nitrogen.

To detect C_4-C_{10} PFCA, the Eu-SAcbisDBM@Au surface was immersed in a C_4-C_{10} PFCA MeOH solution (pH=6.5±0.5) with different concentrations (from 80 nM to 100 μM) for 10 minutes. The

surface was subsequently washed with MeOH and dried with a stream of nitrogen and stored in a dark environment under nitrogen atmosphere until use.

4.2.3 Pre-treatment of waste leather, leatherette and textile samples

Waste leather/leatherette/textile samples (n=34) obtained in the UK were provided by WRc plc, with an additional sample of US firefighter protective clothing provided by Professor Graham Peaslee. Prior to extraction of PFAS, 50 mg (for HPLC-TOF-MS) and 500 mg (for the prepared sensor) of samples were weighed and cut into small pieces. The samples were then transferred to 15 mL PP plastic tubes before addition of 10 mL MeOH and 50 µL of 1 ng/µL internal standard mix (latter not necessary for samples analysed via the sensor). The tubes were then re-capped and inverted 20 times to mix the contents, followed by sonication for 1 hour. The resultant solvent extracts were filtered through a 0.22 µm filter membrane and evaporated to incipient dryness by a gentle stream of nitrogen at 38°C. Following reconstitution to 1 mL with MeOH (pH = 6.5), these final extracts were stored in 2 mL GC vials (for HPLC-TOF-MS) or 10 mL glass vials (for sensor analysis).

4.2.4 LC-MS method for the detection of C_4-C_{10} PFCAs

LC-MS determination of concentrations of PFBA, PFPeA, PFHxA, PFHpA, PFOA, PFNA and PFDA in leather, leatherette and textile samples was conducted using a Sciex Exion HPLC coupled to a Sciex 5600+ triple TOF MS equipped with an Agilent ZORBAX RRHD Eclipse Plus C18 column (2.1 internal diameter, 100 mm length, 1.8 µm particle size). Firstly, 10 µL of extract solution was injected into LC via Raptor C18 column (1.8 µm particle size, 50 mm length, 2.1 mm internal diameter, Restek). Details of the LC conditions employed are provided as Table S3.1. The TOF-MS is equipped with a Turbo V source operated in negative mode using electrospray ionization (ESI) at a voltage of −4500 V. The curtain gas and nebulizer gas (source gas 1) were both 25 psi, while the drying gas (source gas 2) was 35 psi. The CAD gas was set to medium, and the temperature was 450 °C. Mass spectrometric data was acquired using automatic information-dependent acquisition (IDA) with two experiment types: (i)

survey scan, which provided TOF-MS data, and (ii) dependent product ion scan using a collision energy of -40 V and a collision spread of 30 V. The results were quantified in Multiquant 2.0 using MS/MS transitions and retention time for identification (Table S4.2).

4.3 Results and discussion

4.3.1 The morphologies of Eu-SAcbisDBM@Au surface

The morphology of the Eu-functionalised surface was observed by scanning electron microscope (SEM). The surface coated with SAcbisDBM ligand is observed in the shape of rough, unregular and aggregated particulate structure, with a diameter around 90 nm (Figure S4.1a). Upon the coordination of Eu (Figure S4.1b) and the addtion of C_4-C_{10} PFCAs (Figure S4.1c) to the SAcbisDBM@Au surface, their morphlogies are not altered. EDS mapping analysis of Eu-SAcbisDBM@Au surface shows the presence and disturbution of Europium on the Eu-SAcbisDBM@Au surface (Figure S4.2).

4.3.2 Eu(III) amount on surface

The amount of Eu(III) on Eu-SAcbisDBM@Au surface was measured by titration of $EuCl_3$ on the SAcbisDBM@Au surface and monitored the alteration of emission signal of the surface. As depicted in Figure 4.3, the luminescence of the SAcbisDBM@Au surface does not display significant changes with addtion of up to 1 nmol of $EuCl_3$. With further addtion of $EuCl_3$, the luminescence start to increase and reach a plateau at 60 nmol. Upon further addtion of $EuCl_3$ up to 200 nmol, no significant variations was observed in the emission intensity of the Eu-SAcbisDBM@Au surface. For comparison, we added Eu(III) to the cleaned gold surface but do not observe enough optical signal to obtain the emission spectra. It is postulated that the Eu(III) cannot bound on the surface without SAcbisDBM ligand. The load capacity of SAcbisDBM@Au toward Eu(III) is thus calculated to be 86 nmol/cm^2 according to the size of used surface.

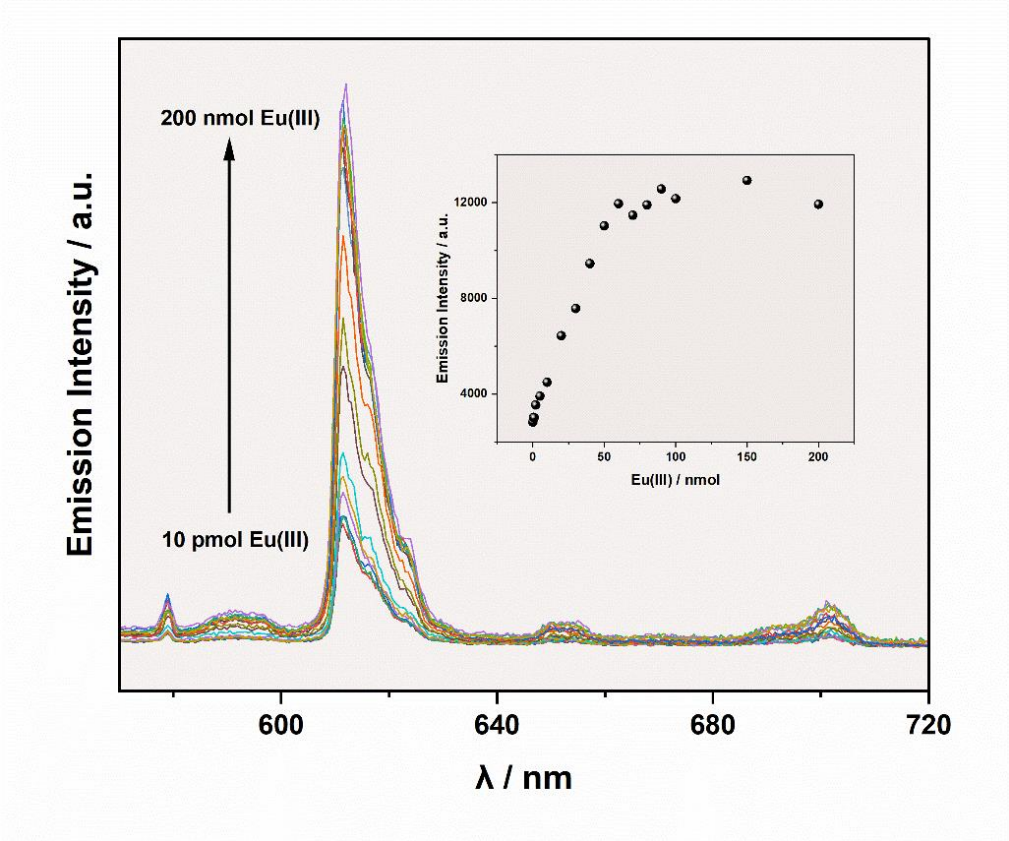

Figure 4.3. Emission spectrum of SAcbisDBM@Au surface with addition of 10 pmol, 100 pmol, 500 pmol, 1 nmol, 2 nmol 5 nmol, 10 nmol, 20 nmol, 30 nmol, 40 nmol, 50 nmol, 60 nmol, 70 nmol, 80 nmol, 90 nmol, 100 nmol, 150 nmol and 200 nmol Eu(III), respectively. Incubation time: 10 minutes. λ_{exc}: 355 nm. Insert: variation of the emission intensity of the SAcbisDBM@Au surface upon the addition of different contents of Eu(III).

4.3.3 X-ray photoelectron spectroscopy analysis

The coating of SAcbisDBM ligand on the surface was confirmed by X-Ray photoelectron spectroscopy (XPS). XPS wide survey (Figure 4.4a) confirms the presence of C (284.8 ev), N (399.8 ev), O (531.8 ev) and S (163.8 ev) on the surface. Furthermore, the elemental ratios obtained from the atomic percentages (At%) of the SAcbisDBM@Au surface agree with those of the SAcbisDBM ligand ($C_{31}H_{27}N_3O_5S$) (Table 4.1). The thiol attachment of SAcbisDBM to the gold surface is displayed in the high resolution spectrum in Figure 4.4b. The S 2p region for the SAcbisDBM@Au surface displays the

S $2p_{3/2}$ and $2P_{1/2}$ peaks at 162.7 ev and 163.9 ev, respectively. The peak at 162.7 ev was assigned to bound thiolate (82%) while the peak at 163.9 ev to unbound thiolate (18%), as previously reported.[204] The appearance of unbound thiolate might be attributed to inadequately thorough rinsing, or the SAcbisDBM ligand assembling on the surface through alkyl-Au interactions instead of Au-S bonds.[205] It is clear that SAcbisDBM ligand was bound to the gold surface.

Upon the coating of Eu(III), the Eu $3d_{5/2}$ peak appears at 1135.5 ev (Figure 4.4c), indicating the presence of Eu(III) on the SAcbisDBM@Au surface. The atomic ratio of Eu to S was calculated as 0.35 according to the wide survey of Eu-SAcbisDBM@Au surface, while that of Eu-SAcbisDBM@Au + PFOA surface is 0.36 (Table 4.2). It is implied that around 2.8 SAcbisDBM ligand on gold surface can bind 1 Eu(III). This phenomenon can be ascribed to the SAcbisDBM ligand pile up on the surface and hiding the binding site. Upon addition of PFCA, herein, we used PFOA ($C_8HF_{15}O_2$), the wide survey (Figure 4.4a) of the Eu-SAcbisDBM@Au + PFOA surface displays the presence of an intense peak in the F 1s region at 689.4 eV, which could not be observed in the spectra of the SAcbisDBM@Au and Eu-SAcbisDBM@Au surfaces. The high resolution F 1s spectrum (Figure 4.4d) also shows both -CF_2-CF_2- and -CF_3 components at 689.3 eV and 687.6 eV, respectively.[206] Interestingly, a metal-fluorine peak located at 684.64 ev was observed,[206] which could be attributed to the PFOA contact with the gold surface directly. Furthermore, the C 1s spectrum of the Eu-SAcbisDBM@Au surface with PFOA displays two new peaks at 292.4 eV and 294.5 eV compared to the SAcbisDBM@Au surface (Figure 4.4e), which can be assigned to CF_2 and CF_3 contributions, respectively. This proves that the Eu-SAcbisDBM@Au surface can capture PFOA. It is noted that the atomic ratio of F to Eu is 47 (Table 4.2), which indicates that each Eu(III) on the Eu-SAcbisDBM@Au surface can bind around 3.1 PFOA. In summary, the ratio of SAcbisDBM ligand to Eu(III) to PFOA is: 2.8 : 1 : 3.1.

Table 4.1. Atomic percentage (At%) of the SAcbisDBM@Au surface measured by XPS, and compared to the real At% of SAcbisDBM ligand. Elemental included C, N, O and S.

SAcbisDBM molecular structure: $C_{31}H_{27}N_3O_5S$				
	Atomic percentage (%)			
	C	N	O	S
SAcbisDBM@Au surface	46.1	3.9	6.7	1.5
Elemental analysis results of powder	46.2	4.5	7.5	1.5

$$At\% = \frac{N_i}{N_{tot}} \times 100$$

Where At% represents the Atomic percentage. N_i represents the number of atoms of interest while N_{tot} represents the total number of atoms.

Table 4.2. At% (C, N, O, F, S and Eu) of the Eu-functionalised surface measured by XPS and their atomic ratio (Ar) of C, N, O, F and Eu to S.

	At%					
	C	N	O	F	S	Eu
Eu-SAcbisDBM@Au	65.8	5.6	13.1	-	2.0	0.7
Eu-SAcbisDBM@Au + PFOA	50.3	3.3	8.0	25.03	1.5	0.54

	Atomic ratio				
	C/S	N/S	O/S	F/S	Eu/S
Eu-SAcbisDBM@Au	32.6	2.8	6.5	-	0.35
1Eu-SAcbisDBM@Au + PFOA	33.3	2.2	5.3	16.7	0.36

$$Ar = \frac{At_i}{At_S}$$

Where Ar represents the atomic ratio of the atoms of interest to sulphur. At_i represents the atomic percentage of atoms of interest while At_S represents the atomic percentage of sulphur.

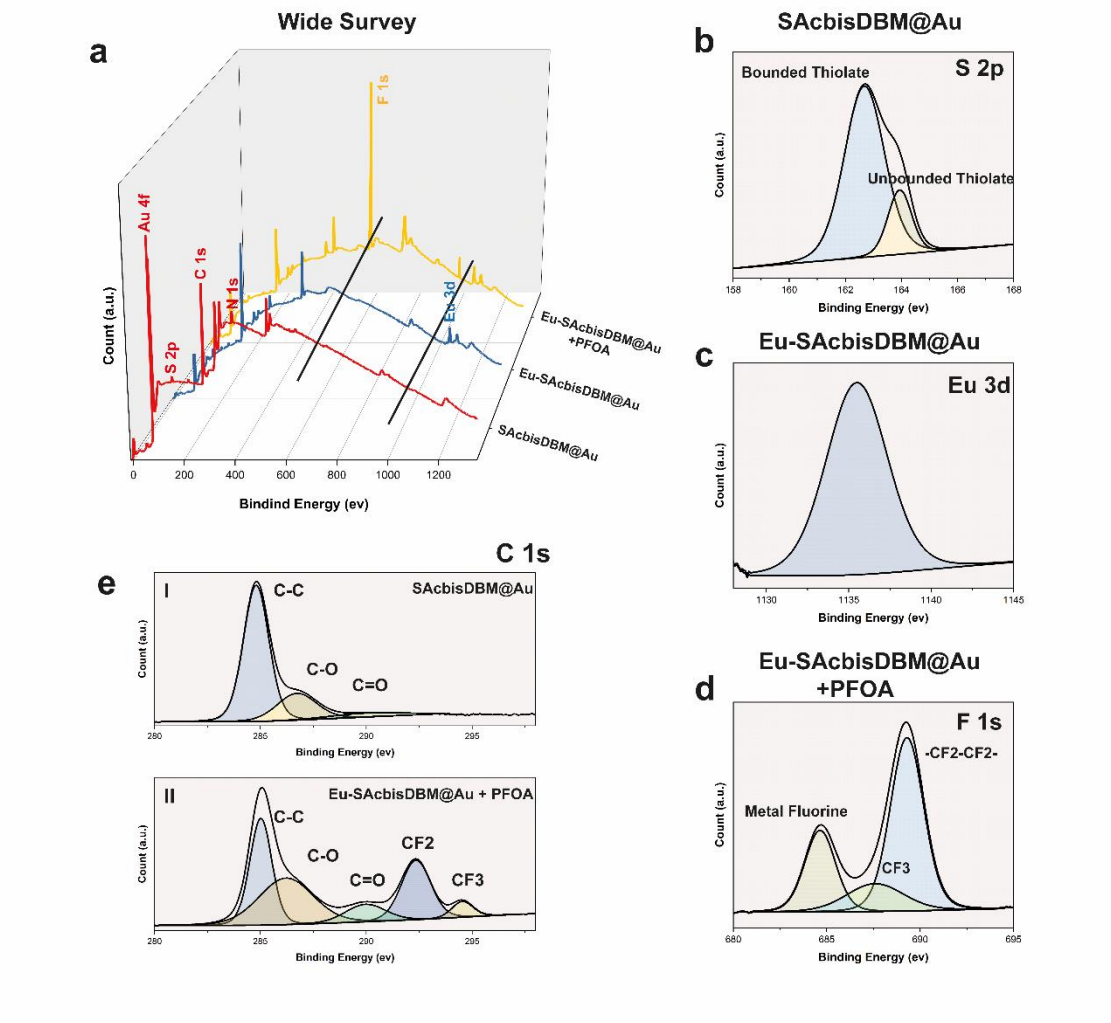

Figure 4.4. XPS images of (a) wide survey for SAcbisDBM@Au, Eu-SAcbisDBM@Au and Eu-SAcbisDBM@Au + PFOA, (b) S 2p spectrum of SAcbisDBM@Au, (c) Eu 3d spectrum of Eu-SAcbisDBM@Au, (d) F 1s spectrum of Eu-SAcbisDBM@Au + PFOA and (e) C 1s spectrum of SAcbisDBM@Au and Eu-SAcbisDBM@Au + PFOA.

4.3.4 Raman spectroscopy analysis

The chemical structures of the SAcbisDBM ligand on the surface, as well as it is coordinated with Eu(III), were analysed by Raman spectroscopy. The Raman spectra of the SAcbisDBM@Au surface displays Raman shifts at 1000 cm^{-1}, 1284 cm^{-1}, 1359 cm^{-1}, 1548 cm^{-1} and 1600 cm^{-1} (Figure 4.5a), which can be assigned to the vibration of aromatic ring and C-C aliphatic chain, C-CH_3, N=N, C=O and C=C, respectively.[207] These observed chemical structures are in agreement with the known structure of the

SAcbisDBM ligand. With the addition of Eu (III), a new peak at 272 cm^{-1} appears (Figure 4.5b), which can be assigned to the vibration of Eu-O.[207] This observation confirms the coordination of Eu (III) to SAcbisDBM ligand on the surface.

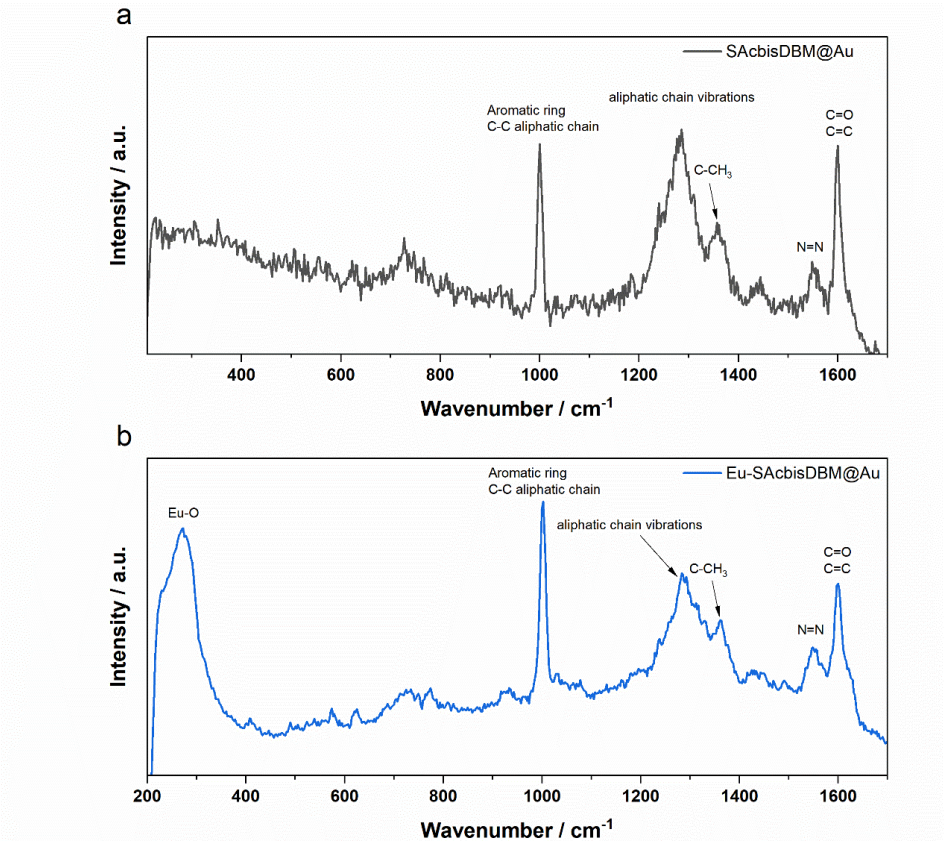

Figure 4.5. Raman spectrum of (a) SAcbisDBM@Au surface and (b) Eu-SAcbisDBM@Au surface. Laser excitation λ: 633 nm.

4.3.5 Effect of C_4-C_{10} PFCAs on Eu (III)

The detection of C_4-C_{10} PFCAs with Eu(III) was initially investigated in solution by monitoring variations of the luminescence lifetime and emission properties of $EuCl_3$ upon the addition of PFCAs in water. The emission spectra of Eu(III) in water displays the characteristic $^5D_0 \rightarrow {}^7F_J$ (J=1-4) transitions at 595 nm, 617 nm, 651 nm and 699 nm, respectively, and a recorded luminescence lifetime of 2 µs (6%) and 110 µs (94%) is recorded (Figure 4.6). Upon addition of C_4-C_{10} PFCA (pH = 6.5, from 2 µM to up to 20 µM), the luminescence intensity of Eu(III) is significantly increased, showing a linear relationship (Figure 4.6a). The relative emission intensity of the $^5D_0$->$^7F_2$ transition (617 nm) to the

$^5D_0$->$^7F_1$ transition (595 nm) has a 49% increase upon the addition of 20 uM of C_4-C_{10} PFCA in comparison with that of without addition of C_4-C_{10} PFCA, indicating a modification to the coordination sphere of the metal. Simultaneously, the luminescence lifetime of Eu(III) displays an increase upon the addition of 2 µM to 20 µM C_4-C_{10} PFCA, reaching up to 100 µs (36%), 440 µs (64%) at the maximum addition of C_4-C_{10} PFCAs (Figure 4.6b). These alterations are consistent with our hypothesis that the coordination of C_4-C_{10} PFCA to the Eu(III) displaces the H_2O molecule, leading the formation of a hydrophobic layer around Eu(III) that prevents quenching caused by H_2O molecules.

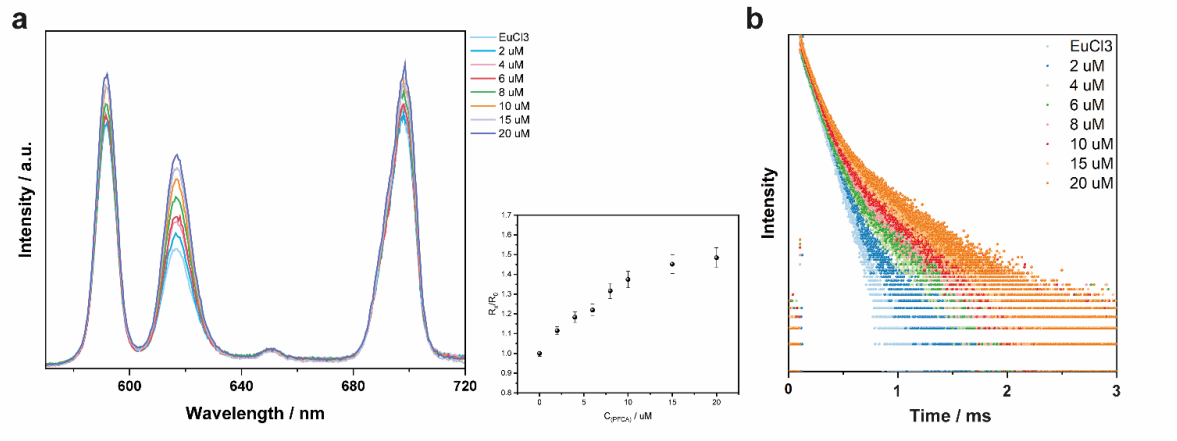

Figure 4.6. (a) luminescence intensity of 1 mM $EuCl_3$ solution, and with the addition of 2 µM, 4 µM, 6 µM, 8 µM, 10 µM, 15 µM and 20 µM C_4-C_{10} PFCAs, respectively, λ_{exc} = 375 nm. Insert: the relationship between the concentration of C_4-C_{10} PFCAs and R_x/R_0, Where Rx represents the ratio of peak area at 617 nm to 595 nm with the addition of different concentration of C_4-C_{10} PFCAs, R_0 represents the ratio of peak at 617 nm to 595 nm without adding C_4-C_{10} PFCAs. (b) luminescence lifetime of 1 mM EuCl3 solution with the addition of 2 µM, 4 µM, 6 µM, 8 µM, 10 µM, 15 µM and 20 µM C4-C6 PFCAs, respectively.

4.3.6 pH optimisation

In comparison to other factors, pH is likely to influence the luminescence lifetime of the luminophore.[208, 209] pH impacts the coordination environment of the luminophore[210] and can alter the protonation state of ligands or functional groups within it,[211] which lead to variations in the luminescent properties of the

luminophore. The pH effect on the Eu-SAcbisDBM@Au surface was examined by analysing its luminescence lifetimes across a range of pH values (0.7-12.9). As depicted in Figure 4.7, the luminescence lifetime is significantly influenced in both extreme acidic (pH < 1.3) and alkaline (pH > 7.4) environments. Specifically, it increases from 28 µs (37%) and 120 µs (63%) at pH 7.4 to 53 µs (39%) and 210 µs (61%) at pH 12.9. Conversely, it declines from 24 µs (38%) and 110 µs (62%) at pH 1.3 to 15 µs (39%) and 100 µs (61%) at pH 0.7. Notably, the luminescence lifetime of Eu-SACbisDBM@Au surface remains stable within the pH range of 1.3 to 7.4. Given the higher pH requirement indicated by the pKa values of the C_4-C_{10} PFCA (Table S4.1), the pH of the C_4-C_{10} PFCA standard solution should be maintained at 6.5±0.5.

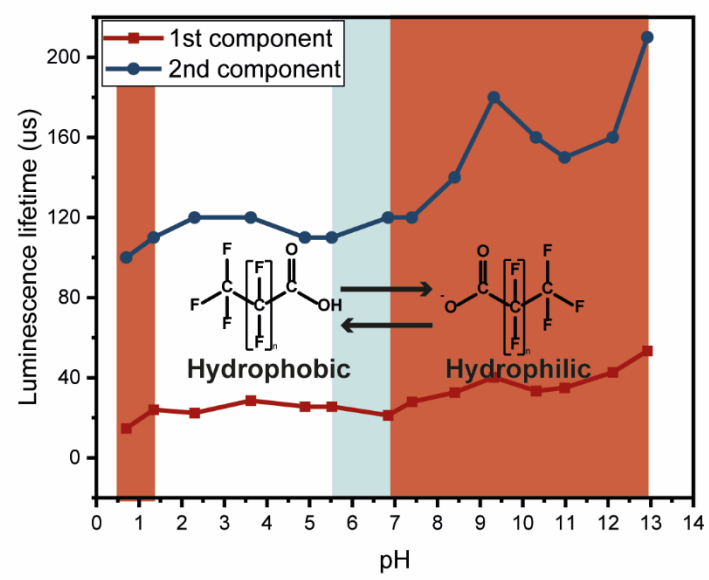

pH	τ / µs
0.7	15 (39%), 100 (61%)
1.3	24 (38%), 110 (62%)
2.3	22 (38%), 120 (62%)
3.6	29 (39%), 120 (61%)
4.9	26 (40%), 110 (60%)
5.5	26 (36%), 110 (64%)
6.8	21 (38%), 120 (62%)
7.4	28 (37%), 120 (63%)
8.4	33 (37%), 140 (63%)
9.3	40 (34%), 180 (60%)
10.3	33 (34%), 160 (66%)
11.0	35 (41%), 150 (59%)
12.1	43 (40%), 160 (60%)
12.9	53 (39%), 210 (61%)

Figure 4.7. pH (0.7-12.9) effect on the luminescence lifetime of Eu-SAcbisDBM@Au surface. White and blue zone indicated no influence on lifetime while red zone indicated a significant effect on lifetime.

4.3.7 Analytical performance for C_4-C_{10} PFCA detection

Sensor response to C_4-C_{10} PFCA

The sensitivity of the Eu-SAcbisDBM@Au surface was defined by the alteration of the luminescence lifetime in the presence of different concentrations of C_4-C_{10} PFCA. The lifetime of Eu-

SAcbisDBM@Au surface shows the expected increase upon increase of C_4-C_{10} PFCA concentrations from 80 nM to 100 µM (Figure 4.8a). Specifically, in the presence of 100 µM analyte, the lifetime of the Eu-SAcbisDBM@Au surface increases from 18±0.6 µs (37%), 105±6 µs (63%) to 110 µs (24%), 448 µs (76%). This represents a nearly 6.5-fold increase for the first component and a 4.3-fold increase for the second component. The rest of the variations caused by the matched C_4-C_{10} PFCA are shown in Table 4.3. Additionally, the emission intensity of the Eu-SAcbisDBM@Au surface also displays a remarkable increase, especially for the hypersensitive $^5D_0 \rightarrow {}^7F_2$ transition (617 nm) displaying nearly a 2.7-fold enhancement (Figure 4.8c). This enhancement in both luminescence lifetime and emission intensity can be attributed to the PFCA displacing the water molecules surrounding Eu(III), thereby reducing luminescence quenching.

The linear relationship between concentrations of C_4-C_{10} PFCA and luminescence lifetime is shown in Figure 4.8b. Both 1st component and 2nd component of luminescence lifetime displayed identical tendencies:

For the 1st component:

$$\tau_1\ (\mu s) = 0.8416\ C_{PFCAs}\ (\mu M) + 19.34,\ R^2 = 0.9928\ (1)$$

For the 2nd component:

$$\tau_2\ (\mu s) = 3.4811\ C_{PFCAs}\ (\mu M) + 120,\ R^2 = 0.9822\ (2)$$

where τ_1 (ns) and τ_2 (ns) represents the 1st and 2nd component luminescence lifetime of Eu-SAcbisDBM@Au surface while C_{PFCAs} (µM) represents the concentration of C_4-C_{10} PFCAs. The detection ranges from 80 nM (29 µg/L) to 100 µM (36 mg/L) with a limit of detection (LOD) of 55 nM (S/N=3).

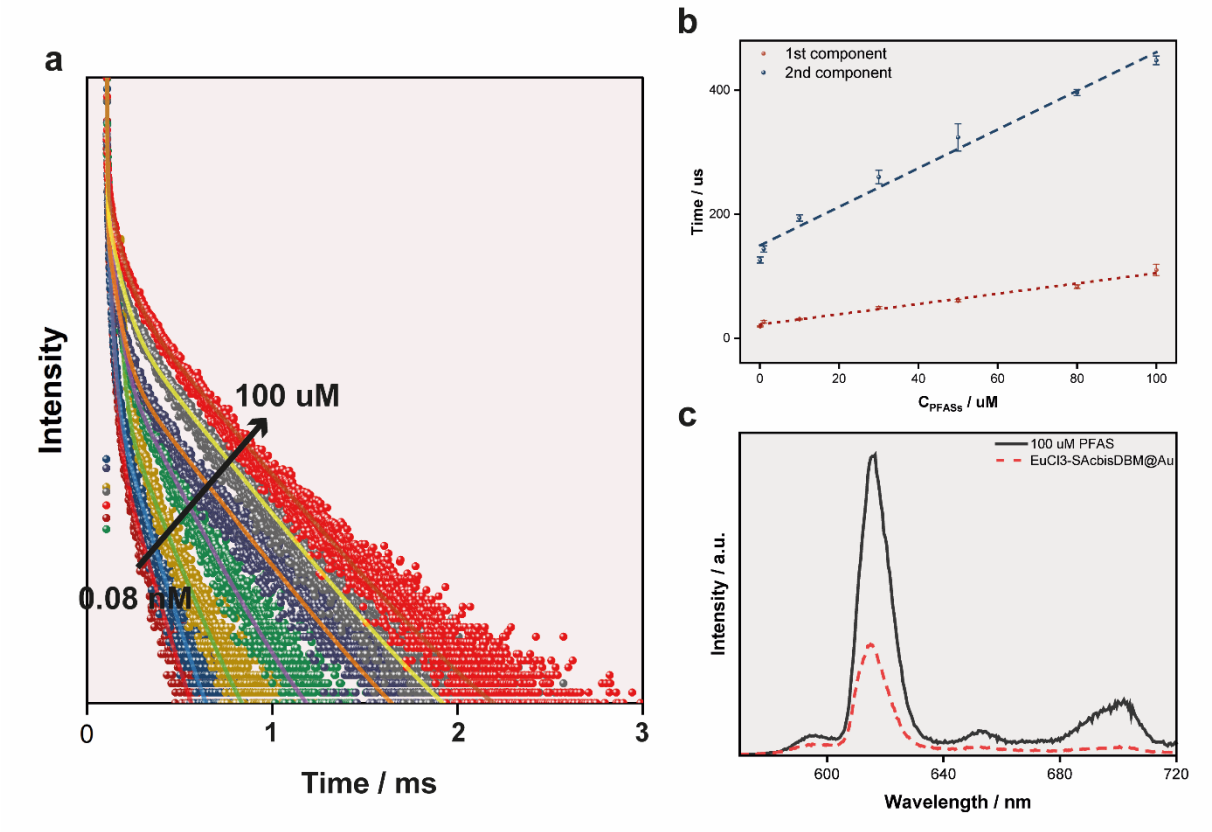

Figure 4.8. (a) Luminescence lifetime spectroscopy of Eu-SAcbisDBM@Au surface upon the addition of 80 nM, 1 µM, 10 µM, 30 µM, 50 µM, 80 µM and 100 µM C_4-C_{10} PFCAs, respectively. (b) Calibration curve (1^{st} component in red and 2^{nd} component in blue) of the concentration of C_4-C_{10} PFCAs to luminescence lifetime. (c) Emission spectrum of Eu-SAcbisDBM@Au surface and its alteration in the presence of 100 µM C_4-C_{10} PFCAs.

Table 4.3. Details of the variation of luminescence lifetime of Eu-SAcbisDBM@Au surface with addition of 80 nM, 1 µM, 10 µM, 30 µM, 50 µM, 80 µM and 100 µM C_4-C_{10} PFCAs.

C (uM)	τ (us)	
	1st component	2nd component
100	106±5 (24%)	444±5 (76%)
80	83±3 (22%)	396±5 (78%)
50	59±2 (25%)	318±16 (75%)
30	48±2 (27%)	258±10 (73%)
10	31±1 (30%)	194±5 (70)
1	24±1 (33%)	136±8 (67%)
0.08	19±1 (39%)	126±5 (61%)

Reusability and possible interference

C_4-C_{10} PFCA can be removed from the surface upon washing with a large amount of milli-Q water. As depicted in Figure 4.9a, the luminescence lifetime of the Eu-SAcbisDBM@Au surface exhibited an anticipated increase (110 µs (24%), 450 µs (76%)) with the addition of 100 µM C_4-C_{10} PFCA. Subsequently, after washing, the lifetime reinstated to its initial decay values (19 µs (33%), 120 µs (67%)), indicating the successful removal of C_4-C_{10} PFCA. The washing process was repeated four times, and the recovery of luminescence lifetime of Eu-SAcbisDBM@Au surface are observed of 99%, 98%, 104% and 94% (1st component), respectively, and 110%, 110%, 93% and 102% (2nd component), respectively, compared to the first cycle. The accuracy of detecting C_4-C_{10} PFCA are around 89%-108% (1st component) and 83%-98% (2nd component), respectively. This demonstrates that the prepared surface can be reused for at least five cycles or more.

Moreover, by employing the washing procedure, this study detected varying concentrations (10 µM, 30 µM, 50 µM, 80 µM, and 100 µM) of C_4-C_{10} PFCA using a single Eu-SAcbisDBM@Au surface. As

illustrated in Figure 4.9b, the luminescence lifetime of the prepared surface displayed the expected increase upon the addition of different concentrations of PFCA. The results observed in Figure 4.9a and Figure 4.9b indicate the excellent reproducibility and reusability of the prepared surface.

To evaluate potential interferences with the sensor response, eight metal ions (Na^{+}, Ca^{2+}, Mg^{2+}, Zn^{2+}, Ni^{2+}, Mn^{2+}, Co^{2+}, and Cu^{2+}) along with six aliphatic acids (valeric acid, hexanoic acid, heptanoic acid, octanoic acid, decanoic acid, and dodecanoic acid) were examined for their impact on the Eu-SAcbisDBM@Au surface. As illustrated in Figure 4.9c, Na^{+}, Ca^{2+}, Mg^{2+}, Zn^{2+}, Ni^{2+}, and the six aliphatic acids displayed no significant effects on the lifetime of the Eu-SAcbisDBM@Au surface. However, Mn^{2+}, Co^{2+}, and Cu^{2+} exhibited notable influences, causing variations of 11%, 33%, and 28% (1st component), and 18%, 41%, and 36% (2nd component) in the lifetime of the Eu-SAcbisDBM@Au surface, respectively. To ensure the accuracy and reliability of the sensor, it is preferable to avoid these substances when detecting samples or to utilize SPE to pre-treat the sample in order to eliminate these metal ions.

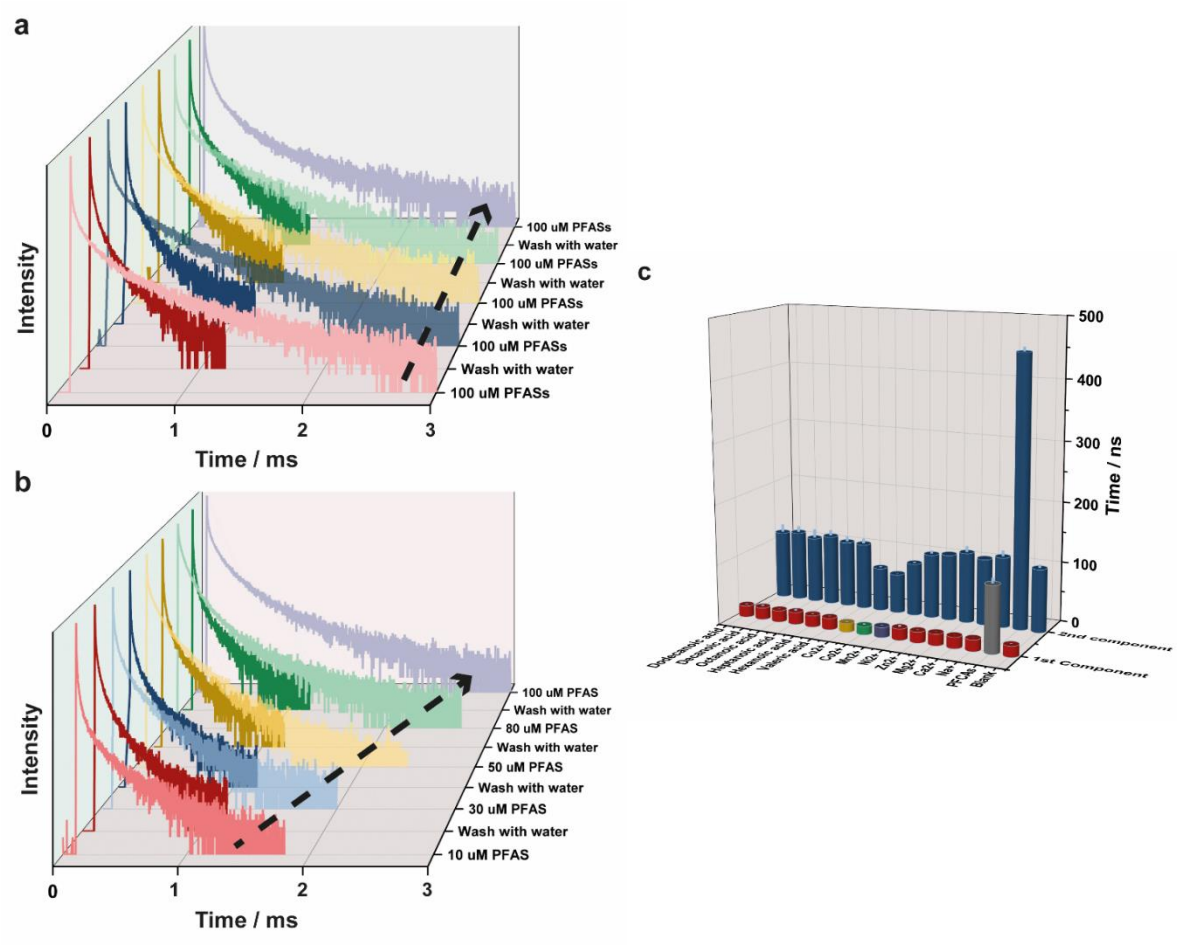

Figure 4.9. (a) Detection of 100 µM concentrations of C_4-C_{10} PFCAs five times by using the same Eu-SAcbisDBM@Au surface. The functionalised surface was washed with milli-Q water everytime after detection. (b) Detection of 10 µM, 30 µM, 50 µM, 80 µM, and 100 µM concentrations of C_4-C_{10} PFCA by the same Eu-SAcbisDBM@Au surface. The functionalised surface was washed with water everytime after detection. (c) Luminescence lifetime of Eu-SAcbisDBM@Au surface in the presence of 100 µM C_4-C_{10} PFCA, 100 µM of Na(I), Ca(II), Mg(II), Zn(II), Ni(II), Mn(II), Co(II) and Cu(II), respectively and 100 µM of valeric acid, hexanoic acid, heptanoic acid, octanoic acid, decanoic acid and dodecanoic acid, respectively.

4.3.8 Waste sample analysis

To evaluate the applicability of the prepared sensor, the Eu-SAcbisDBM@Au surface was tested for the detection of C_4-C_{10} PFCA in 34 samples (Sample information shown in Table S4.3). Before this, all samples were analysed by LC-TOF-MS. As shown in Table 4.4, concentrations of C_4-C_{10} PFCA in the 34 samples ranged between 9 ng/g and 416 ng/g with those in leather (n=5), leatherette (n=23) and fabric (n=6) samples containing 25-320 ng/g, 9-419 ng/g and 59-312 ng/g of C_4-C_{10} PFCAs, respectively. The average concentration of C_4-C_{10} PFCA in leather and leatherette samples was identical at 107 ng/g, while textile samples displayed a higher average concentration of 157 ng/g. Nevertheless, concentrations of C_4-C_{10} PFCA in these three types of sample types vary substantially between individual samples, with standard deviations of ±108 ng/g, ±101 ng/g and ±90 ng/g respectively. Among the 7 PFCA measured, PFOA was present at the highest concentration, comprising up to 89% Σ_7PFCAs in some samples (Figure S4.3). Interestingly, the proportion of long-chained PFNA (average contribution of 12%) and PFDA (12%) is less than the short-chained PFBA (17%) and PFPeA (15%).

Concentrations of C_4-C_{10} PFCAs in the 34 samples analysed using the prepared sensor are reported in Table 4.4. In leather and leatherette samples, C_4-C_{10} PFCAs were detected between 37-467 ng/g and <25-589 ng/g while in textile samples C_4-C_{10} PFCA were detected in the range of 68-401 ng/g. Concentrations detected by the Eu-SAcbisDBM@Au surface are close to the results obtained by LC-TOF-MS, with an accuracy of 71-185% and RSD of 5%-60% (mean: 21%). The difference in concentration values reported by the two methods may be due to several factors: (1) the sample aliquots analysed by the two methods were taken from different regions of the same sample, thus reflecting the inhomogeneous distribution of PFCAs within individual samples; (2) samples contain unknown interfering substances and (3) uncertainty in the LC-TOF-MS based measurements. In conclusion, these data suggest that this luminescence sensor is applicable and reliable for detecting ≥25 ng/g C_4-C_{10} PFCAs in leather, leatherette, and textile samples.

Table 4.4. Concentration (ng/g) of ΣC_4-C_{10} PFCA detected in leather/fabric samples: (a) by LC-TOF-MS, (b) by Eu-SAcbisDBM@Au surface (n=3).

Sample #	Concentration of ΣC_4-C_{10} PFCAs (ng/g) measured by: LC-TOF-MS								Sensor	Accuracy[a] %	RSD %
	PFBA	PFPeA	PFHxA	PFHpA	PFOA	PFNA	PFDA	PFAS total			
Leather											
001	28	8	6	6	32	2	<0.07	80	133±41	165	31
002	52	16	24	17	56	86	70	320	467±46	146	10
003	12	13	4	3	20	4	5	62	97±9	156	9
004	2	6	15	2	13	3	6	48	49±22	102	45
005	2	4	4	2	<0.05	5	7	25	37±10	146	27
Range	2-52	4-16	4-24	2-17	<0.05-56	2-86	<0.07-70	25-320			
Average	19	9	11	6	30	20	22	107			
Median	12	8	6	3	26	4	7	62			
Leatherette											
006	14	6	84	156	23	83	20	387	501±66	130	13
007	25	9	9	25	26	3	3	99	114±6	115	5
008	25	14	13	10	18	55	2	138	127±7	92	6
009	12	4	<0.12	4	24	32	<0.07	76	82±10	108	12
010	15	7	8	7	71	13	2	124	135±11	109	8
011	40	13	110	101	47	90	16	416	589±69	141	12
012	25	15	12	19	16	9	9	104	131±29	126	22
013	10	5	<0.12	<0.15	14	<0.08	<0.07	29	41±11	142	27
014	4	5	<0.12	<0.15	<0.05	<0.08	<0.07	9	<25	-	-

015	15	16	4	4	19	6	8	72	106±10	148	9
016	11	13	<0.12	5	14	5	8	55	82±6	149	7
017	12	14	5	5	16	6	8	67	97±41	146	42
018	11	9	4	3	<0.05	5	7	40	62±37	156	60
019	8	15	6	7	17	11	17	80	92±25	114	27
020	33	12	13	15	30	24	32	159	241±25	152	10
021	12	11	7	12	23	20	25	110	156±54	142	35
022	19	18	23	3	112	4	12	191	273±38	143	14
023	5	4	<0.12	2	18	2	6	37	46±12	123	26
024	5	9	<0.12	3	15	5	8	45	54±18	119	33
025	4	3	<0.12	<0.15	<0.05	2	3	13	<25	-	-
026	8	10	4	4	15	4	11	56	40±17	71	43
027	11	19	10	4	17	12	15	89	140±27	157	19
028	3	10	7	3	14	6	13	57	73±13	129	18
Range	3-40	3-19	<0.12-110	<0.1-156	<0.05-112	<0.08-90	<0.07-32	9-419			
Average	14	10	20	20	27	19	11	107			
Median	12	10	9	5	18	6	8	76			
Textile											
029	12	9	<0.12	19	14	2	2	59	68±16	116	24
030	27	29	41	30	53	28	37	244	250±71	102	28
031	24	11	8	13	43	4	6	109	121±32	111	26
032	10	14	24	15	20	2	7	90	167±48	185	29
033	17	18	9	10	33	16	23	125	153±14	122	9

034	4	5	4	4	277	6	11	312	401±72	129	18
Range	4-27	5-29	4-41	4-30	14-277	2-28	2-37	59-312			
Average	16	14	17	15	73	10	14	157			
Median	15	12	9	14	38	5	9	117			

-: No data available

[a]Accuracy expressed as ratio of concentration recorded via sensor to that recorded via LC-TOF-M

4.4 Conclusion

This study presents the development of a novel luminescence lifetime-based sensing surface for detecting PFCA in various materials, including leather, leatherette, and textiles. Characterization of the modified surface was conducted using various techniques such as SEM-EDX, XPS and Raman spectroscopy, confirming the successful surface modification. Luminescence lifetime variation demonstrated the sensor's excellent sensitivity to PFCA. Also, the sensor exhibited outstanding reproducibility, reusability and minimal interference from other substances. While the sensor does not specifically target PFOA and might sometimes give higher concentration readings, it can easily identify PFCA levels as low as 0.03 mg/kg based on the real sample analysis test. This capability allows the user to check whether the concentration of PFOA exceed the EU LPCL limit of 1 mg/kg. While our sensor is specifically validated for C_4-C_{10} PFCAs, it's important to note that longer or shorter chain PFCAs, such as C_{11}-C_{14} PFCA and C_3 PFCA, could potentially interfere with the detection due to their similar chemical structures. However, given the vast number of these compounds, it is impractical to test them all.

To improve the sensor's performance, several strategies can be employed: (1) implementing pre-concentration steps like SPE to reduce interference, (2) using alternative materials such as plasmonic gold surfaces, and (3) optimizing the ratio and arrangement of Eu(III) and SAcbisDBM ligands on the surface. Despite its limitations, this sensor offers a promising solution to address a major environmental concern. Overall, this study provides a highly sensitive, selective, and portable tool for PFCA detection, which holds promise for practical applications in environmental monitoring and regulatory compliance.

Chapter 5: NIR Detection of PFOA, PFNA and PFDA *via* Nd(III)/Yb(III)-SAcbisDBM in Solution and Immobilised on Plasmonic Gold Surface

5.1 Introduction

5.1.1 NIR emission by Nd(III) and Yb(III)

In the field of luminescent materials, rare earth elements have long been valued for their extraordinary photophysical properties. Among these elements, neodymium(Nd) and ytterbium(Yb) stand out as promising candidates for near-infrared (NIR) emission, an essential wavelength range in fields such as bioimaging,[212, 213] telecommunications,[214] and optical sensing.[215, 216] Yb(III) and Nd(III) are the most studied NIR emitting lanthanides(III), with their emission collectively covering the 850-1650 nm spectral range.[217]

Nd and Yb exhibit sharp, distinctive emission bands, substantial pseudo-Stokes shifts, and remarkable luminescence lifetimes that can extend up to milliseconds.[218, 219] This prolonged luminescence lifetime provides a distinct advantage in sensing applications.[220] Additionally, their NIR emissions serve to mitigate scattering effects, a key benefit in analytical and imaging techniques.[217] Furthermore, operating within the NIR range significantly reduces interference from autofluorescence, commonly encountered in complex samples, further enhancing their utility in various scientific disciplines.[221]

While the luminescent properties of lanthanides(III) ions have captured considerable attention, their application in flat surface complexes remains surprisingly limited. This is attributed to the vibrational excitation of C-H and O-H bonds, which renders Nd(III) and Yb(III) less inclined to exhibit NIR luminescence in aqueous and most organic environments.[222] Strikingly, the utilisation of NIR-emitting lanthanides(III) in such context is notably sparse, with only one instance of a Yb(III) self-assembled

monolayer (SAM) on gold reported, yet no emission could be recorded.[223]

5.1.2 Reinstatement of Ln(III) luminescence

As with the other lanthanides, the emission of Nd and Yb originates from formally forbidden f-f transitions, resulting in extremely low molar absorption coefficients (1-10 $dm^3mol^{-1}cm^{-1}$).[224] Additionally, NIR-emitting lanthanides (III) are highly susceptible to radiationless deactivation caused by high-energy vibrations, owing to the narrow energy gaps between their primary emissive states and the final states.[225] Thus, a proper ligand capable of not only efficiently absorbing and transferring energy to the metal ions but also shielding the lanthanides(III) from the influence of high-energy oscillations is highly desirable.

Among various ligands, β-diketones, a well-known class of acyclic ligands for lanthanides(III), offer notable advantages.[226] Unlike macrocyclic ligands, β-diketones provide superior flexibility and facile metal complexation.[227] As lanthanides(III) act as hard Lewis acids, the negatively charged oxygen atoms within the diketone structure prove to be ideal coordination sites for these ions, facilitating the formation of triple or quadruple-stranded architectures.[228] Notably, bis-β-diketones, featuring two binding sites, enable the incorporation of two lanthanides(III) ions and demonstrate exceptional luminescent properties, with luminescence signals up to 11 times more intense compared to their mononuclear counterparts.[202] Moreover, the terminal units of bis-β-diketones can be tailored to customize the properties of the resulting complexes.

In this study, we utilised a surface-active ligand derived from a novel bis-βdiketonate compound, which was synthesized by our colleague,[203] namely **SAcbisDBM ligand**. The SAcbisDBM ligand exhibits notably high molar absorption coefficients (in the order of 10^5 dm^3mol^{-1} cm^{-1}), making it exceptionally efficient for light harvesting. Furthermore, the complexes formed between SAcbisDBM ligands and lanthanides(III) display robust luminescence, spanning either the visible or NIR regions of the electromagnetic spectrum.

5.1.3 NIR luminescence detection of PFOA, PFDA and PFNA

In this section, we explore the detection of PFOA, PFNA, and PFDA using Nd-SAcbisDBM and Yb-SAcbisDBM either in solvent or immobilised at plasmonic gold (pAu) surface (Figure 5.1). The SAcbisDBM ligand facilitates the reinstatement of NIR luminescence for Nd(III) and Yb(III). pAu is highly efficient at absorbing and scattering light, which is able to increase the sensitivity of the emitter anchored on it.[229] Moreover, the presence of numerous isolated gold islands, each with a size of tens of nanometres on the pAu surface, effectively mitigates the quenching of the lanthanide luminescent complexes caused by aggregation.[230] Regarding detection, PFOA, PFNA, and PFDA, which possess hydrophilic groups and lipophobic chains, may disrupt the local environment of neodymium and ytterbium, leading to changes in luminescence intensity and lifetime. We elucidate this relationship through various surface characterization and analytical techniques. This study contributes to a deeper understanding of how Nd(III) and Yb(III) complexes interact with solid materials, thereby opening up possibilities for their integration into various applications.

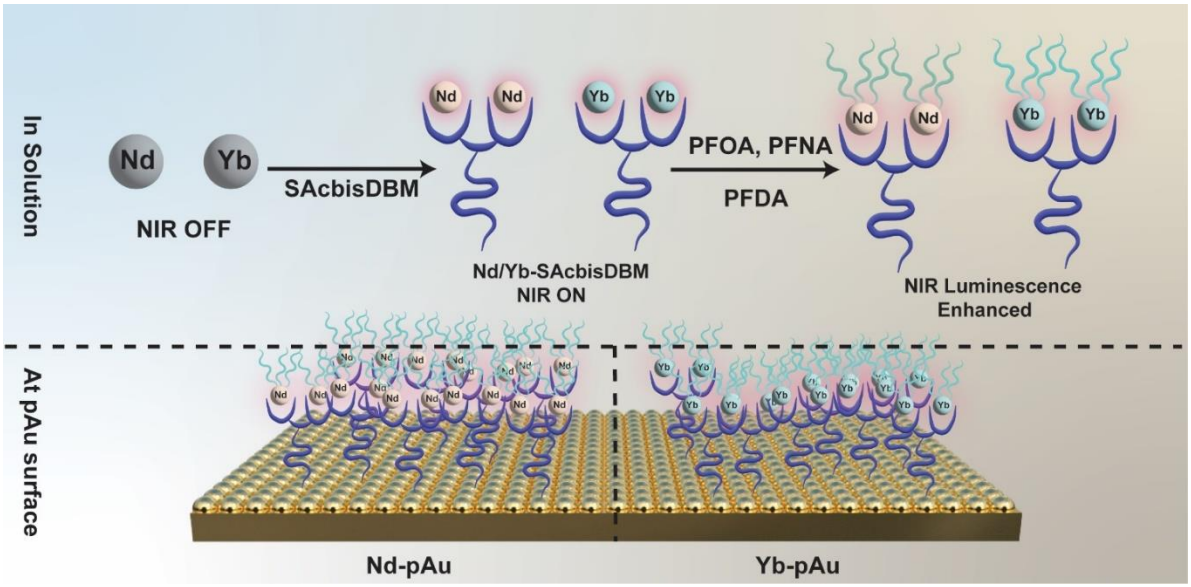

Figure 5.1. Schematic diagram of Nd-SAcbisDBM and Yb-SAcbisDBM in MeOH-Water solution (up) and immobilised on pAu surface (down).

5.2 Experimental

5.2.1 Preparation of Nd/Yb-SAcbisDBM

The synthesis of the SAcbisDBM ligand follows the procedure outlined in Chapter IV, Part 4.2.1.

To prepare Nd-SAcbisDBM and Yb-SAcbisDBM, 50 µM of $NdCl_3 \cdot 6H_2O$ and 50 µM of $YbCl_3 \cdot 6H_2O$ were separately dissolved in a MeOH - H_2O solution (3:7, v/v). Subsequently, 20 µM of the SAcbisDBM ligand was added to each solution. The Nd-SAcbisDBM and Yb-SAcbisDBM solutions should be stored in a nitrogen environment and kept away from light.

5.2.2 Preparation of Nd/Yb-functionalised surface

The plasmonic gold (pAu) slides underwent a thorough rinsing process with acetone followed by milli-Q water, repeated three times to ensure removal of all organic residues from the surface. Subsequently, the cleaned surfaces were dried under a stream of nitrogen and stored in a nitrogen environment.

The SAcbisDBM@pAu surface was prepared by immersing the clean pAu surfaces in a SAcbisDBM solution (1 mM in THF) for 18 hours. The modified surface was then washed with small amounts of tetrahydrofuran and dried under a stream of nitrogen.

To immobilize Nd(III) and Yb(III) at the pAu surface, namely **Nd-pAu** surface and **Yb-pAu** surface, the SAcbisDBM@Au surfaces were immersed in $NdCl_3$ solution (10 mM in H_2O) and YbCl3 solution (10 mM in H_2O), respectively, for 18 hours. Following immersion, the modified surfaces were washed with milli-Q water and subsequently dried under a stream of nitrogen.

5.3 Results and discussion

5.3.1 Morphologies of Nd(III)/Yb(III)-SAcbisDBM in solution and at pAu surface

Scanning electron microscopy (SEM) was used to observe the morphology of the SAcbisDBM ligand, and the ligand coordinated with Nd(III) and Yb(III) in a 30% MeOH-water solution, as well as when

immobilised on the pAu surface. In the MeOH-H_2O solution (3:7, v/v), the SAcbisDBM ligand formed well-dispersed spheres with a measured diameter of approximately 210±40 nm (Figure S5.2a). Upon coordination with Nd(III) and Yb(III), the morphology of the ligand remained unchanged, with the spheres maintaining a size of around 220±40 nm (Figure S5.1a,b). Energy Dispersive Spectroscopy (EDS) analysis confirmed the presence of carbon, neodymium, and ytterbium in the particles, confirming the successful coordination of Nd(III) and Yb(III) to the SAcbisDBM ligand (Figure S5.1c). Interestingly, the atomic ratios of C to Nd and C to Yb were found to be 93:7 and 94:6, respectively, implying that each SAcbisDBM ligand is bound with 2.3 Nd(III) ions and 2.0 Yb(III) ions, consistent with theoretical expectations. Unsurprisingly, upon the addition of PFCA (herein, PFDA), the morphology of the Nd-SAcbisDBM and Yb-SAcbisDBM remained unchanged (Figure S5.2b and Figure S5.2c).

In contrast to the observations made in Chapter IV, where the ligand was affixed to a plain gold surface, in this study, the ligand is anchored on the pAu surface. Interestingly, the pAu surface exhibits numerous gold islands, a feature not observed on the plain gold surface (Figure S5.1d). The morphology of the SAcbisDBM ligand on the pAu surface is observed in the formation of numerous closely connected granular substances, with an average diameter of approximately 85 nm (Figure S5.1d). Upon coordination with Nd(III) and Yb(III), and in the presence of PFCA (specifically PFDA), there were no discernible differences in morphology compared to the SAcbisDBM@pAu surface (Figure S5.1d and Figure S5.1e), consistent with the findings of the previous chapter.

5.3.2 Raman spectroscopy of Nd(III)/Yb(III)-SAcbisDBM at pAu surface

Raman spectroscopy was used to analyse the pAu surface coated with SAcbisDBM ligand, and after the coordination of Nd(III) and Yb(III), respectively. As shown in Figure 5.2a, consistent with previous finding where the SAcbisDBM ligand coated on plain gold surface (part 4.3.4), the Raman spectra of the SAcbisDBM@pAu surface displays peaks at 1000 cm^{-1}, 1278 cm^{-1}, 1360 cm^{-1}, 1549 cm^{-1} and 1600 cm^{-1}, respectively. They could be assigned to the vibration of aromatic ring and C-C aliphatic chain, C-CH_3, N=N, and C=O and C=C, respectively.[207] These observations align with the molecular structure of

the SAcbisDBM ligand. Upon coordination with Nd(III) and Yb(III), additional peaks around 260 cm^{-1} are observed in the Raman spectra of the Nd-pAu surface (Figure 5.2b) and Yb-pAu surface (Figure 5.2c), respectively. These peaks can be attributed to the vibrations of Nd-O and Yb-O,[207] confirming the binding of Nd(III) and Yb(III) to the SAcbisDBM ligand.

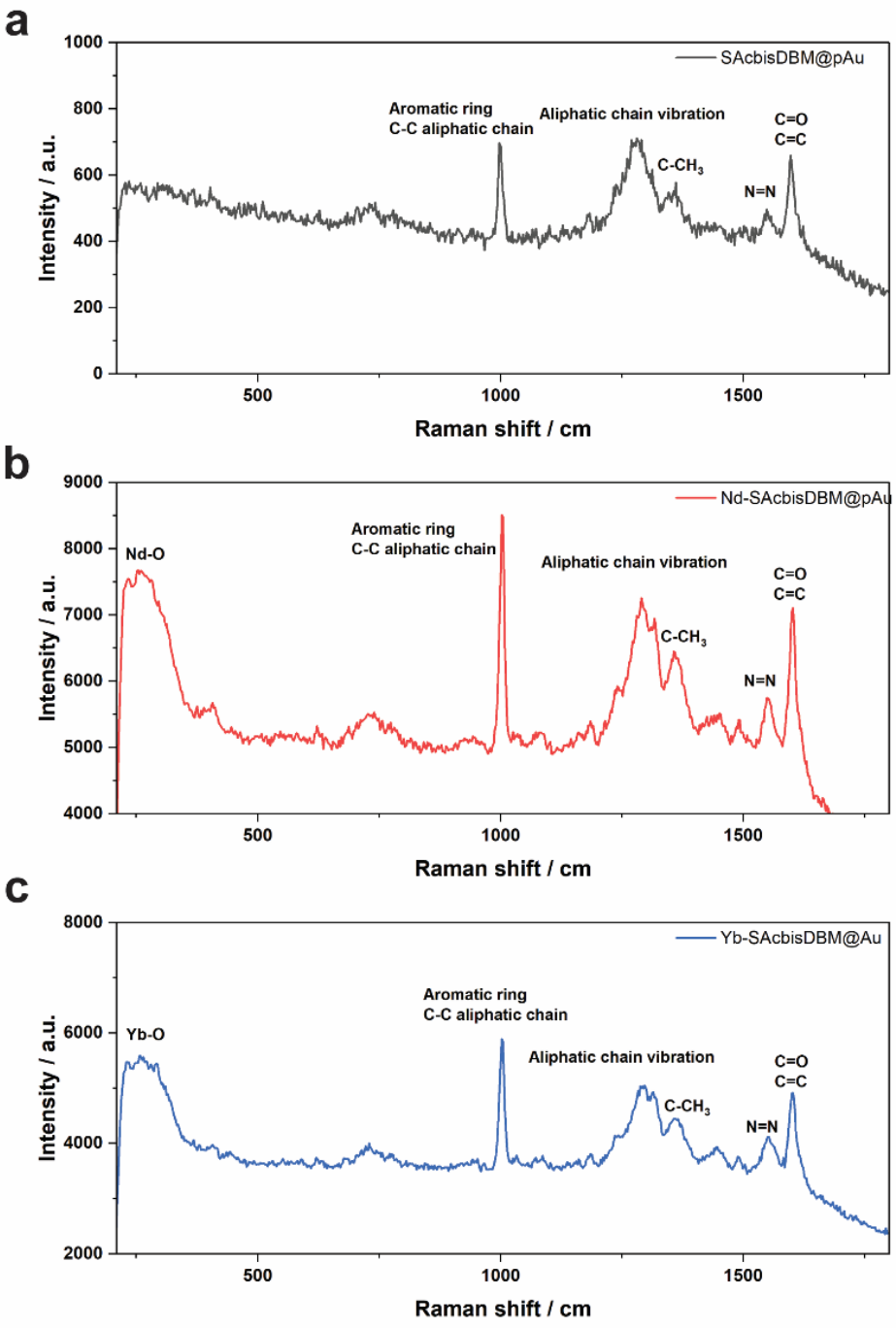

Figure 5.2. Raman spectrum of (a) SAcbisDBM@pAu surface (b) Nd-pAu surface and (c) Yb-pAu surface.

5.3.3 Optical behaviour of Nd(III) and Yb(III)

Due to the presence of C-H and O-H bonds near NIR-emitting lanthanides (III), effective radiationless transitions can occur through vibrational excitation, making it challenging to record emission spectra and lifetime spectra for Nd(III) and Yb(III) in both water and MeOH.[222] However, after coordinating to the SAcbisDBM ligand, Nd(III) and Yb(III) exhibit NIR luminescence at 1060 nm and 980 nm ($^2F_{5/2} \rightarrow {}^2F_{7/2}$), respectively, in 30% MeOH-water solution (Figure 5.3a and Figure 5.3c). Notably, the emission wavelength of the Nd-SAcbisDBM and Yb-SAcbisDBM remain unchanged upon immobilization at the pAu surface (Figure 5.3a and Figure 5.3c). In terms of luminescence lifetime spectra, Nd-SAcbisDBM shows a lifetime of 1.13 µs (31%), 1.13 µs (19%), 9.05 µs (50%) in solution, while its surface coating displays a slightly lower lifetime of 1.09 µs (20%), 1.09 µs (30%), 8.89 µs (50%) (Figure 5.3b). Yb-SAcbisDBM, on the other hand, demonstrates a higher lifetime of 1.59 µs (29%), 5.08 µs (36%), 15.3 µs (34%) in solution compared to Nd-SAcbisDBM, while its surface coating shows a lifetime of 1.30 µs (37%), 4.57 µs (31%), 13.6 µs (32%) (Figure 5.3d). The appearance of the emission spectrum and lifetime spectrum confirms that the SAcbisDBM ligand enhances the luminescence sensitisation of NIR emitting lanthanide(III).

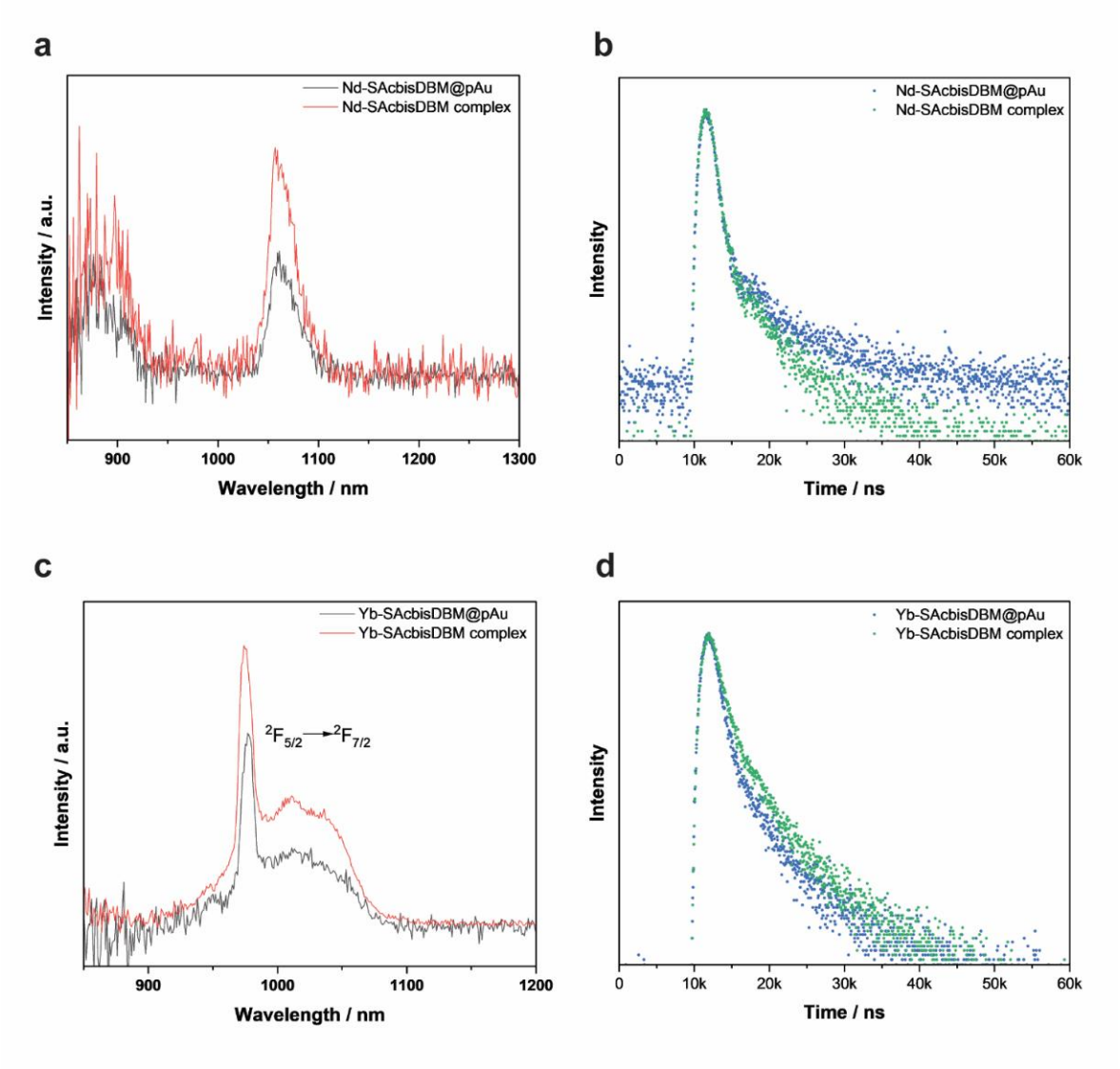

Figure 5.3. (a) Emission spectrum of Nd-SAcbisDBM in 30% MeOH-water solution and immobilised at the pAu surface. (b) Luminescence lifetime spectra of Nd-SAcbisDBM in 30% MeOH-water solution and immobilised at the pAu surface. (c) Emission spectrum of Yb-SAcbisDBM in 30% MeOH-water solution and immobilised at the pAu surface. (d) Luminescence lifetime spectra of Yb-SAcbisDBM in 30% MeOH-water solution and immobilised at the pAu surface.

5.3.4 Optimization of the Nd-SAcbisDBM luminescence

Due to space constraints, this paper only conducted the optimisation of Nd-SAcbisDBM. The conditions set for Yb-SAcbisDBM refer to those of Nd-SAcbisDBM.

The NIR luminescence of the Nd-SAcbisDBM complex is primarily influenced by the concentration of the SAcbisDBM ligand rather than the concentration of Nd(III) and Yb(III). Evidence shown in Figure 5.4a, there is barely any change in the emission intensity using different concentrations (0.05 mM, 0.1 mM, 1 mM, and 10 mM) of Nd(III) to coordinate with SAcbisDBM ligand. Interestingly, the emission intensity of Nd(III) (0.05 mM) increases as the concentration of SAcbisDBM ligand (20 µM, 40 µM, 60 µM, and 80 µM) increases (Figure 5.4b). Among these concentrations, the 80 µM SacbisDBM ligand showed the greatest efficiency in enhancing the luminescence of Nd(III) and Yb(III). However, to conserve reagents, the concentrations of Nd(III) and SAcbisDBM ligand were maintained at 0.05 mM and 20 µM, respectively.

We proceeded to investigate the influence of solvents on the luminescence of the Nd-SAcbisDBM. As depicted in Figure 5.4c, the complex displayed varying emission intensities in THF-water solution (1:1, v/v), MeCN-water solution (1:1, v/v), MeOH-water solution (1:1, v/v), and water. The strongest luminescence was observed in water, followed by MeOH, MeCN, and THF, indicating that polar solvents enhance the luminescence of Nd(III). Further analysis was conducted to assess the impact of the percentage of MeOH (MeOH%) on luminescence. As illustrated in Figure 5.4d, the Nd-SAcbisDBM complex exhibited its weakest luminescence in a 100% MeOH solution while demonstrating the strongest luminescence in 100% water. However, the luminescence remained relatively consistent at MeOH proportions of 30%, 50%, and 70%.

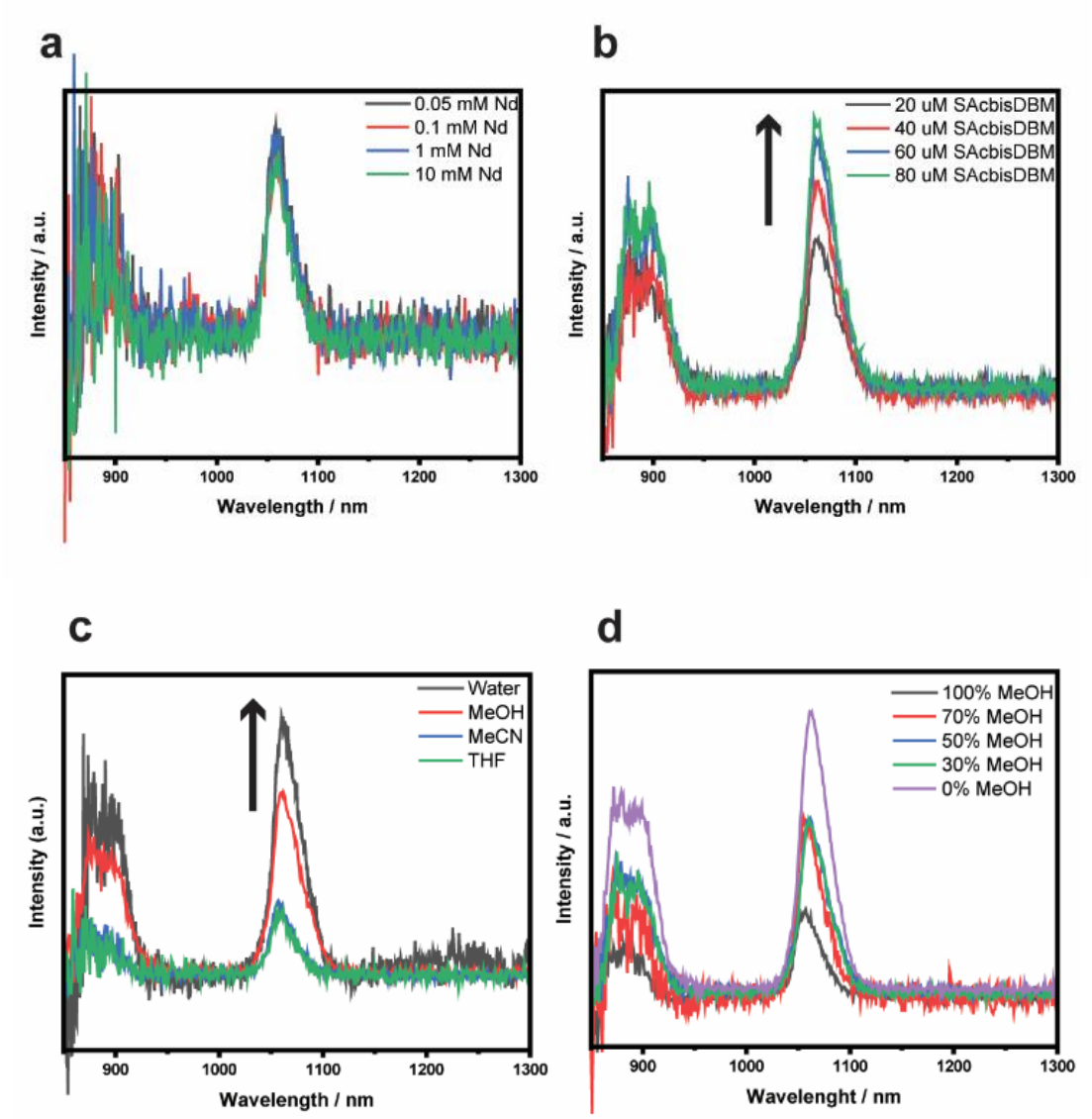

Figure 5.4. Emission spectra of 0.05 mM, 0.1 mM, 1 mM and 10 mM Nd(III) water solution containing 20 µM SAcbisDBM ligand dissolved in MeCN. (b) Emission spectra of 0.05 mM Nd(III) water solution containing 20 µM, 40 µM, 60 µM and 80 µM SAcbisDBM ligand dissolved in MeCN. (c) Emission spectra of 0.05 mM Nd(III) with 20 µM SAcbisDBM ligand dissolved in water, MeOH-water solution (1 : 1, v/v), MeCN-water solution (1 : 1, v/v) and THF-water solution (1 : 1, v/v), respectively. (d) Emission spectra of 0.05 mM Nd(III) with 20 µM SAcbisDBM ligand dissolved in 0%, 30%, 50%, 70% and 100% MeOH-water solution, respectively.

5.3.5 Effect of PFCA on the luminescence of Nd-SAcbisDBM

The Nd-SAcbisDBM demonstrated a significant increase in emission intensity upon the addition of PFCA (exemplify by PFOA). As depicted in Figure 5.5a to Figure 5.5c, the luminescence of Nd-SAcbisDBM dissolved in 30%, 50%, and 70% MeOH-water solutions exhibited varying degrees of enhancement with the addition of PFOA. Particularly, at 30% MeOH (Figure 5.5a), PFOA proved to be the most effective in enhancing the luminescence of Nd-SAcbisDBM, with this effect diminishing as the percentage of MeOH increased. Minimal improvement in luminescence was observed for Nd-SAcbisDBM dissolved in 70% MeOH upon the addition of PFOA (Figure 5.5c), with no noticeable impact on luminescence observed in 100% MeOH. Consequently, the subsequent experiments will utilise a 30% MeOH-water solution.

Furthermore, we explored the influence of other PFCA, such as PFNA and PFDA, on the luminescence of the Nd-SAcbisDBM complex. The prepared sensor chips were not tested on the C_4-C_7 PFCAs because preliminary experiments showed they were less effective in enhancing the luminescence of Nd(III) and Yb(III) compared to PFOA, PFNA, and PFDA. As for C11 and PFCA with longer length, we did not include them in our tests due to the unavailability of relevant standard samples. Our findings revealed that both PFNA and PFDA could enhance the emission intensity of the Nd-SAcbisDBM (Figure 5.5d). Interestingly, PFDA (C10) exhibited the most significant increase in luminescence, followed by PFNA (C9) and PFOA (C8). This observation suggests that the longer fluorocarbon chain of these PFCA may play a more significant role in preventing the quenching of Nd(III) by C-H or O-H bonds.

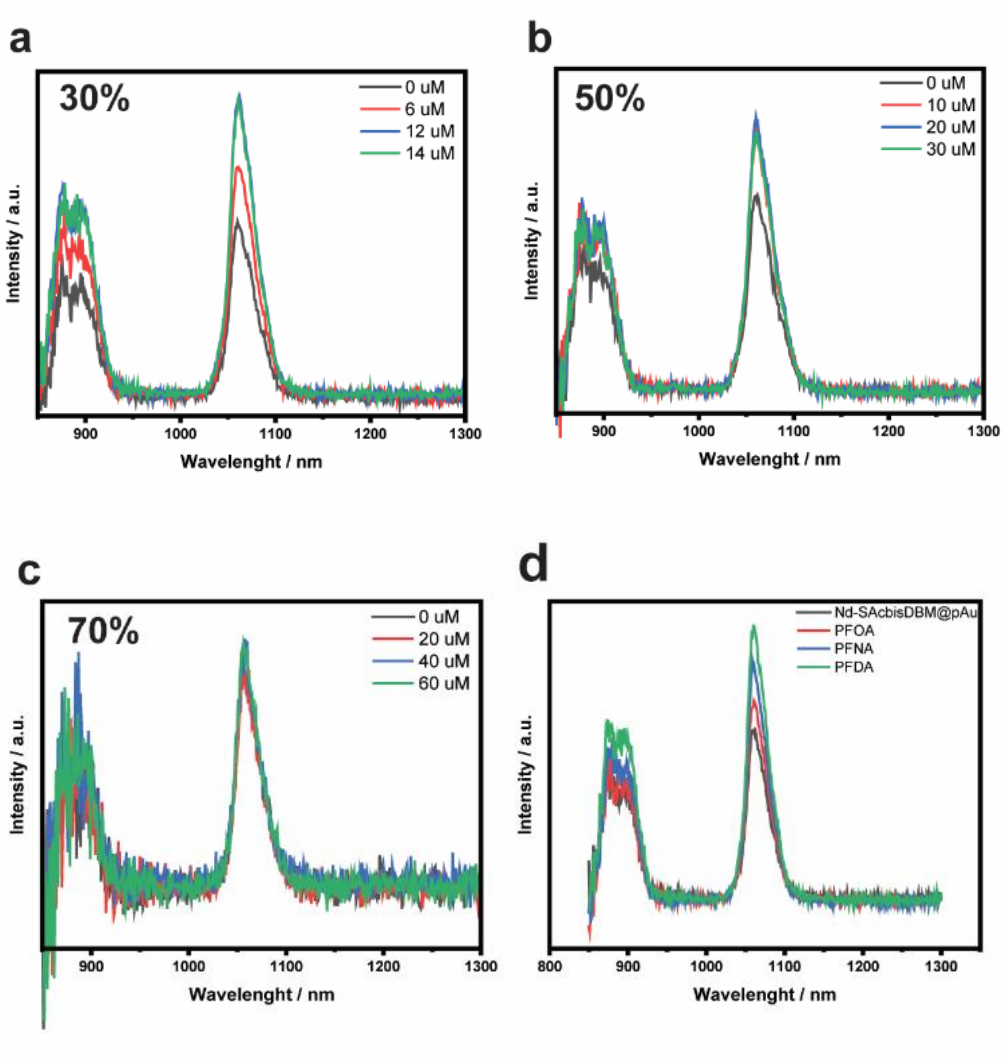

Figure 5.5. (a) Emission spectra of Nd-SAcbisDBM upon the addition of 6 µM, 12 µM and 14 µM PFOA, solvent: 30% MeOH-water solution. (b) Emission spectra of Nd-SAcbisDBM upon the addition of 0 µM, 10 µM, 20 µM and 30 µM PFOA, solvent: 50% MeOH-water solution. (c) Emission spectra of Nd-SAcbisDBM upon the addition of 0 µM, 20 µM, 40 µM and 60 µM PFOA, solvent: 70% MeOH-water solution. (d) Emission spectra of Nd-SAcbisDBM upon the addition of 8 µM PFOA, 8 µM PFNA and 8 µM PFDA, respectively, solvent: 30% MeOH-water solution.

5.3.6 Effect of PFCA on the luminescence of Ln-functionalised surface

As depicted in Figure 5.6a and Figure 5.6c, both the Nd-pAu surface and Yb-pAu surface exhibit a discernible augmentation in emission intensity upon the addition of PFOA, PFNA, and PFDA. Among these PFCA, PFDA elicits the most pronounced enhancement, increasing the emission intensity by approximately 68% for Nd-SAcbisDBM and 35% for Yb-SAcbisDBM. Additionally, PFNA and PFOA induce enhancements of approximately 30% and 17%, respectively, for Nd-SAcbisDBM, and approximately 7% and 14%, respectively, for Yb-SAcbisDBM.

The corresponding lifetime spectra, as illustrated in Figure 5.6b and Figure 5.6d, reveal a similar trend, although the amplification is less conspicuous. According to the calculated results (Table 5.1), the lifetime of the Nd-pAu surface increases to 1.0 µs (40%), 5.0 µs (24%), and 12.1 µs (36%) upon the addition of PFDA, compared to that without adding PFDA, where it showed a lifetime of 1.1 µs (34%), 1.1 µs (23%), and 8.2 µs (43%), respectively. Similarly, the lifetime of the Yb-pAu surface increases from 1.9 µs (34%), 3.0 µs (30%), and 10.6 µs (35%) to 1.6 µs (29%), 5.7 µs (33%), and 13.8 µs (38%). For the modified surfaces with the addition of PFNA and PFDA, the luminescence lifetime spectra also display varying increases, with details provided in Table 5.1.

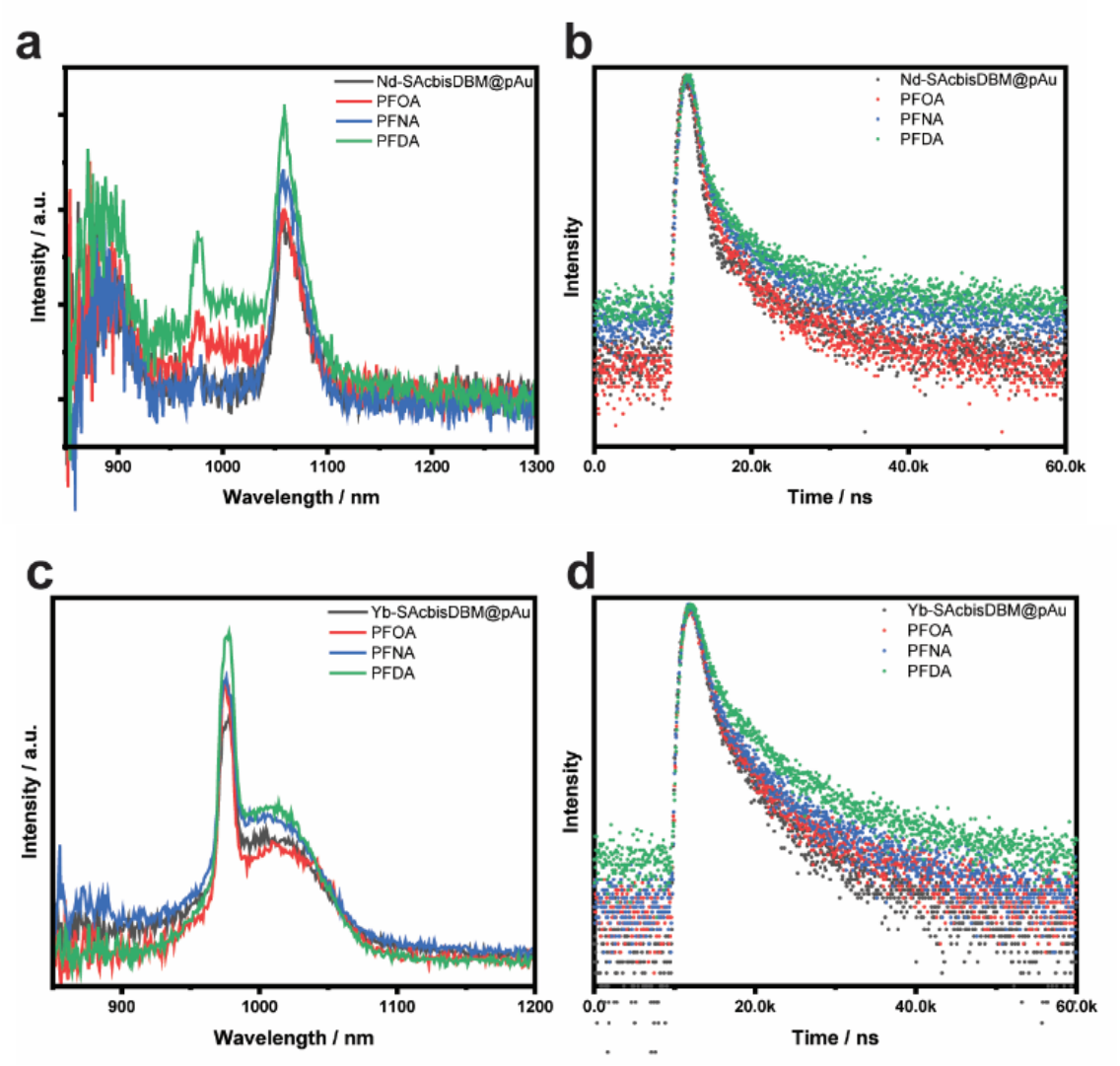

Figure 5.6. (a) Emission spectra of Nd-pAu surface with the addition of 20 nmol PFOA, PFNA and PFDA, respectively. (b) luminescence lifetime spectra of Nd-pAu surface with the addition of 20 nmol PFOA, PFNA and PFDA, respectively. (c) Emission spectra of Yb-pAu surface with the addition of 40 nmol PFOA, PFNA and PFDA, respectively. (d) luminescence lifetime spectra of Yb-pAu surface with the addition of 40 nmol PFOA, PFNA and PFDA, respectively.

Table 5.1. Summary of luminescence lifetime of Nd-pAu surface and Yb-pAu surface, and their alteration with addition of PFDA, PFNA and PFOA, respectively. Used amount of PFDA, PFNA and PFOA: 20 nmol for Nd-pAu surface and 40 nmol for Yb-pAu surface.

Sample	τ / µs		
	1st component	2nd component	3rd component
Nd-pAu surface	0.94 (28%)	0.94 (24%)	8.7 (49%)
Nd-pAu surface + PFDA	1.02 (32%)	4.2 (28%)	11.8 (40%)
Nd-pAu surface + PFNA	0.87 (25%)	4.08 (36%)	11.6 (39%)
Nd-pAu surface +PFOA	1.3 (36%)	1.3 (17%)	9.3 (47%)
Yb-pAu surface	1.4 (33%)	4.8 (31%)	12.9 (36%)
Yb-pAu surface + PFOA	1.5 (38%)	4.7 (27%)	13.2 (35%)
Yb-pAu surface + PFNA	1.3 (37%)	4.6 (31%)	13.6 (31%)
Yb-pAu surface + PFDA	1.5 (38%)	5.4 (24%)	15.0 (38%)

5.3.7 Analytical performance of the Nd/Yb-SAcbisDBM for PFDA

An extensive study was undertaken to assess the sensing capabilities of the Nd/Yb-SAcbisDBM toward PFDA. As depicted in Figure 5.7a and Figure 5.7b, the luminescence of Nd-SAcbisDBM and Yb-SAcbisDBM display a linear relationship with the concentrations of PFDA falling in the ranges of 2 µM to 14 µM and 10 µM to 35 µM. This phenomenon can be attributed to PFDA coordinating with Nd(III)/Yb(III) and displaced with H_2O and methanol molecules, preventing quenching of the Nd/Yb-SAcbisDBM from the vibrational excitation of C-H and O-H bonds. Specifically, the emission intensity of the Nd-SAcbisDBM increased by up to 2.4-fold, while that of the Yb-SAcbisDBM increased by up to 1.3-fold. Their relationship is expressed as follows:

For the Nd-SAcbisDBM complex (2 µM to 14 µM PFDA):

$$I/I_0 = 0.1101\ C_{PFDA}\ (\mu M) + 0.9615,\ R^2 = 0.9835,\ (5.1)$$

For the Yb-SAcbisDBM complex (10 µM to 35 µM PFDA):

$$I/I_0 = 0.0077\ C_{PFDA}\ (\mu M) + 1.0052,\ R^2 = 0.9971,\ (5.2)$$

Where I_0 and I represent the peak area of Nd/Yb-SAcbisDBM before and after the addition of PFDA, respevtively.

As the PFDA concentration was further increased, the luminescence of the Nd-SAcbisDBM and Yb-SAcbisDBM remained stable within the ranges of 14 µM to 20 µM and 35 µM to 50 µM, respectively (Figure 5.7a and Figure 5.7b).

However, upon the addition of PFDA exceeding 20 µM in Nd-SAcbisDBM and 50 µM in Yb-SAcbisDBM, a significant decrease in luminescence was observed, and accompanied by the production of precipitation (Figure 5.7c and Figure 5.7d). The relationships are shown as follows:

For the Nd-SAcbisDBM complex (20 µM to 55 µM PFDA):

$$I/I_0 = -0.016\ C_{PFDA}\ (\mu M) + 1.3323,\ R^2 = 0.9892,\ (5.3)$$

For the Yb-SAcbisDBM complex (50 µM to 500 µM PFDA):

$$I/I_0 = -0.0017\ C_{PFDA}\ (\mu M) + 1.0743,\ R^2 = 0.9861,\ (5.4)$$

Here, I_0 represents the peak area of Nd-SAcbisDBM with the addition of 20 µM PFDA, or Yb-SAcbisDBM with the addition of 50 µM PFDA, while I represents the peak area with further increases in PFDA concentration.

Due to time constraints, some of the experiments were conducted only once and did not include parallel measurements. While this limitation may affect the reproducibility of the results, the data obtained still provide valuable insights into the performance of the sensor.

To explore the connection between the decrease in luminescence and the formation of precipitation, UV-vis spectroscopy was employed to track changes in the absorbance spectrum of the Nd-SAcbisDBM in the presence of PFDA. As demonstrated in Figure S5.3, there was a substantial decrease in absorption peaks at 243 nm and 375 nm. Remarkably, when PFDA was combined with the SAcbisDBM ligand alone, no precipitation occurred; however, upon subsequent addition of Nd(III)/Yb(III), precipitation ensued immediately. This suggests that there is a strong interaction between PFDA and Nd(III) and

Yb(III). Additionally, to confirm that the reduction in luminescence was not solely due to a change in the concentration of the probe solution resulting from the addition of water, we conducted a control experiment. As illustrated in Figure S5.4, the luminescence of the Nd-SAcbisDBM exhibited a slight decline with the addition of up to 200 µL of water. In comparison, the effect of adding PFOA exceeding 20 µM displayed a significant decrease (Figure 5.7c). It is evident that the significant decrease in luminescence is primarily influenced by PFDA.

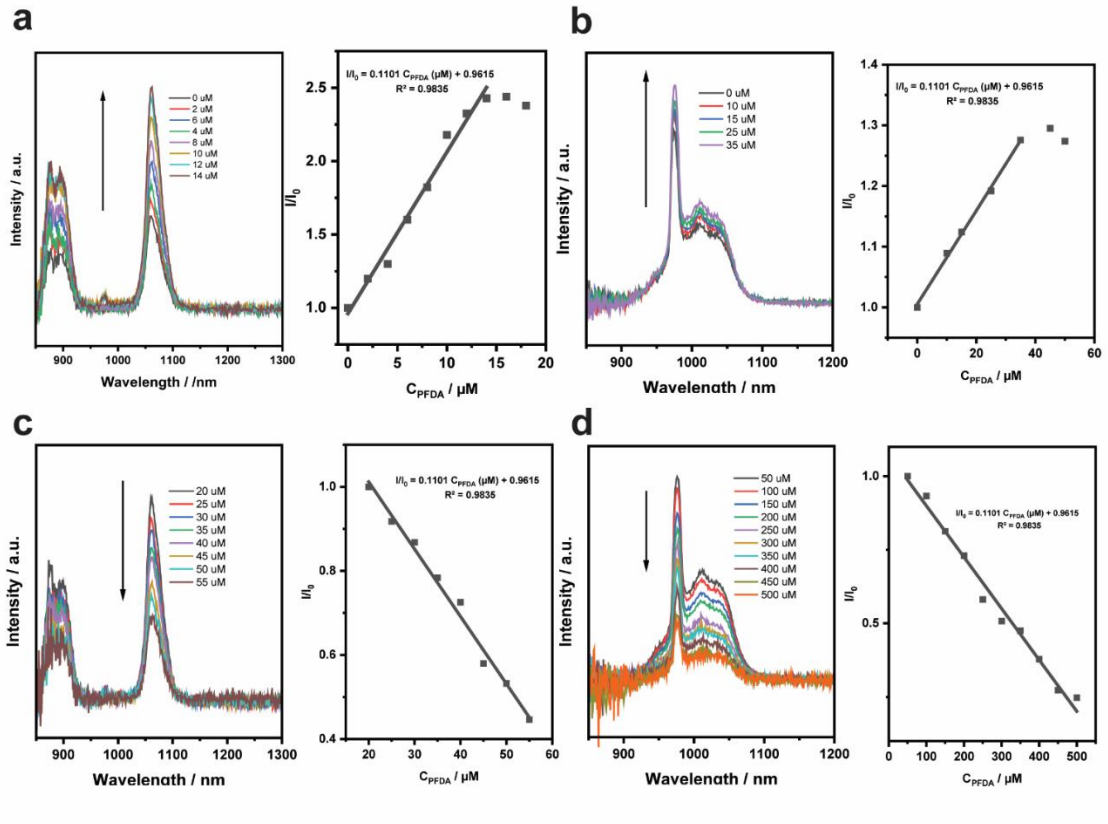

Figure 5.7. (a) Emission spectrum of Nd-SAcbisDBM with the addition of 2 µM to18 µM PFDA and its corresponding calibration curves. λ_{em} = 1060 nm, Solvent: 30% MeOH-Water solution. (b) Emission spectrum of Yb-SAcbisDBM with the addition of 20 µM to 55 µM PFDA and its corresponding calibration curves. λ_{em} = 976 nm, Solvent: 30% MeOH-Water solution. (c) Emission spectrum of Nd-SAcbisDBM with the addition of 10 µM to 35 µM µM PFDA, λ_{em} = 1060 nm and its corresponding calibration curves. Solvent: 30% MeOH-Water solution. (d) Emission spectrum of Yb-SAcbisDBM with the addition of 50 µM to 500 µM PFDA and its corresponding calibration curves. λ_{em} = 976 nm, Solvent: 30% MeOH-Water solution.

5.3.8 Analytical performance of the Nd/Yb-pAu surfaces for PFDA

We subsequently investigated the impact of PFDA on the NIR luminescence of both Nd-pAu and Yb-pAu surfaces. As shown in Figure 5.8a and Figure 5.8c their luminescence also increases with the addition of PFDA, within the ranges of 5 nmol to 20 nmol PFDA and 10 nmol to 40 nmol PFDA. The corresponding linear relationships are expressed as follows:

For Nd-pAu surface (5 nmol to 20 nmol PFDA):

$$I/I_0 = 0.0831\ C_{PFDA}\ (\text{nmol}) + 0.6894,\ R^2 = 0.9803,\ (5.5)$$

For Yb-pAu surface (10 mmol to 40 mmol PFDA):

$$I/I_0 = 0.0682\ C_{PFDA}\ (\text{nmol}) + 0.5186,\ R^2 = 0.9831,\ (5.6)$$

Where I_0 and I represent the peak area of Nd/Yb-pAu surfaces before and after the addition of PFDA. Identically, due to limited time, certain experiments were performed only once. Although this may impact the robustness and reproducibility of the results, the preliminary data generated are nonetheless indicative of the sensor's potential.

Distinct from the behaviour of Nd/Yb-SAcbisDBM in solution, the emission intensity of the Nd-pAu surface and Yb-pAu surface remained unchanged with further additions of PFDA. It can be attributed to the solid pAu surface preventing the Nd-SAcbisDBM and Yb-SAcbisDBM from aggregation.

Furthermore, the luminescence lifetime of Nd-pAu surface and Yb-pAu surface also increased upon the addition of 5 nmol to 20 nmol PFDA and 10 nmol to 40 nmol PFDA, respectively (Figure 5.8b and Figure 5.8d). Specifically, with the addition of PFDA, the lifetime of Nd-pAu surface increased by up to 48%, while that of Yb-pAu surface increased by up to 30%.

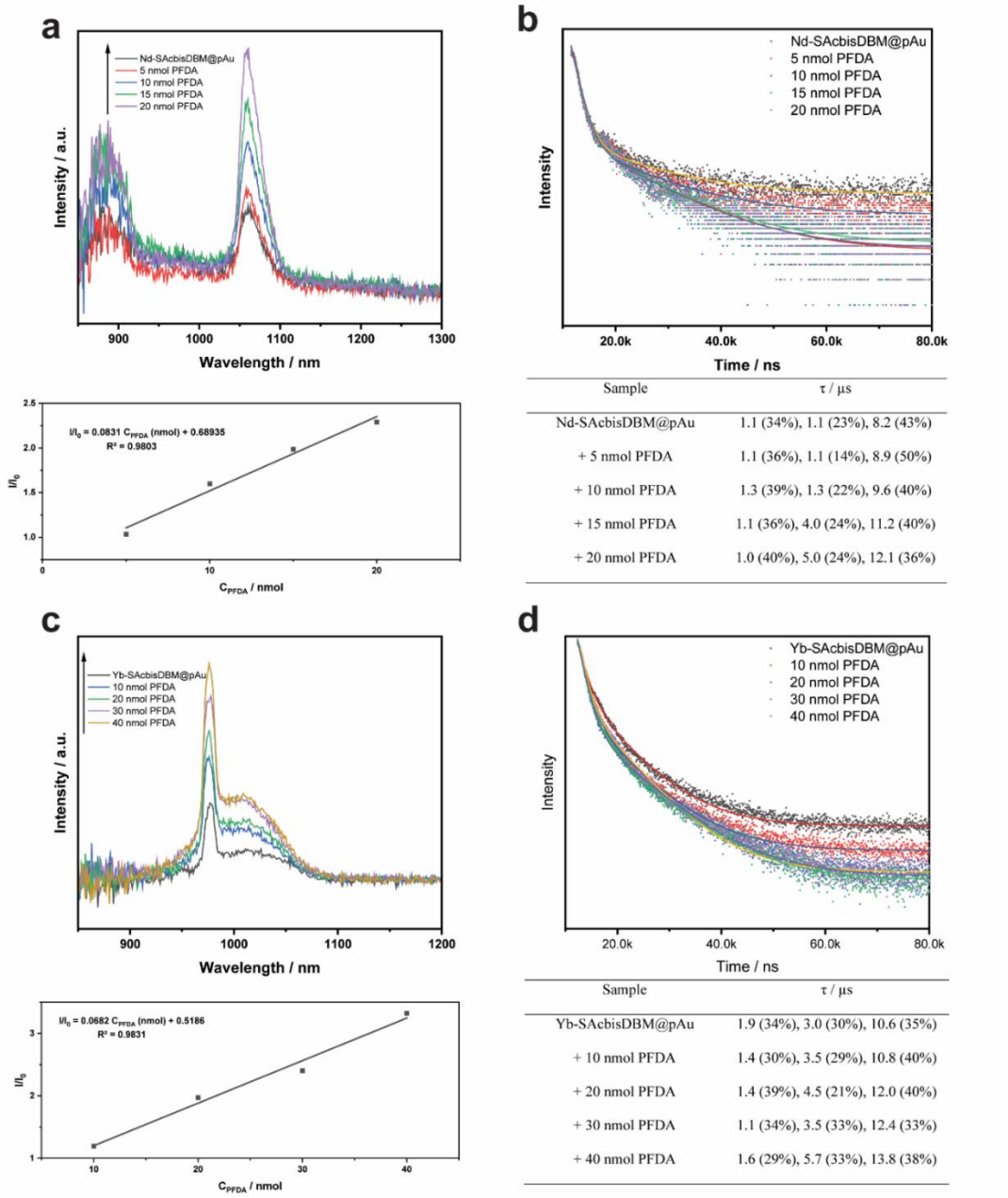

Sample	τ / μs
Nd-SAcbisDBM@pAu	1.1 (34%), 1.1 (23%), 8.2 (43%)
+ 5 nmol PFDA	1.1 (36%), 1.1 (14%), 8.9 (50%)
+ 10 nmol PFDA	1.3 (39%), 1.3 (22%), 9.6 (40%)
+ 15 nmol PFDA	1.1 (36%), 4.0 (24%), 11.2 (40%)
+ 20 nmol PFDA	1.0 (40%), 5.0 (24%), 12.1 (36%)

Sample	τ / μs
Yb-SAcbisDBM@pAu	1.9 (34%), 3.0 (30%), 10.6 (35%)
+ 10 nmol PFDA	1.4 (30%), 3.5 (29%), 10.8 (40%)
+ 20 nmol PFDA	1.4 (39%), 4.5 (21%), 12.0 (40%)
+ 30 nmol PFDA	1.1 (34%), 3.5 (33%), 12.4 (33%)
+ 40 nmol PFDA	1.6 (29%), 5.7 (33%), 13.8 (38%)

Figure 5.8. (a) Emission spectrum of Nd-pAu surface with the addition of 5 nmol to 20 nmol PFDA, λ_{em} = 1060 nm. (c) Emission spectrum of Yb-pAu surface with the addition of 10 nmol to 40 nmol PFDA, λ_{em} = 960 nm. Below figures of (a) and (c): calibration curves of relative intensity (I/I_0) to the concentration of PFDA. (b) Lifetime spectra of Nd-pAu surface with the addition of 5 nmol to 20 nmol PFDA. (d) Lifetime spectra of Yb-pAu surface with the addition of 10 nmol to 40 nmol PFDA. Below figures of (b) and (d): Summary of luminescence lifetime of Nd-pAu surface and Yb-pAu surface, and their alteration with addition of 5 nmol to 20 nmol and 10 nmol to 40 nmol PFDA, respectively.

5.4 Conclusion

In this chapter, the luminescence of Nd-SAcbisDBM and Yb-SAcbisDBM in both solution and at pAu gold surfaces upon the addition of PFOA, PFNA, and PFDA were investigated. SEM imaging revealed the morphology of the SAcbisDBM ligand, while Raman spectroscopy provided insights into the composition of functional groups on these modified surfaces. Our observations underscored the predominant influence of the SAcbisDBM ligand concentration on the luminescence of Nd(III) and Yb(III), particularly in polar solvents. Importantly, the introduction of PFCAs, notably PFDA, resulted in a remarkable enhancement of luminescence. Testing revealed that Nd-SAcbisDBM can detect PFDA at concentrations as low as 2 µM, while Yb-SAcbisDBM can detect PFDA down to 10 µM. Nevertheless, due to time constraints, this work could not delve deeper into the relationship between Nd(III) and Yb(III) complexes and PFOA, PFNA, and PFDA. Consequently, the current analytical performance represents preliminary findings from the initial phase of our study. However, by optimizing the sensor, such as adjusting the pH value, modifying the incubation methods, increasing the amount of SAcbisDBM ligand, etc., it is anticipated that the sensor's performance can be significantly improved in future studies. These findings demonstrate that Nd-SAcbisDBM and Yb-SAcbisDBM are promising candidates for PFDA sensing. This research not only advances our understanding of NIR-emitting lanthanide behavior but also lays the foundation for the development of efficient sensors with versatile applications in analytical chemistry.

Chapter 6: Conclusion and outlook

6.1 Conclusion

In this thesis, three novel luminescence lifetime-based sensing solid interfaces were developed. Two of these sensors, the Ir-functionalised surface and the Eu-functionalised surface, were proven to be capable of detecting PFAS such as PFOA in aqueous environments and waste samples.

Chapter three demonstrates that gold surfaces modified with IrC_6 and IrC_{12} metal probes provide a sensitive optical platform for detecting PFOA based on the iridium luminescence lifetime signal. Addition of PFOA affects the luminescence lifetime of the iridium probes which are known for sensitivity of the luminescence signal on local environment. The largest change of the lifetime which is best suited for analytical detection is observed for the gold surfaces co-coated with the fluorinated surfactant and IrC_6 or IrC_{12}. The surfactant not only enhances PFOA interaction but also, by increasing the luminescence lifetime, provides a significant change in the analytically exploitable luminescence lifetime signal upon displacement with PFOA. The sensing surfaces effectively quantify PFOA concentrations in drinking water, reaching levels as low as 100 µg/L (240 nM), and exhibit strong anti-interference capabilities.

In the fourth chapter, a gold surface modified with Eu(III) and SAcbisDBM ligand is developed for detecting PFCA in materials like leather, leatherette, and textiles. Surface characterization techniques, including SEM, XPS, Raman spectroscopy, etc confirm successful modification, while luminescence lifetime variation demonstrates excellent sensitivity to PFCA. The sensor exhibits remarkable reusability and minimal interference, capable of identifying PFCA levels as low as 0.03 mg/kg based on real sample analysis, aiding assessment of compliance with the EU LPCL limit regulation on maximum permissible concentrations of PFOA in waste fabrics.

Lastly, in the fifth chapter, the luminescence of Nd(III)/Yb(III)-SAcbisDBM in solution and on pAu gold surfaces upon addition of PFOA, PFNA, and PFDA is investigated. SEM imaging and Raman

spectroscopy provide insights into surface morphology and composition. Results highlight the influence of SAcbisDBM ligand concentration on luminescence, particularly in polar solvents, with significant enhancement observed upon introduction of PFCAs, notably PFDA. Nd-SAcbisDBM and Yb-SAcbisDBM are identified as promising candidates for PFDA sensing, capable of detecting concentrations as low as 2 μM and 10 μM, respectively.

In summary, the surface-based luminescence assays reported in this thesis provide a novel approach to monitoring related PFAS based on luminescence lifetime signal with high robustness and reliability Which can be further exploited for development of multi-analyte devices.

6.2 Future outlook

Luminescence sensor for the detection of PFAS in different environmental contexts have concerned with increased interest. Combined with the actual situation, this thesis proposes some suggestions for their future development.

1. Expand Research Scope: The research objects should not be limited to PFOS and PFOA. Other PFAS, such as PFBS, PFHxS, PFBA, PFNA, and PFDA, have attracted much attention in recent years as they have been labelled as Bioaccumulative (B) and Toxic (T)[2] and listed as Substances of Very High Concern (SVHC) by the EU.[52] It is valuable to develop luminescence assays to detect these PFAS.

2. Utilise Stokes Shift: Use the stokes shift of the sensing material in the presence of PFAS as the optical signal. Compared to luminescence intensity-based sensing, wavelength-based sensing is less susceptible to high electron affinity interferents, such as paramagnetic metal ions (Mn^{2+}, Co^{2+}, Ni^{2+}, and Cu^{2+}) and nitroaromatics,[231, 232] offering a much more accurate and stable approach to detect PFAS. Furthermore, no relevant studies have been reported so far to our knowledge.

3. Address Probe Concentration Dependency: Solve the problem of the probe luminescence being easily affected by the concentration of the probe. This influence greatly reduces the real-world applications of luminescence intensity-based sensors. Luminescence lifetime can be an alternative sensing signal, which is barely independent of the probe concentration.

4. Enhance Selectivity: Employ array-based sensing technology or molecularly imprinted technology to

improve the selectivity of the sensing material toward PFAS. Distinguishing and accurately quantifying different PFAS analogues is essential given the differences in toxicity between different PFAS.

Chapter 7: Appendix

7.1 Tables

Table S3.1. Liquid chromatography elution program

Mobile Phase	A: 5 mM ammonium formate in water B: 5 mM ammonium formate in methanol		
Column	Restek Raptor C18 column 1.8 µm particle size, 50 mm length, 2.1 mm internal diameter		
Flow Rate	0.4 mL/min		
Gradient	**Time**	**A (%)**	**B (%)**
	0.00	80	20
	6	5	95
	6.5	5	95
	6.51	80	20
	8	80	20

Table S3.2. MS/MS transitions and PFOA retention times

Compound	**MS/MS Transition**	**Retention Time**
Native Compounds		
PFOA	413.16 → 369.12	4.51
Internal Standards		
M8-PFOA	421.3 → 377.12	4.50
Recovery determination standard		
M4-PFOA	417 → 372	4.50

Table S3.3. PFOA concentration in different countries' drinking water.

Country	**Sampling site**	**C_{PFOA} (ng/L)**	**Ref.**
Ireland	Tap water samples were collected from home and office connected to municipal water supplies	0.04-1.76	[3]
Norway	3 drinking water samples were collected from the tap in households receiving water from different water works	0.65-2.5	[233]
German	5 tap water samples were collected from potable water treatment plant located at the federal state of Hesse	0.16-1.9	[234]
Belgium	Drinking water samples were collected from local origin	1-5	[235]
Netherlands	Drinking water samples were collected from the cities in the vicinity from the PFAS production plant. The cities include Zwijndrecht, Dordrecht, Papendrecht, Sliedrecht, Utrecht, Wageningen.	<0.3-2.7	[236]
Italy	Samples were collected from North of Milan (industrialised area)	10-47	[237]
Spain	30 drinking water samples collected in 10 Catalonia area drinking water treatment plants	<0.40-9.6	[238]
US	Samples collected from 25 drinking water treatment plants located in 24 contiguous states	0.56-104	[239]
China	The tap water samples were collected from 79 cities in 31 provincial-level administrative regions throughout China	n.d. - 26.33	[240]

Table S4.1. The chemical structure of C_4-C_{10} PFCAs

Name	Acronym name	Molecular weight	Chemical structure	pKa	Ref.
Perfluorobutyric acid	(PFBA)	214.04	C_3F_7COOH	0.394	[8]
Perfluoropentanoic acid	PFPeA	264.05	C_4F_9COOH	0.569	[8]
Perfluorohexanoic acid	(PFHxA)	314.05	$C_5F_{11}COOH$	0.84	[8]
Perfluoroheptanoic acid	(PFHpA)	364.06	$C_6F_{13}COOH$	2.4	[9]
Perfluorooctanoic acid	(PFOA)	414.07	$C_7F_{15}COOH$	3.8±0.1	[10]
Perfluorononanoic acid	(PFNA)	464.08	$C_8F_{17}COOH$	2.575	[8]
Perfluorodecanoic acid	(PFDA)	514.09	$C_9F_{19}COOH$	2.606	[8]

Table S4.2. MS/MS transitions and PFOA retention times

Compound	MS/MS Transition	Retention Time
Native Compounds		
PFBA	214 → 169	1.83
PFPeA	264 → 219	2.22
PFHxA	314 → 269	2.40
PFHpA	364 → 319	2.52
PFOA	413 → 369	2.61
PFNA	463 → 419	2.69
PFDA	514 → 469	2.75
Internal Standards		
^{13}C-PFBA	214 → 170	1.83
$^{13}C_3$-PFPeA	266 → 222	2.22
^{13}C-PFHxA	314 → 269	2.40
$^{13}C_4$-PFHpA	367 → 322	2.52
$^{13}C_8$-PFOA	421 → 376	2.61
^{13}C-PFNA	464 → 419	2.69
$^{13}C_6$-PFDA	519 → 474	2.75
$^{13}C_4$-PFOA	417 → 372	2.61

Table S4.3. Category of the leather, leatherette and textile samples

Sample #	Material	Category	Sample #	Material	Category
1	Leather	Sofa	18	Leatherette	Sofa
2	Leather	Sofa	19	Leatherette	Sofa
3	Leather	Sofa	20	Leatherette	Chair
4	Leather	Armchair	21	Leatherette	Chair
5	Leather	Sofa	22	Leatherette	Other
6	Leatherette	Sofa	23	Leatherette	Chair
7	Leatherette	Chair	24	Leatherette	Armchair
8	Leatherette	Sofa	25	Leatherette	Chair
9	Leatherette	Sofa	26	Leatherette	Armchair
10	Leatherette	Sofa	27	Leatherette	Armchair
11	Leatherette	Armchair	28	Leatherette	Sofa
12	Leatherette	Armchair	29	Textile	Sofa
13	Leatherette	Sofa	30	Textile	Sofa
14	Leatherette	Sofa	31	Textile	Infant Changing mat
15	Leatherette	Armchair	32	Textile	Firefighter uniform
16	Leatherette	Chair	33	Textile	Armchair
17	Leatherette	Sofa	34	Textile	Other

7.2 Figures

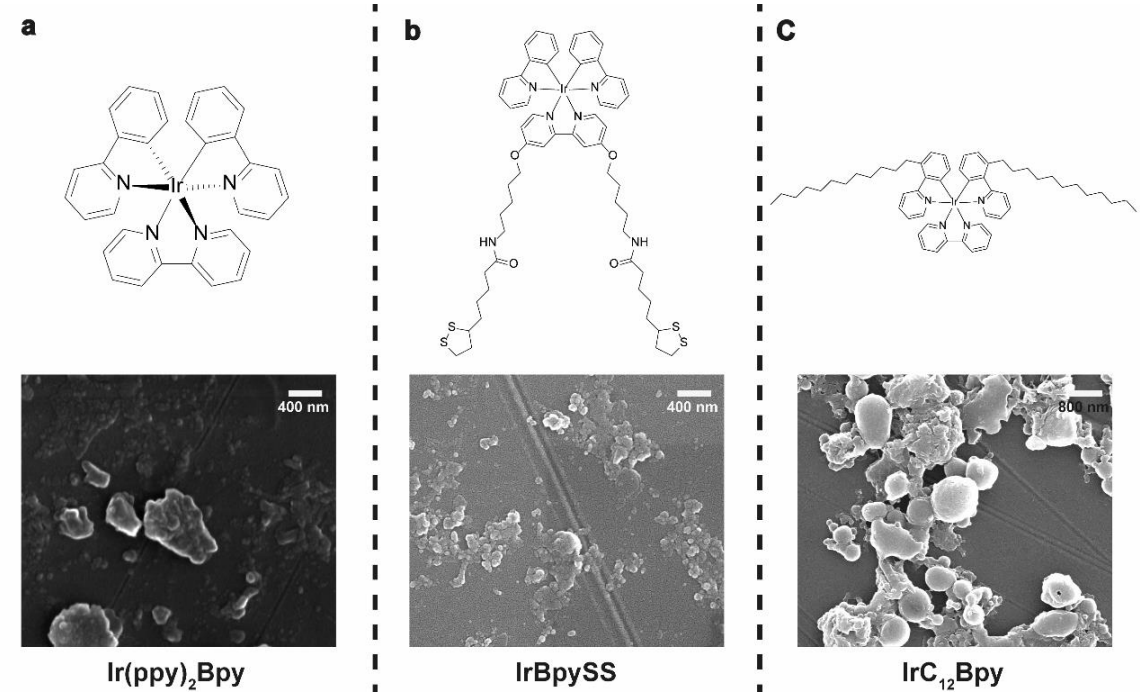

Figure S3.1. Chemical structure and SEM images of (a) Ir(ppy)$_2$bpy@Au, (b) IrbpySS@Au and (c) IrC$_{12}$bpy@Au deposited as acetonitrile solutions on Au surfaces.

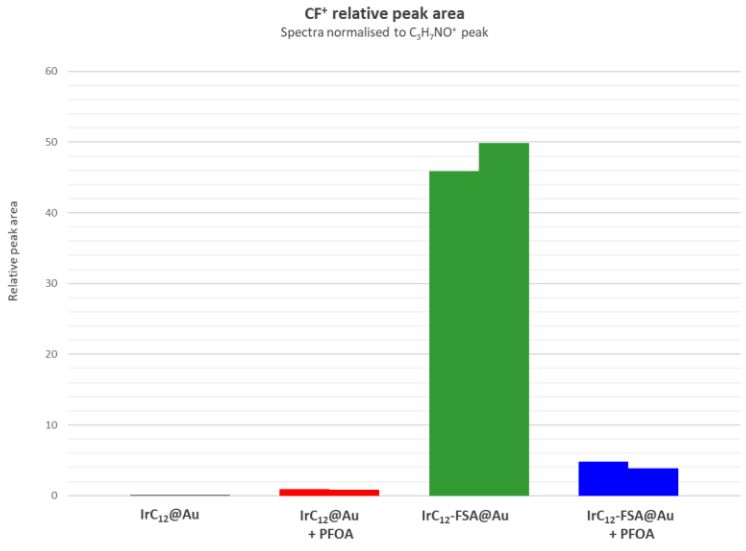

Figure S3.2. Relative CF^+ peak areas for different substrates (top). Relative peak areas of the Li^+ peak unique to Zonyl-FSA (bottom).

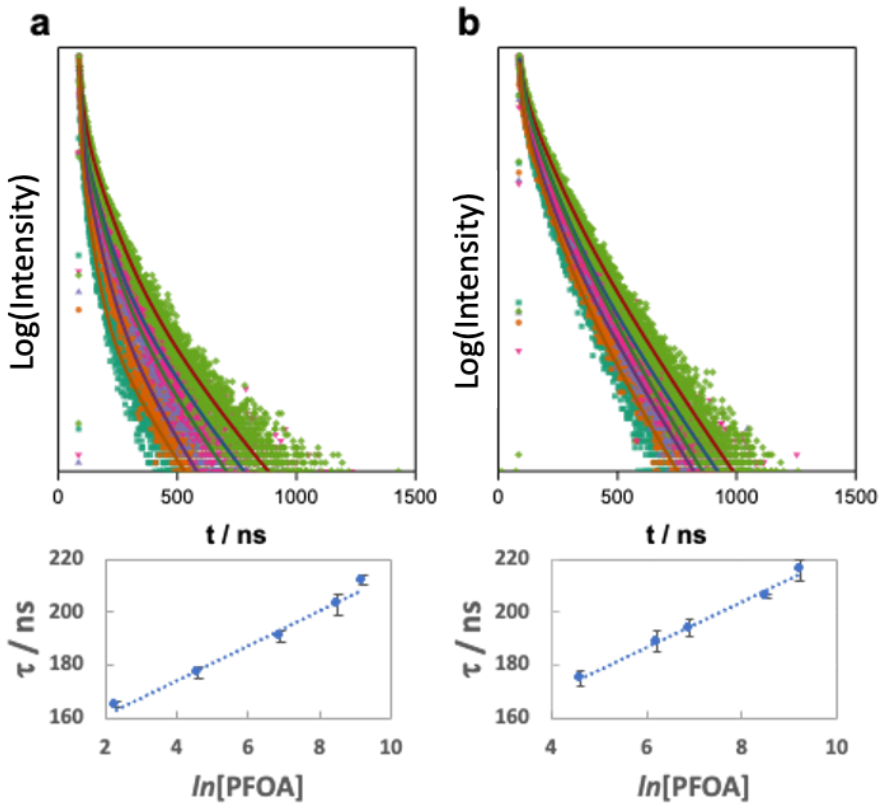

Figure S3.3. Luminescence lifetime decays (normalised plots -showing fitting in solid line) of (a) IrC_6@Au and (b) IrC_{12}@Au surfaces upon addition of PFOA, $\chi^2 = 1.0 \pm 0.2$, accompanied by plots of the luminescence lifetime (major component) with ln[PFOA]. The minor lifetime component showed same dependency.

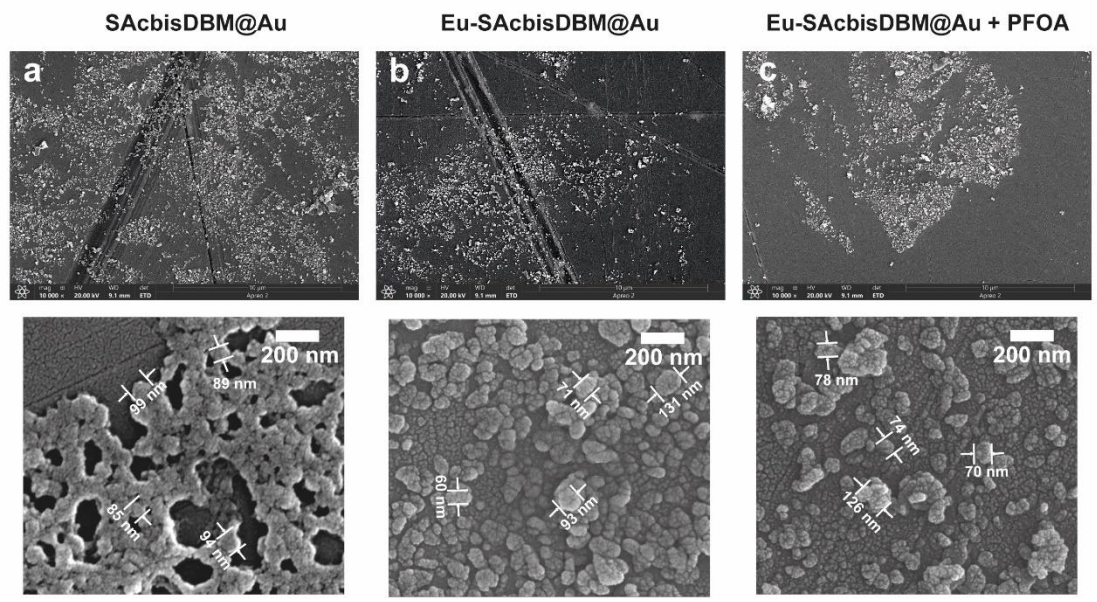

Figure S4.1. SEM images of (a) SAcbisDBM@Au surface, (b) Eu-SAcbisDBM@Au surface and (c) Eu-SAcbisDBM@Au surface + C_4-C_{10} PFCA, solution of C_4-C_{10} PFCA: 50 µM.

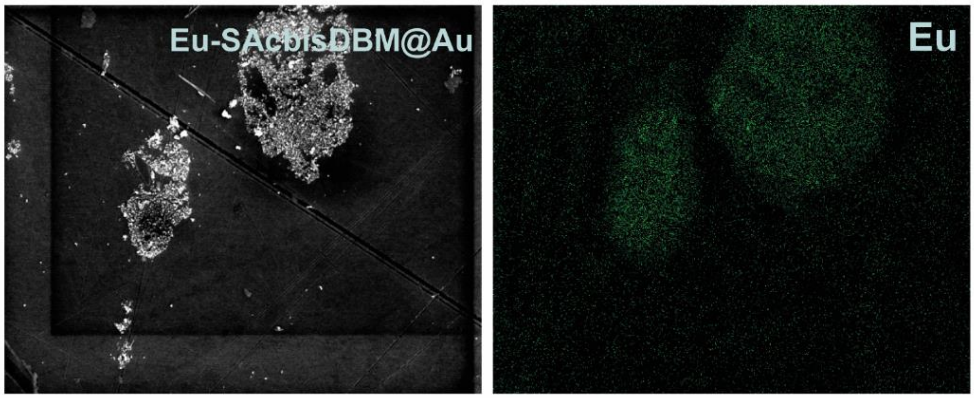

Figure S4.2. EDX elemental mapping analysis, europium mapping of Eu-SAcbisDBM@Au surface.

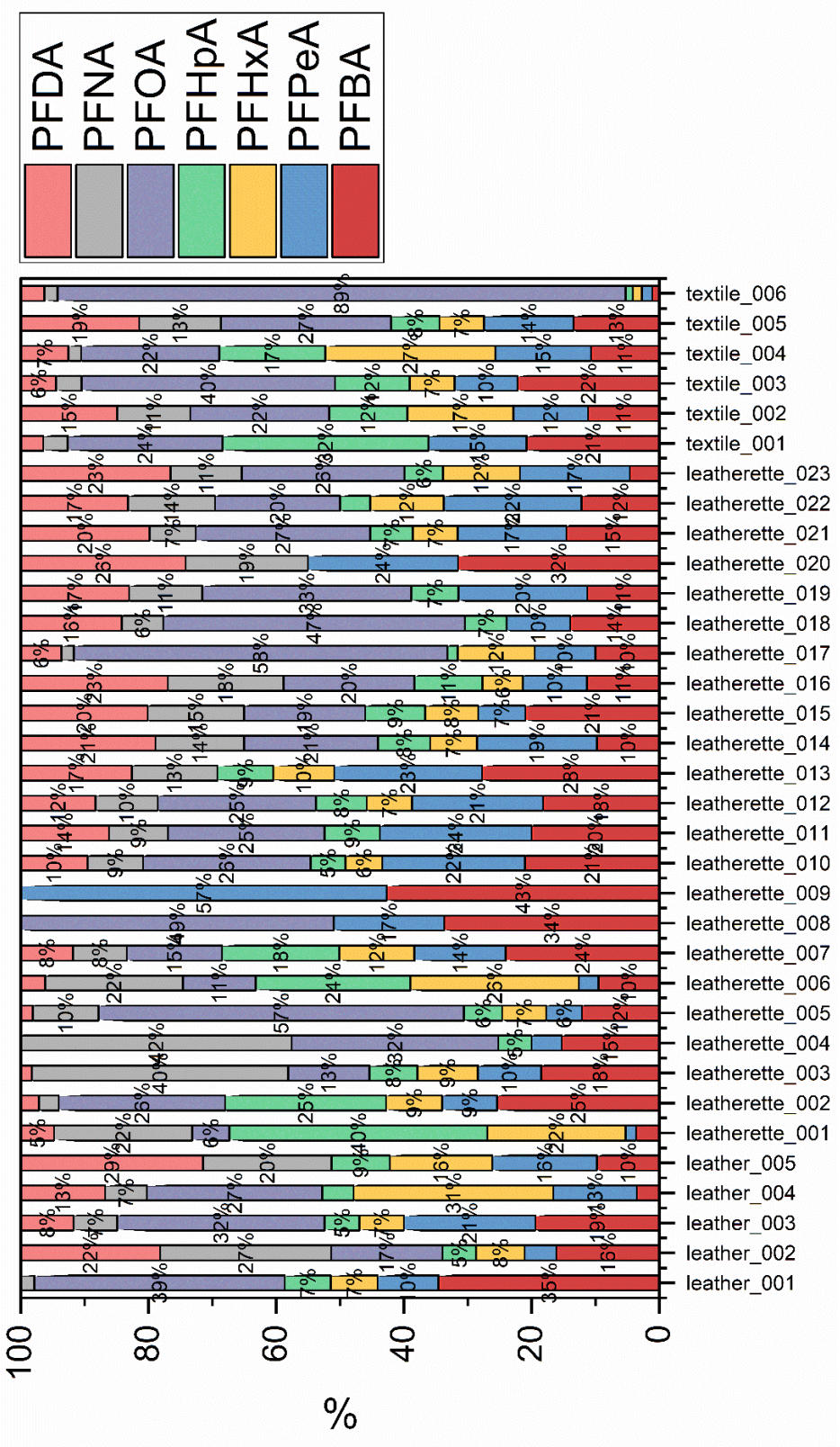

Figure S4.3. Proportion of each PFCA compound (PFBA, PFPeA, PFHxA, PFHpA, PFOA, PFNA and PFDA) in every samples. Percentage lower than 5% did not show in the figure.

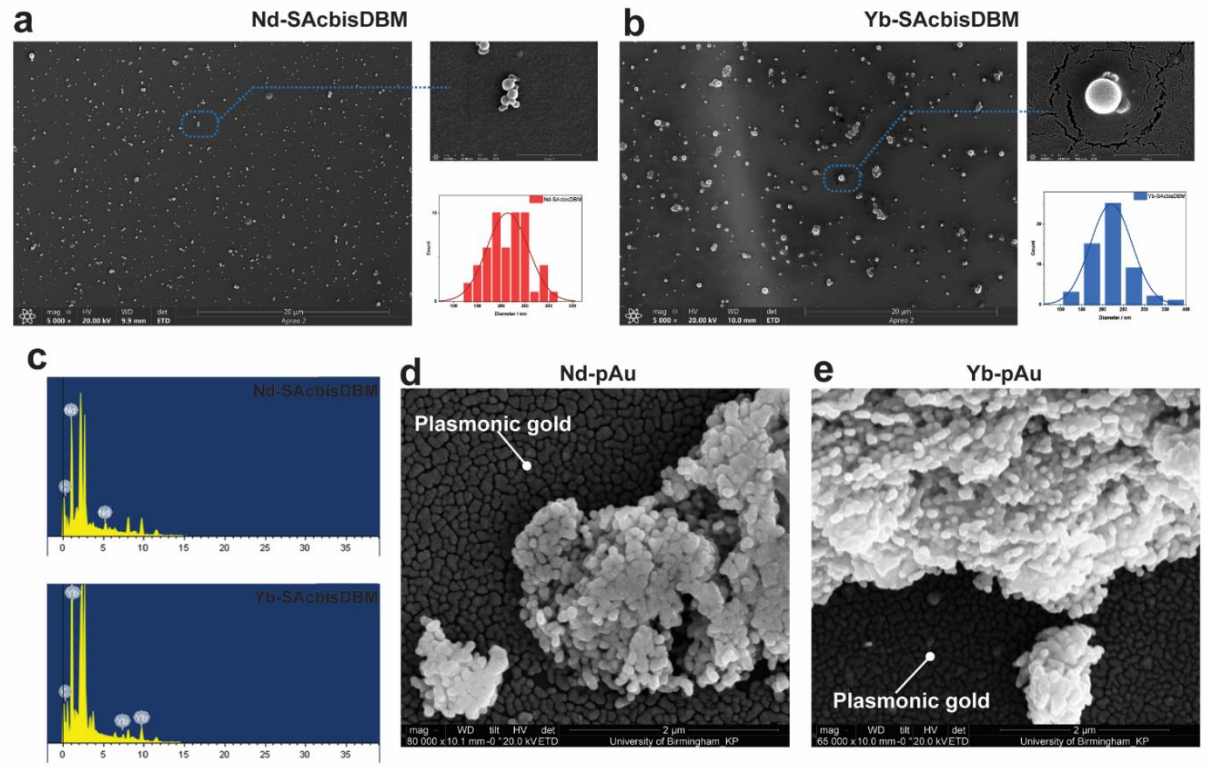

Figure S5.1. (a) and (b) SEM images of Nd-SAcbisDBM and Yb-SAcbisDBM in 30% MeOH-water solution. Insert: magnified selected spot (up), and size distribution of Nd/Yb-SAcbisDBM (down). (c) EDS spectrum of Nd-SAcbisDBM and Yb-SAcbisDBM in 30% MeOH-water solution. (d) and (e) SEM images of Nd-pAu surface and Yb-pAu surface.

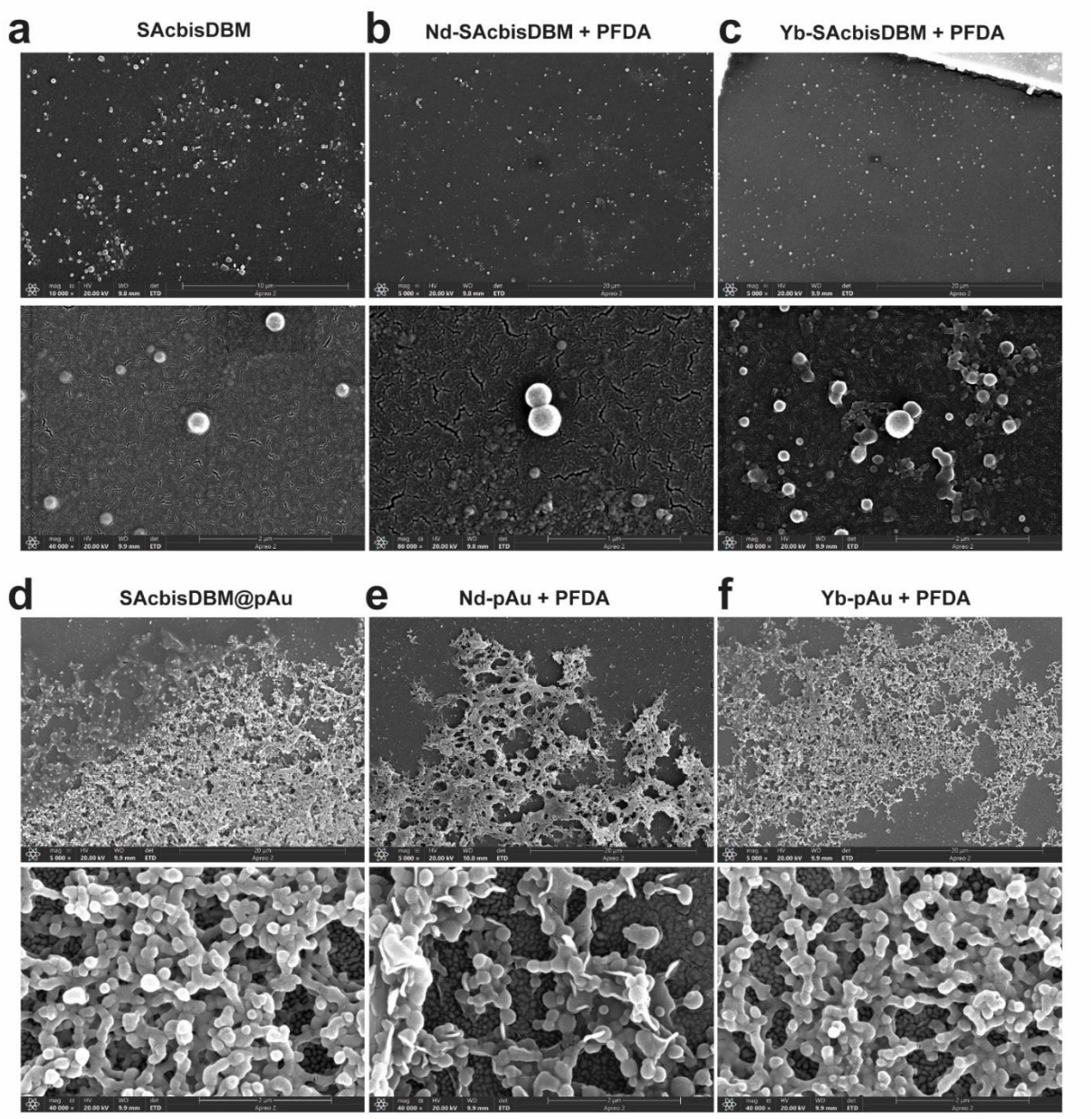

Figure S5.2. SEM image of (a) SAcbisDBM ligand, solvent: in 30% MeOH-water solution, (b) Nd-SAcbisDBM + 10 µM PFDA, Solvent: in 30% MeOH-water solution, (c) Yd-SAcbisDBM + 30 µM PFDA, Solvent: in 30% MeOH-water solution, (e) SAcbisDBM@pAu surface, (e) Nd-SAcbisDBM@pAu surface + 10 nmol PFDA, (f) Yd-SAcbisDBM@pAu surface + 20 nmol PFDA.

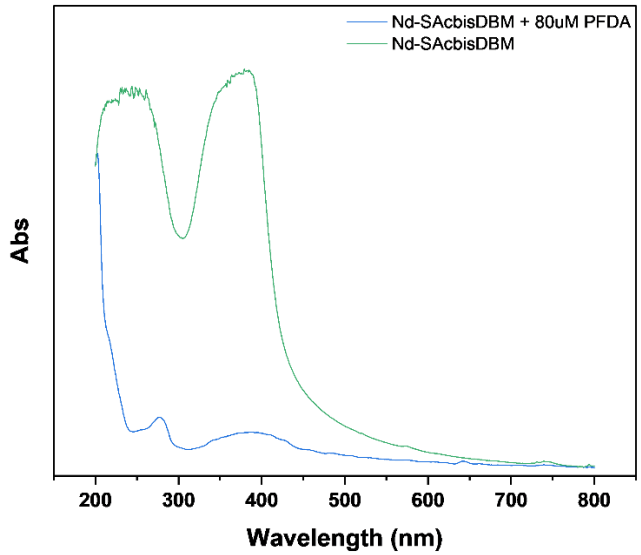

Figure S5.3. UV-vis spectra of Nd-SAcbisDBM complex in 30% MeOH-water solution before and after the addition of 80 µM PFDA.

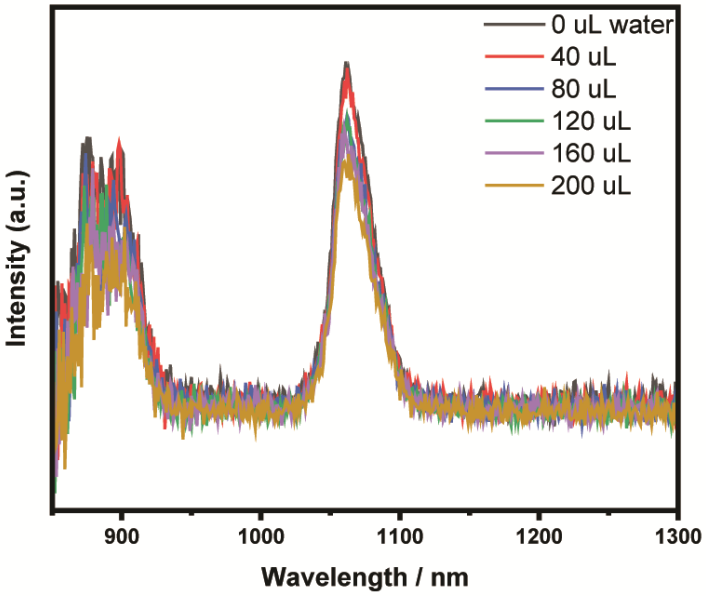

Figure S5.4. Emission spectra of Nd-SAcbisDBM with addition of 40 µL, 80 µL, 120 µL, 160 µL and 200 µL water. λ_{em} = 1060 nm, Solvent: 30% MeOH-water solution.

Chapter 8: References

1. United State Environmental Protection Agency Per- and Polyfluoroalkyl Substances (PFAS). https://www.epa.gov/pfas

2. European chemicals agency Perfluoroalkyl chemicals (PFASs). https://echa.europa.eu/hot-topics/perfluoroalkyl-chemicals-pfas

3. Harrad, S.; Wemken, N.; Drage, D. S.; Abdallah, M. A.; Coggins, A. M., Perfluoroalkyl Substances in Drinking Water, Indoor Air and Dust from Ireland: Implications for Human Exposure. *Environ Sci Technol* **2019,** *53*, (22), 13449-13457.

4. Xiao, F.; Simcik, M. F.; Halbach, T. R.; Gulliver, J. S., Perfluorooctane sulfonate (PFOS) and perfluorooctanoate (PFOA) in soils and groundwater of a U.S. metropolitan area: migration and implications for human exposure. *Water Res* **2015,** *72*, 64-74.

5. Kissa, E., Fluorinated Surfactants and Repellents, 2nd ed. Marcel Dekker, Inc: New York. **2001,** *97*, 640.

6. Sonne, C., Health effects from long-range transported contaminants in Arctic top predators: An integrated review based on studies of polar bears and relevant model species. *Environ Int* **2010,** *36*, (5), 461-91.

7. Swedish Food Agency PFAS in drinking water and fish-risk management. https://www.livsmedelsverket.se/en/food-and-content/oonskade-amnen/miljogifter/pfas-in-drinking-water-fish-risk-management#Action%20levels

8. Moroi, Y.; Yano, H.; Shibata, O.; Yonemitsu, T., Determination of Acidity Constants of Perfluoroalkanoic Acids. *Bull. Chem. Soc. Jpn.* **2001,** *74*, 667—672.

9. Rayne, S.; Forest, K., Theoretical studies on the pKa values of perfluoroalkyl carboxylic acids. *Journal of Molecular Structure: THEOCHEM* **2010,** *949*, (1-3), 60-69.

10. D Burns; D Ellis; H Li; C Mcmurdo; Webster, E., Experimental pKa Determination for Perfluorooctanoic Acid (PFOA) and the Potential Impact of pKa Concentration Dependence on

Laboratory-Measured Partitioning Phenomena and Environmental Modeling. *Environ Sci Technol* **2008,** *42*, 9283–9288.

11. Xu, B.; Yang, G.; Lehmann, A.; Riedel, S.; Rillig, M. C., Effects of perfluoroalkyl and polyfluoroalkyl substances (PFAS) on soil structure and function. *Soil Ecology Letters* **2022,** *5*, (1), 108-117.

12. Wang, Z.; MacLeod, M.; Cousins, I. T.; Scheringer, M.; Hungerbühler, K., Using COSMOtherm to predict physicochemical properties of poly- and perfluorinated alkyl substances (PFASs). *Environmental Chemistry* **2011,** *8*, (4).

13. D Brooke; A Footitt; Nwaogu, T. A. Environmental Risk Evaluation Report: Perfluorooctanesulphonate (PFOS), Environment Agency, Chemicals Assessment Section, Wallingford, UK. http://chm.pops.int/Portals/0/docs/from_old_website/documents/meetings/poprc/submissions/Comments_2006/sia/pfos.uk.risk.eval.report.2004.pdf

14. Cui, D.; Li, X.; Quinete, N., Occurrence, fate, sources and toxicity of PFAS: What we know so far in Florida and major gaps. *TrAC Trends in Analytical Chemistry* **2020,** *130*, 115976.

15. Davis, K. L.; Aucoin, M. D.; Larsen, B. S.; Kaiser, M. A.; Hartten, A. S., Transport of ammonium perfluorooctanoate in environmental media near a fluoropolymer manufacturing facility. *Chemosphere* **2007,** *67*, (10), 2011-9.

16. Castiglioni, S.; Valsecchi, S.; Polesello, S.; Rusconi, M.; Melis, M.; Palmiotto, M.; Manenti, A.; Davoli, E.; Zuccato, E., Sources and fate of perfluorinated compounds in the aqueous environment and in drinking water of a highly urbanized and industrialized area in Italy. *J Hazard Mater* **2015,** *282*, 51-60.

17. D'Ambro, E. L.; Pye, H. O. T.; Bash, J. O.; Bowyer, J.; Allen, C.; Efstathiou, C.; Gilliam, R. C.; Reynolds, L.; Talgo, K.; Murphy, B. N., Characterizing the Air Emissions, Transport, and Deposition of Per- and Polyfluoroalkyl Substances from a Fluoropolymer Manufacturing Facility. *Environmental Science & Technology* **2021,** *55*, (2), 862-870.

18. Sima, M. W.; Jaffé, P. R., A critical review of modeling Poly- and Perfluoroalkyl Substances

(PFAS) in the soil-water environment. *Science of The Total Environment* **2021,** *757*, 143793.

19. Heydebreck, F.; Tang, J.; Xie, Z.; Ebinghaus, R., Emissions of Per- and Polyfluoroalkyl Substances in a Textile Manufacturing Plant in China and Their Relevance for Workers' Exposure. *Environ Sci Technol* **2016,** *50*, (19), 10386-10396.

20. Schellenberger, S.; Liagkouridis, I.; Awad, R.; Khan, S.; Plassmann, M.; Peters, G.; Benskin, J. P.; Cousins, I. T., An Outdoor Aging Study to Investigate the Release of Per- And Polyfluoroalkyl Substances (PFAS) from Functional Textiles. *Environ Sci Technol* **2022,** *56*, (6), 3471-3479.

21. Thompson, J. T.; Robey, N. M.; Tolaymat, T. M.; Bowden, J. A.; Solo-Gabriele, H. M.; Townsend, T. G., Underestimation of Per- and Polyfluoroalkyl Substances in Biosolids: Precursor Transformation During Conventional Treatment. *Environmental Science & Technology* **2023,** *57*, (9), 3825-3832.

22. Adamson, D. T.; Nickerson, A.; Kulkarni, P. R.; Higgins, C. P.; Popovic, J.; Field, J.; Rodowa, A.; Newell, C.; DeBlanc, P.; Kornuc, J. J., Mass-Based, Field-Scale Demonstration of PFAS Retention within AFFF-Associated Source Areas. *Environmental Science & Technology* **2020,** *54*, (24), 15768-15777.

23. Seltenrich, N., PFAS in Food Packaging: A Hot, Greasy Exposure. *Environ Health Perspect* **2020,** *128*, (5), 54002.

24. Putz, K. W.; Namazkar, S.; Plassmann, M.; Benskin, J. P., Are cosmetics a significant source of PFAS in Europe? product inventories, chemical characterization and emission estimates. *Environ Sci Process Impacts* **2022,** *24*, (10), 1697-1707.

25. Herzke, D.; Olsson, E.; Posner, S., Perfluoroalkyl and polyfluoroalkyl substances (PFASs) in consumer products in Norway - a pilot study. *Chemosphere* **2012,** *88*, (8), 980-7.

26. Vestergren, R.; Herzke, D.; Wang, T.; Cousins, I. T., Are imported consumer products an important diffuse source of PFASs to the Norwegian environment? *Environ Pollut* **2015,** *198*, 223-30.

27. Tittlemier, S. A.; Pepper, K.; Seymour, C.; Moisey, J.; Bronson, R.; Cao, X.-L.; Dabeka, R. W. J. J. o. a.; chemistry, f., Dietary exposure of Canadians to perfluorinated carboxylates and perfluorooctane sulfonate via consumption of meat, fish, fast foods, and food items prepared in their

packaging. **2007,** *55*, (8), 3203-3210.

28. Seshasayee, S. M.; Rifas-Shiman, S. L.; Chavarro, J. E.; Carwile, J. L.; Lin, P.-I. D.; Calafat, A. M.; Sagiv, S. K.; Oken, E.; Fleisch, A. F., Dietary patterns and PFAS plasma concentrations in childhood: Project Viva, USA. *Environment International* **2021,** *151*, 106415.

29. Schaider, L. A.; Balan, S. A.; Blum, A.; Andrews, D. Q.; Strynar, M. J.; Dickinson, M. E.; Lunderberg, D. M.; Lang, J. R.; Peaslee, G. F. J. E. s.; letters, t., Fluorinated compounds in US fast food packaging. **2017,** *4*, (3), 105-111.

30. Thomas, P., The use of fluoropolymers for non-stick cooking utensils. *Surface coatings international* **1998,** *81*, (12), 604-609.

31. European Food Safety Authority PFAS in food: EFSA assesses risks and sets tolerable intake. https://www.efsa.europa.eu/en/news/pfas-food-efsa-assesses-risks-and-sets-tolerable-intake (17 September, 2020),

32. Domingo, J. L.; Nadal, M., Human exposure to per- and polyfluoroalkyl substances (PFAS) through drinking water: A review of the recent scientific literature. *Environmental Research* **2019,** *177*, 108648.

33. Heydebreck, F.; Tang, J.; Xie, Z.; Ebinghaus, R., Emissions of Per- and Polyfluoroalkyl Substances in a Textile Manufacturing Plant in China and Their Relevance for Workers' Exposure. *Environmental Science & Technology* **2016,** *50*, (19), 10386-10396.

34. Tanner, E. M.; Bloom, M. S.; Wu, Q.; Kannan, K.; Yucel, R. M.; Shrestha, S.; Fitzgerald, E. F., Occupational exposure to perfluoroalkyl substances and serum levels of perfluorooctanesulfonic acid (PFOS) and perfluorooctanoic acid (PFOA) in an aging population from upstate New York: a retrospective cohort study. *International archives of occupational environmental health perspectives* **2018,** *91*, 145-154.

35. Ragnarsdottir, O.; Abdallah, M. A.; Harrad, S., Dermal uptake: An important pathway of human exposure to perfluoroalkyl substances? *Environ Pollut* **2022,** *307*, 119478.

36. Poothong, S.; Padilla-Sánchez, J. A.; Papadopoulou, E.; Giovanoulis, G.; Thomsen, C.; Haug, L. S., Hand Wipes: A Useful Tool for Assessing Human Exposure to Poly- and Perfluoroalkyl

Substances (PFASs) through Hand-to-Mouth and Dermal Contacts. *Environmental Science & Technology* **2019,** *53*, (4), 1985-1993.

37. Nicole, W., PFOA and cancer in a highly exposed community: new findings from the C8 science panel. In Environmental Health Sciences: 2013; Vol. 121, pp A340-A340.

38. Antonia M. Calafat; Lee-Yang Wong; Zsuzsanna Kuklenyik; John A. Reidy; Needham, L. L., Polyfluoroalkyl chemicals in the U.S. population: data from the National Health and Nutrition Examination Survey (NHANES) 2003-2004 and comparisons with NHANES 1999-2000. *Environ Health Perspect* **2007,** *115*, (11), 1596-602.

39. Winquist, A.; Steenland, K., Perfluorooctanoic Acid Exposure and Thyroid Disease in Community and Worker Cohorts. *Epidemiology* **2014,** *25*, (2), 255-264.

40. Barry, V.; Winquist, A.; Steenland, K., Perfluorooctanoic acid (PFOA) exposures and incident cancers among adults living near a chemical plant. *Environmental health perspectives* **2013,** *121*, (11-12), 1313-1318.

41. Zahm, S.; Bonde, J. P.; Chiu, W. A.; Hoppin, J.; Kanno, J.; Abdallah, M.; Blystone, C. R.; Calkins, M. M.; Dong, G.-H.; Dorman, D. C., Carcinogenicity of perfluorooctanoic acid and perfluorooctanesulfonic acid. *The Lancet Oncology* **2023**.

42. Sagiv, S. K.; Rifas-Shiman, S. L.; Fleisch, A. F.; Webster, T. F.; Calafat, A. M.; Ye, X.; Gillman, M. W.; Oken, E., Early-Pregnancy Plasma Concentrations of Perfluoroalkyl Substances and Birth Outcomes in Project Viva: Confounded by Pregnancy Hemodynamics? *American Journal of Epidemiology* **2017,** *187*, (4), 793-802.

43. Salihovic, S.; Stubleski, J.; Kärrman, A.; Larsson, A.; Fall, T.; Lind, L.; Lind, P. M., Changes in markers of liver function in relation to changes in perfluoroalkyl substances - A longitudinal study. *Environment International* **2018,** *117*, 196-203.

44. Grandjean, P.; Heilmann, C.; Weihe, P.; Nielsen, F.; Mogensen, U. B.; Timmermann, A.; Budtz-Jørgensen, E., Estimated exposures to perfluorinated compounds in infancy predict attenuated vaccine antibody concentrations at age 5-years. *Journal of Immunotoxicology* **2017,** *14*, (1), 188-195.

45. EFSA Panel on Contaminants in the Food Chain; Schrenk, D.; Bignami, M.; Bodin, L.;

Chipman, J. K.; del Mazo, J.; Grasl-Kraupp, B.; Hogstrand, C.; Hoogenboom, L.; Leblanc, J.-C.; Nebbia, C. S.; Nielsen, E.; Ntzani, E.; Petersen, A.; Sand, S.; Vleminckx, C.; Wallace, H.; Barregård, L.; Ceccatelli, S.; Cravedi, J.-P.; Halldorsson, T. I.; Haug, L. S.; Johansson, N.; Knutsen, H. K.; Rose, M.; Roudot, A.-C.; Van Loveren, H.; Vollmer, G.; Mackay, K.; Riolo, F.; Schwerdtle, T., Risk to human health related to the presence of perfluoroalkyl substances in food. *EFSA Journal* **2020,** *18*, (9).

46. European Commission, COMMISSION REGULATION (EU) No 757/2010, amending Regulation (EC) No 850/2004 of the European Parliament and of the Council on persistent organic pollutants as regards Annexes I and III. Official Journal of the European Union. In 24 August 2010.

47. European chemicals agency Pre-registered substances. https://echa.europa.eu/web/guest/information-on-chemicals/pre-registered-substances (01 December, 2008),

48. European chemicals agency Registered Substances. https://echa.europa.eu/information-on-chemicals/registered-substances (19th May, 2023),

49. Olsen, G. W.; Burris, J. M.; Ehresman, D. J.; Froehlich, J. W.; Seacat, A. M.; Butenhoff, J. L.; Zobel, L. R., Half-life of serum elimination of perfluorooctanesulfonate, perfluorohexanesulfonate, and perfluorooctanoate in retired fluorochemical production workers. *Environmental health perspectives* **2007,** *115*, (9), 1298-1305.

50. Olsen, G. W.; Chang, S.-C.; Noker, P. E.; Gorman, G. S.; Ehresman, D. J.; Lieder, P. H.; Butenhoff, J. L., A comparison of the pharmacokinetics of perfluorobutanesulfonate (PFBS) in rats, monkeys, and humans. *Toxicology* **2009,** *256*, (1), 65-74.

51. Chang, S.-C.; Das, K.; Ehresman, D. J.; Ellefson, M. E.; Gorman, G. S.; Hart, J. A.; Noker, P. E.; Tan, Y.-M.; Lieder, P. H.; Lau, C., Comparative pharmacokinetics of perfluorobutyrate in rats, mice, monkeys, and humans and relevance to human exposure via drinking water. *Toxicological Sciences* **2008,** *104*, (1), 40-53.

52. European Chemicals Agency Candidate List of substances of very high concern for authorisation. https://echa.europa.eu/candidate-list-table (July 26, 2019),

53. Lou, Q.-Q.; Zhang, Y.-F.; Zhou, Z.; Shi, Y.-L.; Ge, Y.-N.; Ren, D.-K.; Xu, H.-M.; Zhao, Y.-X.;

Wei, W.-J.; Qin, Z.-F., Effects of perfluorooctanesulfonate and perfluorobutanesulfonate on the growth and sexual development of Xenopus laevis. *Ecotoxicology* **2013,** *22*, (7), 1133-1144.

54. United Nations Environment Programme Stockholm Convention All POPs listed in the Stockholm Convention. http://www.pops.int/TheConvention/ThePOPs/AllPOPs/tabid/2509/Default.aspx (3 April, 2023),

55. Schrenk, D.; Bignami, M.; Bodin, L.; Chipman, J. K.; Del Mazo, J.; Grasl-Kraupp, B.; Hogstrand, C.; Hoogenboom, L. R.; Leblanc, J. C.; Nebbia, C. S.; Nielsen, E.; Ntzani, E.; Petersen, A.; Sand, S.; Vleminckx, C.; Wallace, H.; Barregard, L.; Ceccatelli, S.; Cravedi, J. P.; Halldorsson, T. I.; Haug, L. S.; Johansson, N.; Knutsen, H. K.; Rose, M.; Roudot, A. C.; Van Loveren, H.; Vollmer, G.; Mackay, K.; Riolo, F.; Schwerdtle, T., Risk to human health related to the presence of perfluoroalkyl substances in food. *EFSA J* **2020,** *18*, (9), 6223.

56. European Union, Position of the Council at first reading with a view to the adoption of a Directive of the European Parliament and of the Council on the quality of water intended for human consumption (recast) 6230/20. In **2020**.

57. United State Environmental Protection Agency Per- and Polyfluoroalkyl Substances (PFAS), Proposed PFAS National Primary Drinking Water Regulation. https://www.epa.gov/sdwa/and-polyfluoroalkyl-substances-pfas (14th March, 2023),

58. European Council Council and Parliament agree to reduce limit values for the presence of persistent organic pollutants in waste. https://www.consilium.europa.eu/en/press/press-releases/2022/06/21/council-and-parliament-agree-to-reduce-limit-values-for-the-presence-of-persistent-organic-pollutants-in-waste/ (21 June 2022),

59. European Commission, COMMISSION REGULATION (EU) No 757/2010 of 24 August 2010 amending Regulation (EC) No 850/2004 of the European Parliament and of the Council on persistent organic pollutants as regards Annexes I and III. In Official Journal of the European Union, Ed. The European Commission, 2010.

60. United State Environmental Protection Agency PFAS Analytical Methods Development and Sampling Research. https://www.epa.gov/water-research/pfas-analytical-methods-development-and-

sampling-research#:~:text=In%20order%20to%20identify%20unknown,on%20known%2C%20structurally%20similar%20analytes.

61. Coggan, T. L.; Anumol, T.; Pyke, J.; Shimeta, J.; Clarke, B. O., A single analytical method for the determination of 53 legacy and emerging per- and polyfluoroalkyl substances (PFAS) in aqueous matrices. *Anal Bioanal Chem* **2019,** *411*, (16), 3507-3520.

62. Monteleone, M.; Naccarato, A.; Sindona, G.; Tagarelli, A., A rapid and sensitive assay of perfluorocarboxylic acids in aqueous matrices by headspace solid phase microextraction-gas chromatography-triple quadrupole mass spectrometry. *J Chromatogr A* **2012,** *1251*, 160-168.

63. Bakker, E.; Telting-Diaz, M., Electrochemical Sensors. *Analytical Chemistry* **2002,** *74*, (12), 2781-2800.

64. Kazemi, R.; Potts, E. I.; Dick, J. E., Quantifying Interferent Effects on Molecularly Imprinted Polymer Sensors for Per- and Polyfluoroalkyl Substances (PFAS). *Anal Chem* **2020,** *92*, (15), 10597-10605.

65. Karimian, N.; Stortini, A. M.; Moretto, L. M.; Costantino, C.; Bogialli, S.; Ugo, P., Electrochemosensor for Trace Analysis of Perfluorooctanesulfonate in Water Based on a Molecularly Imprinted Poly(o-phenylenediamine) Polymer. *ACS Sens* **2018,** *3*, (7), 1291-1298.

66. Glasscott, M. W.; Vannoy, K. J.; Kazemi, R.; Verber, M. D.; Dick, J. E., μ-MIP: Molecularly Imprinted Polymer-Modified Microelectrodes for the Ultrasensitive Quantification of GenX (HFPO-DA) in River Water. *Environmental Science & Technology Letters* **2020,** *7*, (7), 489-495.

67. Lu, D.; Zhu, D. Z.; Gan, H.; Yao, Z.; Luo, J.; Yu, S.; Kurup, P., An ultra-sensitive molecularly imprinted polymer (MIP) and gold nanostars (AuNS) modified voltammetric sensor for facile detection of perfluorooctance sulfonate (PFOS) in drinking water. *Sensors and Actuators B: Chemical* **2022,** *352*.

68. Clark, R. B.; Dick, J. E., Electrochemical Sensing of Perfluorooctanesulfonate (PFOS) Using Ambient Oxygen in River Water. *ACS Sens* **2020,** *5*, (11), 3591-3598.

69. Cheng, Y. H.; Barpaga, D.; Soltis, J. A.; Shutthanandan, V.; Kargupta, R.; Han, K. S.; McGrail, B. P.; Motkuri, R. K.; Basuray, S.; Chatterjee, S., Metal-Organic Framework-Based Microfluidic

Impedance Sensor Platform for Ultrasensitive Detection of Perfluorooctanesulfonate. *ACS Appl Mater Interfaces* **2020,** *12*, (9), 10503-10514.

70. Wang, Y.; Ren, R.; Chen, F.; Jing, L.; Tian, Z.; Li, Z.; Wang, J.; Hou, C., Molecularly imprinted MOFs-driven carbon nanofiber for sensitive electrochemical detection and targeted electro-Fenton degradation of perfluorooctanoic acid. *Separation and Purification Technology* **2023,** *310*.

71. Shanbhag, M. M.; Shetti, N. P.; Kalanur, S. S.; Pollet, B. G.; Nadagouda, M. N.; Aminabhavi, T. M., Hafnium doped tungsten oxide intercalated carbon matrix for electrochemical detection of perfluorooctanoic acid. *Chemical Engineering Journal* **2022,** *434*.

72. Garada, M. B.; Kabagambe, B.; Kim, Y.; Amemiya, S., Ion-transfer voltammetry of perfluoroalkanesulfonates and perfluoroalkanecarboxylates: picomolar detection limit and high lipophilicity. *Anal Chem* **2014,** *86*, (22), 11230-7.

73. A. Prasanna de Silva; H. Q. Nimal Gunaratne; Thorfinnur Gunnlaugsson; Allen J. M. Huxley; Colin P. McCoy; Jude T. Rademacher; Rice, T. E., Signaling Recognition Events with Fluorescent Sensors and Switches. *Chemical Review* **1997,** *97*, 1515-1566.

74. Hwang, H.; Myong, S., Protein induced fluorescence enhancement (PIFE) for probing protein-nucleic acid interactions. *Chem Soc Rev* **2014,** *43*, (4), 1221-9.

75. Yan, Y.; Sun, J.; Zhang, K.; Zhu, H.; Yu, H.; Sun, M.; Huang, D.; Wang, S., Visualizing gaseous nitrogen dioxide by ratiometric fluorescence of carbon nanodots-quantum dots hybrid. *Anal Chem* **2015,** *87*, (4), 2087-93.

76. Zhao, S.-N.; Li, L.-J.; Song, X.-Z.; Zhu, M.; Hao, Z.-M.; Meng, X.; Wu, L.-L.; Feng, J.; Song, S.-Y.; Wang, C.; Zhang, H.-J., Lanthanide Ion Codoped Emitters for Tailoring Emission Trajectory and Temperature Sensing. *Advanced Functional Materials* **2015,** *25*, (9), 1463-1469.

77. Liu, Q.; Huang, A.; Wang, N.; Zheng, G.; Zhu, L., Rapid fluorometric determination of perfluorooctanoic acid by its quenching effect on the fluorescence of quantum dots. *Journal of Luminescence* **2015,** *161*, 374-381.

78. Lin, L.; Zhou, S.; Guo, H.; Chen, Y.; Lin, S.; Yan, L.; Li, K.; Li, J., Nitrogen-doped carbon dots as an effective fluorescence enhancing system for the determination of perfluorooctyl sulfonate.

Microchimica Acta **2019,** *186*, (6), 380.

79. Walekar, L. S.; Zheng, M.; Zheng, L.; Long, M., Selenium and nitrogen co-doped carbon quantum dots as a fluorescent probe for perfluorooctanoic acid. *Microchim Acta* **2019,** *186*, (5), 278.

80. Zheng, L.; Zheng, Y.; Liu, Y.; Long, S.; Du, L.; Liang, J.; Huang, C.; Swihart, M. T.; Tan, K., Core-shell quantum dots coated with molecularly imprinted polymer for selective photoluminescence sensing of perfluorooctanoic acid. *Talanta* **2019,** *194*, 1-6.

81. Zheng, Z.; Yu, H.; Geng, W. C.; Hu, X. Y.; Wang, Y. Y.; Li, Z.; Wang, Y.; Guo, D. S., Guanidinocalix[5]arene for sensitive fluorescence detection and magnetic removal of perfluorinated pollutants. *Nat Commun* **2019,** *10*, (1), 5762.

82. Liang, J.; Deng, X.; Tan, K., An eosin Y-based "turn-on" fluorescent sensor for detection of perfluorooctane sulfonate. *Spectrochim Acta A Mol Biomol Spectrosc* **2015,** *150*, 772-7.

83. Cheng, Z.; Du, L.; Zhu, P.; Chen, Q.; Tan, K., An erythrosin B-based "turn on" fluorescent sensor for detecting perfluorooctane sulfonate and perfluorooctanoic acid in environmental water samples. *Spectrochim Acta A Mol Biomol Spectrosc* **2018,** *201*, 281-287.

84. Wang, H.; Zhang, X.; Liu, Y.; Liu, J., Stabilization of Liposomes by Perfluorinated Compounds. *ACS Omega* **2018,** *3*, (11), 15353-15360.

85. Fitzgerald, N. J. M.; Simcik, M. F.; Novak, P. J., Perfluoroalkyl Substances Increase the Membrane Permeability and Quorum Sensing Response inAliivibrio fischeri. *Environ Sci Technol* **2017,** *5*, (1), 26-31.

86. He, J.; Qiu, P.; Song, J.; Zhang, S.; Bai, Y., A resonance Rayleigh scattering and colorimetric dual-channel sensor for sensitive detection of perfluorooctane sulfonate based on toluidine blue. *Anal Bioanal Chem* **2020,** *412*, (22), 5329-5339.

87. H Feng; N Wang; T Tran T; L Yuan; J Li; Cai., Q., Surface molecular imprinting on dye–(NH2)–SiO2 NPs for specific recognition and direct fluorescent quantification of perfluorooctane sulfonate. *Sens Actuators B Chem* **2014,** *196*, 266-273.

88. Niu, H.; Wang, S.; Zhou, Z.; Ma, Y.; Ma, X.; Cai, Y., Sensitive colorimetric visualization of perfluorinated compounds using poly(ethylene glycol) and perfluorinated thiols modified gold

nanoparticles. *Anal Chem* **2014,** *86*, (9), 4170-7.

89. Takayose, M.; Akamatsu, K.; Nawafune, H.; Murashima, T.; Matsui, J., Colorimetric Detection of Perfluorooctanoic Acid (PFOA) Utilizing Polystyrene-Modified Gold Nanoparticles. *Analytical Letters* **2012,** *45*, (18), 2856-2864.

90. Yin, M.; Che, L.; Jiang, S.; Deng, Q.; Wang, S., Sensing of perfluorinated compounds using a functionalized tricolor upconversion nanoparticle based fluorescence sensor array. *Environmental Science: Nano* **2020,** *7*, (10), 3036-3046.

91. Li, J.; Zhang, C.; Yin, M.; Zhang, Z.; Chen, Y.; Deng, Q.; Wang, S., Surfactant-Sensitized Covalent Organic Frameworks-Functionalized Lanthanide-Doped Nanocrystals: An Ultrasensitive Sensing Platform for Perfluorooctane Sulfonate. *ACS Omega* **2019,** *4*, (14), 15947-15955.

92. Yin, H. Q.; Tan, K.; Jensen, S.; Teat, S. J.; Ullah, S.; Hei, X.; Velasco, E.; Oyekan, K.; Meyer, N.; Wang, X. Y.; Thonhauser, T.; Yin, X. B.; Li, J., A switchable sensor and scavenger: detection and removal of fluorinated chemical species by a luminescent metal-organic framework. *Chem Sci* **2021,** *12*, (42), 14189-14197.

93. Chen, B.; Yang, Z.; Qu, X.; Zheng, S.; Yin, D.; Fu, H., Screening and Discrimination of Perfluoroalkyl Substances in Aqueous Solution Using a Luminescent Metal-Organic Framework Sensor Array. *ACS Appl Mater Interfaces* **2021,** *13*, (40), 47706-47716.

94. Faiz, F.; Baxter, G.; Collins, S.; Sidiroglou, F.; Cran, M., Polyvinylidene fluoride coated optical fibre for detecting perfluorinated chemicals. *Sensors and Actuators B: Chemical* **2020,** *312*.

95. Cennamo, N.; Zeni, L.; Tortora, P.; Regonesi, M. E.; Giusti, A.; Staiano, M.; D'Auria, S.; Varriale, A., A High Sensitivity Biosensor to detect the presence of perfluorinated compounds in environment. *Talanta* **2018,** *178*, 955-961.

96. Cennamo, N.; D'Agostino, G.; Sequeira, F.; Mattiello, F.; Porto, G.; Biasiolo, A.; Nogueira, R.; Bilro, L.; Zeni, L., A Simple and Low-Cost Optical Fiber Intensity-Based Configuration for Perfluorinated Compounds in Water Solution. *Sensors (Basel)* **2018,** *18*, (9).

97. S B Bambot; J Sipior; J R Lakowicz; Rao, G., Lifetime-based optical sensing of pH using resonance energy transfer in sol-gel films. *Sens Actuators B Chem* **1994,** *22*, 181-188.

98. Lakowicz, J. R., *Principles of Fluorescence Spectroscopy, Third Edition*. springer: New York, 2010.

99. A. Prasanna de Silva; H. Q. Nimal Gunaratne; McCoy, C. P., Direct visual indication of pH windows: 'offkm-off' fluorescent PET (photoinduced electron transfer) sensors/switches. *Chem. Commun., 1996 2399* **1996**, 2399.

100. Sun, W.; Li, M.; Fan, J.; Peng, X., Activity-Based Sensing and Theranostic Probes Based on Photoinduced Electron Transfer. *Acc Chem Res* **2019,** *52*, (10), 2818-2831.

101. Lan, M.; Di, Y.; Zhu, X.; Ng, T. W.; Xia, J.; Liu, W.; Meng, X.; Wang, P.; Lee, C. S.; Zhang, W., A carbon dot-based fluorescence turn-on sensor for hydrogen peroxide with a photo-induced electron transfer mechanism. *Chem Commun (Camb)* **2015,** *51*, (85), 15574-7.

102. Birks, J. B., *Photophysics of Aromatic Molecule*. Wiley: London, 1970.

103. Huang, Y.; Xing, J.; Gong, Q.; Chen, L. C.; Liu, G.; Yao, C.; Wang, Z.; Zhang, H. L.; Chen, Z.; Zhang, Q., Reducing aggregation caused quenching effect through co-assembly of PAH chromophores and molecular barriers. *Nat Commun* **2019,** *10*, (1), 169.

104. Kang, T.; Um, K.; Park, J.; Chang, H.; Lee, D. C.; Kim, C.-K.; Lee, K., Minimizing the fluorescence quenching caused by uncontrolled aggregation of CdSe/CdS core/shell quantum dots for biosensor applications. *Sensors and Actuators B: Chemical* **2016,** *222*, 871-878.

105. Jelinek, R., *Carbon Quantum Dots : Synthesis, Properties and Applications*. Springer International Publishing AG: 2016.

106. Hua, B.; Zhang, C.; Zhou, W.; Shao, L.; Wang, Z.; Wang, L.; Zhu, H.; Huang, F., Pillar[5]arene-Based Solid-State Supramolecular Polymers with Suppressed Aggregation-Caused Quenching Effects and Two-Photon Excited Emission. *J Am Chem Soc* **2020,** *142*, (39), 16557-16561.

107. Luo, J.; Xie, Z.; Lam, J. W.; Cheng, L.; Chen, H.; Qiu, C.; Kwok, H. S.; Zhan, X.; Liu, Y.; Zhu, D.; Tang, B. Z., Aggregation-induced emission of 1-methyl-1,2,3,4,5-pentaphenylsilole. *Chem Commun (Camb)* **2001**, (18), 1740-1.

108. Tang, B. Z.; Zhan, X.; Yu, G.; Sze Lee, P. P.; Liu, Y.; Zhu, D., *Journal of Materials Chemistry* **2001,** *11*, (12), 2974-2978.

109. Zhao, Z.; Lu, P.; Lam, J. W. Y.; Wang, Z.; Chan, C. Y. K.; Sung, H. H. Y.; Williams, I. D.; Ma, Y.; Tang, B. Z., Molecular anchors in the solid state: Restriction of intramolecular rotation boosts emission efficiency of luminogen aggregates to unity. *Chem. Sci.* **2011,** *2*, (4), 672-675.

110. Nitti, A.; Pasini, D., Aggregation-Induced Circularly Polarized Luminescence: Chiral Organic Materials for Emerging Optical Technologies. *Adv Mater* **2020,** *32*, (41), e1908021.

111. Hong, Y.; Lam, J. W. Y.; Tang, B. Z., Aggregation-induced emission: phenomenon, mechanism and applications. *Chemical Communications* **2009**, (29).

112. Kleszczynski, K.; Skladanowski, A. C., Mechanism of cytotoxic action of perfluorinated acids. I. alteration in plasma membrane potential and intracellular pH level. *Toxicol Appl Pharmacol* **2009,** *234*, (3), 300-5.

113. Fitzgerald, N. J. M.; Wargenau, A.; Sorenson, C.; Pedersen, J.; Tufenkji, N.; Novak, P. J.; Simcik, M. F., Partitioning and Accumulation of Perfluoroalkyl Substances in Model Lipid Bilayers and Bacteria. *Environ Sci Technol* **2018,** *52*, (18), 10433-10440.

114. Wielsoe, M.; Long, M.; Ghisari, M.; Bonefeld-Jorgensen, E. C., Perfluoroalkylated substances (PFAS) affect oxidative stress biomarkers in vitro. *Chemosphere* **2015,** *129*, 239-45.

115. Zhang, J.; Wan, Y.; Li, Y.; Zhang, Q.; Xu, S.; Zhu, H.; Shu, B., A rapid and high-throughput quantum dots bioassay for monitoring of perfluorooctane sulfonate in environmental water samples. *Environ Pollut* **2011,** *159*, (5), 1348-53.

116. Joel Bernstein; Raymond E. Davis; Liat Shimoni; Chang., N.-L., Patterns in Hydrogen Bonding: Functionality and Graph Set Analysis in Crystals. *Angew. Chem. Int. Ed. Engl* **1995,** *34*, 1555-1573.

117. Steiner, T., The Hydrogen Bond in the Solid State. *Angew. Chem. Int. Ed.* **2002,** *41*, 48-76.

118. Cabaleiro-Lago, E. M.; Otero, J. R. g., Ab Initioand density functional theory study of the interaction in formamide and thioformamide dimers and trimers. *The Journal of Chemical Physics* **2002,** *117*, (4), 1621-1632.

119. Schneider, H.-J., Hydrogen bonds with fluorine. Studies in solution, in gas phase and by computations, conflicting conclusions from crystallographic analyses. *Chemical Science* **2012,** *3*, (5).

120. Nakamoto, K.; Margoshes, M.; Rundle, R. E., Stretching Frequencies as a Function of Distances

in Hydrogen Bonds. *Journal of the American Chemical Society* **1955,** *77*, (24), 6480-6486.

121. Von R. Schleyer, P.; West, R., Comparison of Covalently Bonded Electro-Negative Atoms as Proton Acceptor Groups in Hydrogen Bonding. *Journal of the American Chemical Society* **1959,** *81*, (12), 3164-3165.

122. Wood, P. A.; McKinnon, J. J.; Parsons, S.; Pidcock, E.; Spackman, M. A., Analysis of the compression of molecular crystal structures using Hirshfeld surfaces. *CrystEngComm* **2008**.

123. Chęcińska, L.; Grabowski, S. J., F–H···F–C hydrogen bonds – The influence of hybridization of carbon atom connected with F-acceptor on their properties. *Chemical Physics* **2006,** *327*, (2-3), 202-208.

124. Judith A. K. Howard; Vanessa J. Hoy; David O'Hagan; Smith., G. T., How Good is Fluorine as a Hydrogen Bond Acceptor. *Tetrahedron* **1996,** *52*, 12613-12622.

125. Yanzhi Liu; Kun Yuan; Zhao Yuan; Yuancheng Zhu; Lv., L., Fluorine substitution effects of halide anion receptors based on the combination of a distinct hydrogen bond and anion–p noncovalent interactions: a theoretical investigation. *RSC Adv.*, **2016,** *6*, 14666–14677.

126. Ibon Alkorta; Isabel Rozas; Elguero., J., Effects of fluorine substitution on hydrogen bond interactions. *Journal of Fluorine Chemistry* **2000,** *101*, 233–238.

127. Baker, R. J.; Colavita, P. E.; Murphy, D. M.; Platts, J. A.; Wallis, J. D., Fluorine-fluorine interactions in the solid state: an experimental and theoretical study. *J Phys Chem A* **2012,** *116*, (5), 1435-44.

128. Karnoukhova, V. A.; Fedyanin, I. V.; Lyssenko, K. A., Directionality of intermolecular C–F···F–C interactions in crystals: experimental and theoretical charge density study. *Structural Chemistry* **2015,** *27*, (1), 17-24.

129. Sharp, K. A.; Honig, B., Electrostatic interactions in macromolecules: theory and applications. *Annual review of biophysics*

biophysical chemistry **1990,** *19*, (1), 301-332.

130. Plimpton, S.; Lawton, W., A very accurate test of Coulomb's law of force between charges.

Physical Review **1936,** *50*, (11), 1066.

131. Aguado, R. J.; Mazega, A.; Tarrés, Q.; Delgado-Aguilar, M., The role of electrostatic interactions of anionic and cationic cellulose derivatives for industrial applications: A critical review. *Industrial Crops and Products* **2023,** *201*, 116898.

132. Sabnis, R. W., *Handbook of Fluorescent Dyes and Probes*. John Wiley & Sons: 2015.

133. Lippitsch, M. E.; Draxler, S.; Kieslinger, D., Luminescence lifetime-based sensing: new materials, new devices. *Sensors*

Actuators B: Chemical **1997,** *38*, (1-3), 96-102.

134. Lippitsch, M. E.; Draxler, S.; Kieslinger, D., Luminescence lifetime-based sensing: new materials, new devices. *Sensors*

Actuators B: Chemical

1997, *38*, (1-3), 96-102.

135. Xu, R.; Wang, Y.; Duan, X.; Lu, K.; Micheroni, D.; Hu, A.; Lin, W., Nanoscale Metal-Organic Frameworks for Ratiometric Oxygen Sensing in Live Cells. *J Am Chem Soc* **2016,** *138*, (7), 2158-61.

136. Chen, D.; Wan, Z.; Zhou, Y., Optical spectroscopy of Cr3+-doped transparent nano-glass ceramics for lifetime-based temperature sensing. *Opt. Lett.* **2015,** *40*, (15), 3607-3610.

137. Trettnak, W.; Kolle, C.; Reininger, F.; Dolezal, C.; O'Leary, P., Miniaturized luminescence lifetime-based oxygen sensor instrumentation utilizing a phase modulation technique. *Sensors and Actuators B: Chemical* **1996,** *36*, (1), 506-512.

138. Zhang, G.; Chen, R.; Gao, Y.; Yu, B.; Qin, C.; Xiao, L.; Jia, S., High visibility fluorescence imaging for nanoparticles based on acousto-optic time delay effect. *Sensors and Actuators B: Chemical* **2015,** *208*, 464-467.

139. Liu, S.-Y.; Qi, X.-L.; Lin, R.-B.; Cheng, X.-N.; Liao, P.-Q.; Zhang, J.-P.; Chen, X.-M., Porous Cu(I) Triazolate Framework and Derived Hybrid Membrane with Exceptionally High Sensing Efficiency for Gaseous Oxygen. *Advanced Functional Materials* **2014,** *24*, (37), 5866-5872.

140. Berezin, M. Y.; Achilefu, S., Fluorescence Lifetime Measurements and Biological Imaging. *Chemical Reviews* **2010,** *110*, (5), 2641-2684.

141. Adams, S. J.; Carrod, A. J.; Rochford, L. A.; Walker, M.; Pikramenou, Z., Surfactant-Enhanced Luminescence Lifetime for Biomolecular Detection on Luminescent Gold Surfaces Decorated with Transition Metal Complexes. *ChemistrySelect* **2018,** *3*, (11), 3251-3257.

142. Rogers, N. J.; Claire, S.; Harris, R. M.; Farabi, S.; Zikeli, G.; Styles, I. B.; Hodges, N. J.; Pikramenou, Z., High coating of Ru(II) complexes on gold nanoparticles for single particle luminescence imaging in cells. *Chem Commun (Camb)* **2014,** *50*, (5), 617-9.

143. Mercier, D.; Boujday, S.; Annabi, C.; Villanneau, R.; Pradier, C.-M.; Proust, A., Bifunctional Polyoxometalates for Planar Gold Surface Nanostructuration and Protein Immobilization. *The Journal of Physical Chemistry C* **2012,** *116*, (24), 13217-13224.

144. Laibinis, P. E.; Whitesides, G. M.; Allara, D. L.; Tao, Y. T.; Parikh, A. N.; Nuzzo, R. G., Comparison of the structures and wetting properties of self-assembled monolayers of n-alkanethiols on the coinage metal surfaces, copper, silver, and gold. *Journal of the American Chemical Society* **1991,** *113*, (19), 7152-7167.

145. Perl, A.; Reinhoudt, D. N.; Huskens, J., Microcontact Printing: Limitations and Achievements. **2009,** *21*, (22), 2257-2268.

146. Mitzi, D. B.; Kosbar, L. L.; Murray, C. E.; Copel, M.; Afzali, A., High-mobility ultrathin semiconducting films prepared by spin coating. *Nature* **2004,** *428*, (6980), 299-303.

147. Acharya, S.; Hill, J. P.; Ariga, K., Soft Langmuir–Blodgett Technique for Hard Nanomaterials. **2009,** *21*, (29), 2959-2981.

148. Ashfold, M. N. R.; Claeyssens, F.; Fuge, G. M.; Henley, S. J., Pulsed laser ablation and deposition of thin films. *Chemical Society Reviews* **2004,** *33*, (1), 23-31.

149. Vidic, J.; Pla-Roca, M.; Grosclaude, J.; Persuy, M.-A.; Monnerie, R.; Caballero, D.; Errachid, A.; Hou, Y.; Jaffrezic-Renault, N.; Salesse, R.; Pajot-Augy, E.; Samitier, J., Gold Surface Functionalization and Patterning for Specific Immobilization of Olfactory Receptors Carried by Nanosomes. *Analytical Chemistry* **2007,** *79*, (9), 3280-3290.

150. Adams, S. J.; Lewis, D. J.; Preece, J. A.; Pikramenou, Z., Luminescent gold surfaces for sensing and imaging: patterning of transition metal probes. *ACS Appl Mater Interfaces* **2014,** *6*, (14), 11598-

608.

151. King, S. M.; Claire, S.; Teixeira, R. I.; Dosumu, A. N.; Carrod, A. J.; Dehghani, H.; Hannon, M. J.; Ward, A. D.; Bicknell, R.; Botchway, S. W.; Hodges, N. J.; Pikramenou, Z., Iridium Nanoparticles for Multichannel Luminescence Lifetime Imaging, Mapping Localization in Live Cancer Cells. *J Am Chem Soc* **2018,** *140*, (32), 10242-10249.

152. Carrod, A.; Graglia, F.; Male, L.; Le Duff, C.; Simpson, P.; Elsherif, M.; Ahmed, Z.; Butt, H.; Xu, G. X.; Lo, K. K.; Bertoncello, P.; Pikramenou, Z., Photo- and electrochemical dual-responsive iridium probe for saccharide detection. *Chem Eur J* **2021**.

153. Lewis, D. J.; Pikramenou, Z., Lanthanide-coated gold nanoparticles for biomedical applications. *Coord Chem Rev* **2014,** *273-274*, 213-225.

154. Poole, C. F., New trends in solid-phase extraction. *TrAC Trends in Analytical Chemistry* **2003,** *22*, (6), 362-373.

155. OECD, Toward a new comprehensive global database of per- and polyfluoroalkyl substances (PFAS): summary report on updating the OECD 2007 list of per and polyfluoroalkyl Substances (PFASs). In 2018.

156. Kissa, E., *Fluorinated surfactants and repellents*. CRC Press: 2001; Vol. 97.

157. Chaemfa, C.; Barber, J. L.; Huber, S.; Breivik, K.; Jones, K. C., Screening for PFOS and PFOA in European air using passive samplers. *J Environ Monit* **2010,** *12*, (5), 1100-9.

158. Zhao, Y. G.; Wong, C. K.; Wong, M. H., Environmental contamination, human exposure and body loadings of perfluorooctane sulfonate (PFOS), focusing on Asian countries. *Chemosphere* **2012,** *89*, (4), 355-68.

159. Abraham, K.; Mielke, H.; Fromme, H.; Volkel, W.; Menzel, J.; Peiser, M.; Zepp, F.; Willich, S. N.; Weikert, C., Internal exposure to perfluoroalkyl substances (PFASs) and biological markers in 101 healthy 1-year-old children: associations between levels of perfluorooctanoic acid (PFOA) and vaccine response. *Arch Toxicol* **2020,** *94*, (6), 2131-2147.

160. U.S. Environmental Protection Agency Per- and Polyfluoroalkyl Substances (PFAS), Proposed PFAS National Primary Drinking Water Regulation. https://www.epa.gov/sdwa/and-polyfluoroalkyl-

substances-pfas

161. Wu, J.; Liu, W.; Ge, J.; Zhang, H.; Wang, P., New sensing mechanisms for design of fluorescent chemosensors emerging in recent years. *Chem Soc Rev* **2011,** *40*, (7), 3483-95.

162. Janjić, G. V.; Jelić, S. T.; Trišović, N. P.; Popović, D. M.; Đorđević, I. S.; Milčić, M. K., New Theoretical Insight into Fluorination and Fluorine–Fluorine Interactions as a Driving Force in Crystal Structures. *Cryst Growth Des* **2020,** *20*, (5), 2943-2951.

163. Rocha, M.; Echeverría, G. A.; Piro, O. E.; Jios, J. L.; Ulic, S. E.; Gil, D. M., Role of fluorine-fluorine and weak intermolecular interactions in the supramolecular network of a new trifluoromethyl-1,5-benzodiazepine: Crystal structure, Hirshfeld surface analysis and theoretical study. *J Fluor Chem* **2021,** *242*.

164. Taylor, C. M.; Ellingsen, T. A.; Breadmore, M. C.; Kilah, N. L., Porphyrin-based colorimetric sensing of perfluorooctanoic acid as proof of concept for perfluoroalkyl substance detection. *Chem comm* **2021,** *57*, (88), 11649-11652.

165. Szmacinski, H.; Lakowicz, J. R., Fluorescence lifetime-based sensing and imaging. *Sens Actuators B: Chem* **1995,** *29*, (1), 16-24.

166. Fan, Y.; Wang, S.; Zhang, F., Optical Multiplexed Bioassays for Improved Biomedical Diagnostics. *Angew Chem Int Ed Engl* **2019,** *58*, (38), 13208-13219.

167. Zhou, J.; Li, J.; Zhang, K. Y.; Liu, S.; Zhao, Q., Phosphorescent iridium(III) complexes as lifetime-based biological sensors for photoluminescence lifetime imaging microscopy. *Coord Chem Rev* **2022,** *453*, 214334.

168. Zhang, K. Y.; Zhang, T.; Wei, H.; Wu, Q.; Liu, S.; Zhao, Q.; Huang, W., Phosphorescent iridium(iii) complexes capable of imaging and distinguishing between exogenous and endogenous analytes in living cells. *Chem Sci* **2018,** *9*, (36), 7236-7240.

169. Tang, Q.; Zhang, X.; Cao, H.; Chen, G.; Huang, H.; Zhang, P.; Zhang, Q., A phosphorescent iridium probe for sensing polarity in the endoplasmic reticulum and in vivo. *Dalton Trans* **2019,** *48*, (22), 7728-7734.

170. Zhang, K. Y.; Liu, H.-W.; Tang, M.-C.; Choi, A. W.-T.; Zhu, N.; Wei, X.-G.; Lau, K.-C.; Lo,

K. K.-W., Dual-Emissive Cyclometalated Iridium(III) Polypyridine Complexes as Ratiometric Biological Probes and Organelle-Selective Bioimaging Reagents. *Inorg Chem* **2015,** *54*, (13), 6582-6593.

171. Pramod, P.; Sudeep, P. K.; Thomas, K. G.; Kamat, P. V., Photochemistry of Ruthenium Trisbipyridine Functionalized on Gold Nanoparticles. *J Mater Chem B* **2006,** *110*, (42), 20737-20741.

172. Ramachandra, S.; Schuermann, K. C.; Edafe, F.; Belser, P.; Nijhuis, C. A.; Reus, W. F.; Whitesides, G. M.; De Cola, L., Luminescent Ruthenium Tripod Complexes: Properties in Solution and on Conductive Surfaces. *Inorganic Chemistry* **2011,** *50*, (5), 1581-1591.

173. Tachiya, M., Kinetics of quenching of luminescent probes in micellar systems. II. *J Chem Phys* **1982,** *76*, (1), 340-348.

174. Turro, N. J.; Grätzel, M.; Braun, A. M., Photophysical and photochemical processes in micellar systems. *Angew Chem, Int Ed* **1980,** *19*, (9), 675-696.

175. Uchiyama, S.; Fukatsu, E.; McClean, G. D.; de Silva, A. P., Measurement of Local Sodium Ion Levels near Micelle Surfaces with Fluorescent Photoinduced-Electron-Transfer Sensors. *Angew Chem, Int Ed* **2016,** *55*, (2), 768-771.

176. Ding, L.; Bai, Y.; Cao, Y.; Ren, G.; Blanchard, G. J.; Fang, Y., Micelle-Induced Versatile Sensing Behavior of Bispyrene-Based Fluorescent Molecular Sensor for Picric Acid and PYX Explosives. *Langmuir* **2014,** *30*, (26), 7645-7653.

177. Chen, H.; Zhang, C.; Han, J.; Yu, Y.; Zhang, P., PFOS and PFOA in influents, effluents, and biosolids of Chinese wastewater treatment plants and effluent-receiving marine environments. *Environ Pollut* **2012,** *170*, 26-31.

178. Ranaweera, R.; Ghafari, C.; Luo, L., Bubble-Nucleation-Based Method for the Selective and Sensitive Electrochemical Detection of Surfactants. *Anal Chem* **2019,** *91*, (12), 7744-7748.

179. Romani, A.; Clementi, C.; Miliani, C.; Brunetti, B. G.; Sgamellotti, A.; Favaro, G., Portable Equipment for Luminescence Lifetime Measurements on Surfaces. *Appl. Spectrosc.* **2008,** *62*, (12), 1395-1399.

180. Backe, W. J.; Day, T. C.; Field, J. A., Zwitterionic, Cationic, and Anionic Fluorinated Chemicals

in Aqueous Film Forming Foam Formulations and Groundwater from U.S. Military Bases by Nonaqueous Large-Volume Injection HPLC-MS/MS. *Environ Sci Technol* **2013,** *47*, (10), 5226-5234.

181. Susmann, H. P.; Schaider, L. A.; Rodgers, K. M.; Rudel, R. A., Dietary Habits Related to Food Packaging and Population Exposure to PFASs. *Environ Health Perspect* **2019,** *127*, (10), 107003.

182. Zheng, G.; Boor, B. E.; Schreder, E.; Salamova, A., Indoor exposure to per- and polyfluoroalkyl substances (PFAS) in the childcare environment. *Environ Pollut* **2020,** *258*, 113714.

183. Domingo, J. L.; Nadal, M., Human exposure to per- and polyfluoroalkyl substances (PFAS) through drinking water: A review of the recent scientific literature. *Environ Res* **2019,** *177*, 108648.

184. Xu, Y.; Fletcher, T.; Pineda, D.; Lindh, C. H.; Nilsson, C.; Glynn, A.; Vogs, C.; Norstrom, K.; Lilja, K.; Jakobsson, K.; Li, Y., Serum Half-Lives for Short- and Long-Chain Perfluoroalkyl Acids after Ceasing Exposure from Drinking Water Contaminated by Firefighting Foam. *Environ Health Perspect* **2020,** *128*, (7), 77004.

185. Li, Y.; Andersson, A.; Xu, Y.; Pineda, D.; Nilsson, C. A.; Lindh, C. H.; Jakobsson, K.; Fletcher, T., Determinants of serum half-lives for linear and branched perfluoroalkyl substances after long-term high exposure-A study in Ronneby, Sweden. *Environ Int* **2022,** *163*, 107198.

186. Berg, V.; Nost, T. H.; Hansen, S.; Elverland, A.; Veyhe, A. S.; Jorde, R.; Odland, J. O.; Sandanger, T. M., Assessing the relationship between perfluoroalkyl substances, thyroid hormones and binding proteins in pregnant women; a longitudinal mixed effects approach. *Environ Int* **2015,** *77*, 63-9.

187. Starling, A. P.; Engel, S. M.; Whitworth, K. W.; Richardson, D. B.; Stuebe, A. M.; Daniels, J. L.; Haug, L. S.; Eggesbo, M.; Becher, G.; Sabaredzovic, A.; Thomsen, C.; Wilson, R. E.; Travlos, G. S.; Hoppin, J. A.; Baird, D. D.; Longnecker, M. P., Perfluoroalkyl substances and lipid concentrations in plasma during pregnancy among women in the Norwegian Mother and Child Cohort Study. *Environ Int* **2014,** *62*, 104-12.

188. Petersen, K. U.; Larsen, J. R.; Deen, L.; Flachs, E. M.; Haervig, K. K.; Hull, S. D.; Bonde, J. P. E.; Tottenborg, S. S., Per- and polyfluoroalkyl substances and male reproductive health: a systematic review of the epidemiological evidence. *J Toxicol Environ Health B Crit Rev* **2020,** *23*, (6), 276-291.

189. Stanifer, J. W.; Stapleton, H. M.; Souma, T.; Wittmer, A.; Zhao, X.; Boulware, L. E., Perfluorinated Chemicals as Emerging Environmental Threats to Kidney Health: A Scoping Review. *Clin J Am Soc Nephrol* **2018,** *13*, (10), 1479-1492.

190. Grandjean, P.; Heilmann, C.; Weihe, P.; Nielsen, F.; Mogensen, U. B.; Budtz-Jorgensen, E., Serum Vaccine Antibody Concentrations in Adolescents Exposed to Perfluorinated Compounds. *Environ Health Perspect* **2017,** *125*, (7), 077018.

191. Stockholm Convention All POPs listed in the Stockholm Convention. http://chm.pops.int/TheConvention/ThePOPs/ListingofPOPs/tabid/2509/Default.aspx

192. Union, C. o. t. E. Council and Parliament agree to reduce limit values for the presence of persistent organic pollutants in waste. https://www.consilium.europa.eu/en/press/press-releases/2022/06/21/council-and-parliament-agree-to-reduce-limit-values-for-the-presence-of-persistent-organic-pollutants-in-waste/

193. Eurostat Waste statistics. https://ec.europa.eu/eurostat/statistics-explained/index.php?title=Waste_statistics#:~:text=Hazardous%20waste%20treatment-,Total%20waste%20generation,4%20815%20kg%20per%20capita.

194. Kotthoff, M.; Muller, J.; Jurling, H.; Schlummer, M.; Fiedler, D., Perfluoroalkyl and polyfluoroalkyl substances in consumer products. *Environ Sci Pollut Res Int* **2015,** *22*, (19), 14546-59.

195. Madou, M. J.; Morrison, S. R., *Chemical sensing with solid state devices*. Elsevier: 2012.

196. Wang, C.; Wang, C.; Jin, D.; Yu, Y.; Yang, F.; Zhang, Y.; Yao, Q.; Zhang, G. J., AuNP-Amplified Surface Acoustic Wave Sensor for the Quantification of Exosomes. *ACS Sens* **2020,** *5*, (2), 362-369.

197. Lee, E.; Yoon, Y. S.; Kim, D. J., Two-Dimensional Transition Metal Dichalcogenides and Metal Oxide Hybrids for Gas Sensing. *ACS Sens* **2018,** *3*, (10), 2045-2060.

198. Bishop, K. J.; Wilmer, C. E.; Soh, S.; Grzybowski, B. A., Nanoscale forces and their uses in self-assembly. *Small* **2009,** *5*, (14), 1600-30.

199. Zhang, K.; Carrod, A. J.; Del Giorgio, E.; Hughes, J.; Rurack, K.; Bennet, F.; Hodoroaba, V.-D.; Harrad, S.; Pikramenou, Z., Luminescence Lifetime-Based Sensing Platform Based on

Cyclometalated Iridium(III) Complexes for the Detection of Perfluorooctanoic Acid in Aqueous Samples. *Analytical Chemistry* **2024,** *96*, (4), 1565-1575.

200. Stefan Lis; Choppin, G. R., Determination of Small Amounts of Water in Dimethylformamide and Dlmethylsulfoxlde Using Luminescence Lifetime Measurements of Europlum(III). *Anal. Chem.* **1991,** *63*, 2542-2543.

201. Yao, M.; Chen, W., Hypersensitive luminescence of Eu^{3+} in dimethyl sulfoxide as a new probing for water measurement. *Anal Chem* **2011,** *83*, (6), 1879-82.

202. Bassett, A. P.; Magennis, S. W.; Glover, P. B.; Lewis, D. J.; Spencer, N.; Parsons, S.; Williams, R. M.; De Cola, L.; Pikramenou, Z., Highly Luminescent, Triple- and Quadruple-Stranded, Dinuclear Eu, Nd, and Sm(III) Lanthanide Complexes Based on Bis-Diketonate Ligands. *Journal of the American Chemical Society* **2004,** *126*, (30), 9413-9424.

203. Giorgio, E. D. Dinuclear Lanthanide(Iii) Complexes for Light Emitting Surfaces and Plasmonic Nanomaterials. University of Birmingham, 2023.

204. Castner, D. G., X-ray Photoelectron Spectroscopy Sulfur 2p Study of Organic Thiol and Disulfide Binding Interactions with Gold Surfaces. *Langmuir* **1996,** *12*, 5083-5086.

205. Berisha, A.; Combellas, C.; Kanoufi, F.; Medard, J.; Decorse, P.; Mangeney, C.; Kherbouche, I.; Seydou, M.; Maurel, F.; Pinson, J., Alkyl-Modified Gold Surfaces: Characterization of the Au-C Bond. *Langmuir* **2018,** *34*, (38), 11264-11271.

206. Alexander V. Naumkin; Anna Kraut-Vass; Stephen W. Gaarenstroom; Powell, C. J., NIST X-ray Photoelectron Spectroscopy Database. In 2012.

207. Horiba Jobin Yvon Raman Data and Analysis, Raman Spectroscopy for Analysis and Monitoring. https://static.horiba.com/fileadmin/Horiba/Technology/Measurement_Techniques/Molecular_Spectroscopy/Raman_Spectroscopy/Raman_Academy/Raman_Tutorial/Raman_bands.pdf?utm_source=uhw&utm_medium=301&utm_campaign=uhw-redirect

208. Nakabayashi, T.; Oshita, S.; Sumikawa, R.; Sun, F.; Kinjo, M.; Ohta, N., pH dependence of the fluorescence lifetime of enhanced yellow fluorescent protein in solution and cells. *Journal of*

Photochemistry

Photobiology A: Chemistry **2012,** *235*, 65-71.

209. Lin, H. J.; Herman, P.; Lakowicz, J. R., Fluorescence lifetime-resolved pH imaging of living cells. *the journal of the international society for analytical cytology* **2003,** *52*, (2), 77-89.

210. Crans, D. C.; Baruah, B.; Ross, A.; Levinger, N. E., Impact of confinement and interfaces on coordination chemistry: Using oxovanadate reactions and proton transfer reactions as probes in reverse micelles. *J Coordination Chemistry Reviews* **2009,** *253*, (17-18), 2178-2185.

211. Magalhães, P. R.; Oliveira, A. S. F.; Campos, S. R.; Soares, C. M.; Baptista, A. M. J. J. o. C. I.; Modeling, Effect of a pH gradient on the protonation states of cytochrome c oxidase: A continuum electrostatics study. **2017,** *57*, (2), 256-266.

212. Hemmer, E.; Venkatachalam, N.; Hyodo, H.; Hattori, A.; Ebina, Y.; Kishimoto, H.; Soga, K., Upconverting and NIR emitting rare earth based nanostructures for NIR-bioimaging. *Nanoscale* **2013,** *5*, (23), 11339-11361.

213. Sava Gallis, D. F.; Rohwer, L. E. S.; Rodriguez, M. A.; Barnhart-Dailey, M. C.; Butler, K. S.; Luk, T. S.; Timlin, J. A.; Chapman, K. W., Multifunctional, Tunable Metal–Organic Framework Materials Platform for Bioimaging Applications. *ACS Applied Materials & Interfaces* **2017,** *9*, (27), 22268-22277.

214. Bai, G.; Yang, Z.; Lin, H.; Jie, W.; Hao, J., Lanthanide Yb/Er co-doped semiconductor layered WSe2 nanosheets with near-infrared luminescence at telecommunication wavelengths. *Nanoscale* **2018,** *10*, (19), 9261-9267.

215. Tang, M.; Huang, Y.; Wang, Y.; Fu, L., An ytterbium complex with unique luminescence properties: detecting the temperature based on a luminescence spectrum without the interference of oxygen. *Dalton Transactions* **2015,** *44*, (16), 7449-7457.

216. Kazakov, D. V.; Safarov, F. E., A novel chemiluminescence from the reaction of singlet oxygen with β-diketonates of europium(iii), neodymium(iii) and ytterbium(iii). *Photochemical & Photobiological Sciences* **2014,** *13*, (12), 1646-1649.

217. Bünzli, J.-C. G.; Eliseeva, S. V., Lanthanide NIR luminescence for telecommunications,

bioanalyses and solar energy conversion. *Journal of Rare Earths* **2010,** *28*, (6), 824-842.

218. Ma, Q.; Wang, J.; Li, Z.; Lv, X.; Liang, L.; Yuan, Q., Recent Progress in Time-Resolved Biosensing and Bioimaging Based on Lanthanide-Doped Nanoparticles. **2019,** *15*, (32), 1804969.

219. Li, X.; Lu, S.; Tu, D.; Zheng, W.; Chen, X., Luminescent lanthanide metal–organic framework nanoprobes: from fundamentals to bioapplications. *Nanoscale* **2020,** *12*, (28), 15021-15035.

220. Cui, Y.; Chen, B.; Qian, G., Lanthanide metal-organic frameworks for luminescent sensing and light-emitting applications. *Coordination Chemistry Reviews* **2014,** *273-274*, 76-86.

221. Kenry; Duan, Y.; Liu, B., Recent Advances of Optical Imaging in the Second Near-Infrared Window. **2018,** *30*, (47), 1802394.

222. Hasegawa, Y.; Ohkubo, T.; Sogabe, K.; Kawamura, Y.; Wada, Y.; Nakashima, N.; Yanagida, S., Luminescence of Novel Neodymium Sulfonylaminate Complexes in Organic Media. *Angewandte Chemie International Edition* **2000,** *39*, (2), 357-360.

223. Mulas, A.; Dubacheva, G. V.; Al Sabea, H.; Miomandre, F.; Audibert, J.-F.; Norel, L.; Rigaut, S.; Lagrost, C., Self-Assembled Monolayers of Redox-Active 4d–4f Heterobimetallic Complexes. *Langmuir* **2019,** *35*, (42), 13711-13717.

224. Armelao, L.; Quici, S.; Barigelletti, F.; Accorsi, G.; Bottaro, G.; Cavazzini, M.; Tondello, E., Design of luminescent lanthanide complexes: From molecules to highly efficient photo-emitting materials. *Coordination Chemistry Reviews* **2010,** *254*, (5), 487-505.

225. Crawford, S. E.; Andolina, C. M.; Kaseman, D. C.; Ryoo, B. H.; Smith, A. M.; Johnston, K. A.; Millstone, J. E., Efficient Energy Transfer from Near-Infrared Emitting Gold Nanoparticles to Pendant Ytterbium(III). *Journal of the American Chemical Society* **2017,** *139*, (49), 17767-17770.

226. Bellusci, A.; Barberio, G.; Crispini, A.; Ghedini, M.; La Deda, M.; Pucci, D., Synthesis and luminescent properties of novel lanthanide (III) β-diketone complexes with nitrogen p, p ‘-disubstituted aromatic ligands. *Inorganic chemistry* **2005,** *44*, (6), 1818-1825.

227. Li, H.-F.; Yan, P.-F.; Chen, P.; Wang, Y.; Xu, H.; Li, G.-M., Highly luminescent bis-diketone lanthanide complexes with triple-stranded dinuclear structure. *Dalton Transactions* **2012,** *41*, (3), 900-907.

228. Binnemans, K. J. H. o. t. p.; earths, c. o. r., Rare-earth beta-diketonates. **2005,** *35*, (5), 107-272.

229. Eichelbaum, M.; Rademann, K., Plasmonic Enhancement or Energy Transfer? On the Luminescence of Gold-, Silver-, and Lanthanide-Doped Silicate Glasses and Its Potential for Light-Emitting Devices. **2009,** *19*, (13), 2045-2052.

230. Sun, Q.-C.; Mundoor, H.; Ribot, J. C.; Singh, V.; Smalyukh, I. I.; Nagpal, P., Plasmon-Enhanced Energy Transfer for Improved Upconversion of Infrared Radiation in Doped-Lanthanide Nanocrystals. *Nano Letters* **2014,** *14*, (1), 101-106.

231. Jayaramulu, K.; Narayanan, R. P.; George, S. J.; Maji, T. K., Luminescent microporous metal-organic framework with functional lewis basic sites on the pore surface: specific sensing and removal of metal ions. *Inorg Chem* **2012,** *51*, (19), 10089-91.

232. Nagarkar, S. S.; Joarder, B.; Chaudhari, A. K.; Mukherjee, S.; Ghosh, S. K., Highly selective detection of nitro explosives by a luminescent metal-organic framework. *Angew Chem Int Ed Engl* **2013,** *52*, (10), 2881-5.

233. Haug, L. S.; Salihovic, S.; Jogsten, I. E.; Thomsen, C.; van Bavel, B.; Lindström, G.; Becher, G., Levels in food and beverages and daily intake of perfluorinated compounds in Norway. *Chemosphere* **2010,** *80*, (10), 1137-1143.

234. Llorca, M.; Farré, M.; Picó, Y.; Müller, J.; Knepper, T. P.; Barceló, D., Analysis of perfluoroalkyl substances in waters from Germany and Spain. *Science of The Total Environment* **2012,** *431*, 139-150.

235. Cornelis, C.; D'Hollander, W.; Roosens, L.; Covaci, A.; Smolders, R.; Van Den Heuvel, R.; Govarts, E.; Van Campenhout, K.; Reynders, H.; Bervoets, L., First assessment of population exposure to perfluorinated compounds in Flanders, Belgium. *Chemosphere* **2012,** *86*, (3), 308-314.

236. Gebbink, W. A.; van Asseldonk, L.; van Leeuwen, S. P. J., Presence of Emerging Per- and Polyfluoroalkyl Substances (PFASs) in River and Drinking Water near a Fluorochemical Production Plant in the Netherlands. *Environmental Science & Technology* **2017,** *51*, (19), 11057-11065.

237. Castiglioni, S.; Valsecchi, S.; Polesello, S.; Rusconi, M.; Melis, M.; Palmiotto, M.; Manenti, A.; Davoli, E.; Zuccato, E., Sources and fate of perfluorinated compounds in the aqueous environment

and in drinking water of a highly urbanized and industrialized area in Italy. *Journal of Hazardous Materials* **2015,** *282,* 51-60.

238. Domingo, J. L.; Ericson-Jogsten, I.; Perelló, G.; Nadal, M.; Van Bavel, B.; Kärrman, A., Human Exposure to Perfluorinated Compounds in Catalonia, Spain: Contribution of Drinking Water and Fish and Shellfish. *Journal of Agricultural and Food Chemistry* **2012,** *60*, (17), 4408-4415.

239. Boone, J. S.; Vigo, C.; Boone, T.; Byrne, C.; Ferrario, J.; Benson, R.; Donohue, J.; Simmons, J. E.; Kolpin, D. W.; Furlong, E. T.; Glassmeyer, S. T., Per- and polyfluoroalkyl substances in source and treated drinking waters of the United States. *Science of The Total Environment* **2019,** *653*, 359-369.

240. Li, Y.; Li, J.; Zhang, L.; Huang, Z.; Liu, Y.; Wu, N.; He, J.; Zhang, Z.; Zhang, Y.; Niu, Z., Perfluoroalkyl acids in drinking water of China in 2017: Distribution characteristics, influencing factors and potential risks. *Environment International* **2019,** *123*, 87-95.